Doctoral Thesis

Analysis of the Functional Connectivity Patterns in the Brain of Mental Disorder Patients and Epilepsy Patients using Wavelet-crosscorrelation Analysis and Graph Theory

by

Steven M.A. Carpels

March 2022

Graduate School of Applied Informatics
University of Hyogo

A dissertation

submitted to the Graduate School of Applied Informatics

University of Hyogo

in partial fulfillment of the requirements

for the degree of Doctor of Philosophy in Applied Informatics

Acknowledgments

The research for this doctoral dissertation has been carried out in the Graduate School of Applied Informatics, University of Hyogo, Hyogo prefecture, Japan, during the year 2015−2022.

I want to thank everyone who helped me create this dissertation. First of all, I wish to express my gratitude to Professor Yuko Mizuno−Matsumoto. This work could not be completed without Professor Mizuno's guidance and helpful comments. She was always prepared to help me and answered my questions whenever possible. I am very grateful for her assistance and the time she spent discussing with me on my work.

I also wish to thank all current and former members of the Mizuno laboratory. They helped me in my study and my daily life in Japan. I am grateful to them for sharing their knowledge and expertise with me. I would like to thank my seniors Ms. Kozue Yamaguchi, Mr. Shun Sakuma, Mr. Yoshihiro Tsuji, Mr. Ayumi Muramatsu, and my juniors Mr. Yuji Inoguchi, Mr. Shohei Kobayashi, Mr. Yusuke Yamamoto, Mr. Masato Ito, Mr. Yoshiyaki Tsujii, Ms. Misato Mochizuki, Mr. Kento Harachi, Mr. Koki Tamura, and Ms. Saya Tanaka.

Lastly, I would like to express my gratitude to my parents for their endless and unconditional support throughout my entire life, and for allowing me to come to Japan for studying.

Steven M.A. Carpels
University of Hyogo
March 2022

Abstract

A lot of recent studies have shown that analyzing functional connectivity in the brain may be useful to study and understand brain function, as well as help in the diagnosis of epilepsy and mental diseases. In this thesis, engineering theory and engineering methodology were applied to the field of clinical neurophysiology. The main purpose of this thesis is to examine the functional connectivity and changes in connectivity patterns in the brain derived from EEG data, and to use wavelet-crosscorrelation analysis and graph theory analysis in order to make the pathology clear in the diseased brain. Connectivity patterns, information transfer in the brain, and changes in brain activity were examined in the alpha band in healthy individuals, mental disorder patients and epilepsy patients. After constructing functional networks, the spatial distribution of the constructed functional networks was analyzed based on graph theory to further characterize the connectivity in the healthy brain and in the diseased brain.

As described in chapter II, the first goal of this dissertation was to investigate and compare the functional connectivity in the brain between healthy individuals and individuals suffering from mental diseases in the alpha band. In some individuals, alpha waves appear in broad regions of the brain, and this is considered abnormal electroencephalography (EEG). This phenomenon is known as diffuse alpha pattern. The EEGs of 10 healthy individuals and 10 neuropsychiatric disorder patients with the diffuse alpha pattern were analyzed using wavelet–crosscorrelation analysis. Five epochs of 2 seconds were analyzed for each subject. Wavelet–crosscorrelation coefficients (WCC) were calculated for frequencies in the alpha band for all epochs in each subject. This study wanted to examine how the functional connectivity in the alpha band between the parts of the brain is different between healthy individuals and mental disorder patients with the diffuse alpha pattern. Wavelet-crosscorrelation analysis was used to visualize the connectivity pattern and the connectivity strength between the brain of healthy individuals and mental disorder individuals. It was hypothesized that the connectivity strength between the parts in the brain could be different between these two groups of subjects. The novelty of this study is abstracting the alpha band to visualize and make the connectivity pattern and connectivity strength clear in the healthy brain and the diseased brain. The results showed that the WCC values were higher in the patients with diffuse alpha, as well as a different connectivity pattern between the healthy individuals and the patients. The results suggest that the connectivity strength in the entire brain, as well as along the sagittal and coronal orientations may be stronger in the brain of the patients than in the healthy individuals in order to compensate for a less time-efficient information transfer.

The study in chapter III aims to compare the functional brain networks derived from electroencephalography (EEG) of 10 patients suffering from epilepsy with 10 healthy subjects based on graph theory to analyze the spatial distribution of the functional network in the brain. This study compared the interictal functional network of the brain of epilepsy patients during epileptiform discharge with during non-discharge. Five epochs per healthy subject, and ten epochs (during epileptiform discharge and non-discharge) per patient were selected and analyzed using wavelet–crosscorrelation analysis. The clustering coefficient, characteristic path length, small-worldness, and nodal betweenness centrality were calculated using graph analysis. The results showed that in the patients, Wavelet-crosscorrelation Coefficients (WCC) were significantly higher, and clustering and path length were significantly lower during discharge compared with the healthy subjects, along with alterations in the hub regions. The functional connectivity strength and the functional network configuration in the brain of the epilepsy patients were altered compared to the healthy subjects. Even though in the patients, the functional connectivity and small-worldness of the brain did not show significant differences between discharge and non-discharge, the centrality and the spatial distribution of the hub regions were different between during epileptiform discharge and during non-discharge. The results showed a loss of small-world topology in the functional brain network of epilepsy patients. A more random topology was found during discharge and non-discharge, therefore network indices may aid to distinguish epilepsy patients from healthy individuals, and diagnose epilepsy with a higher sensitivity. The nodal betweenness centrality index may aid to distinguish EEGs at the time of epileptiform discharges from EEGs at the time of non-discharges. The novel finding of this study is that a very short characteristic path length was found which causes the brain in epilepsy patients to synchronize too much, resulting in epileptic seizures to occur easier (seizure-prone state).

The results of both studies show that the functional connectivity differs between healthy individuals and neuropsychiatric and epilepsy patients. Performing graph theory analysis in addition to wavelet-crosscorrelation analysis provides further characterization of the functional network and information transfer in the brain. Combining WCC or other connectivity measures with network measures could make the pathology in the brain clear by revealing failing network characteristics of individuals suffering from brain disorders. This could lead to a deeper understanding of how the information transfer between brain areas fails, and may reveal the causes of brain dysfunction. The study in chapter III revealed a facilitation of synchronization in the epileptic brain due to more random topology, potentially explaining the cause of seizures. The value of this dissertation is that these results could aid in the future diagnosis and treatment of neuropsychiatric diseases and epilepsy, as well as predict a potential brain disorder or a potential patient.

Contents

Chapter I

Introduction

1.1 Background

Many studies have shown that neurophysiological and neuroimaging techniques could be useful for the assessment of clinical pathologies. Currently, there are several neurophysiological and neuroimaging techniques being used in hospitals and clinics: Computed Tomography (CT) scans, structural and functional Magnetic Resonance Imaging (MRI) scans, Electrocorticography (ECoG), and Electroencephalography (EEG). CT and MRI scans have a strong spatial resolution, but low temporal resolution. ECoG and EEG have a relatively low spatial resolution but a higher temporal resolution than CT and MRI, enabling to analyze transient changes in neuronal activity [1,2]. Therefore, it has been suggested that EEG analysis may to be useful as a supplement for the diagnosis of neuropsychiatric diseases. Nowadays, the clinical application of EEG is being carried out in many hospitals, and because (as opposed to ECoG) it is non-invasive, it is often being used as aid for the assessment of neurophysiological pathologies [3].

Electroencephalography is a medical imaging technique that reads scalp electrical activity generated by brain structures [4]. The electrical activity inside the brain is recorded by means of electrodes placed on the scalp [5]. Electroencephalography is usually abbreviated to EEG and can be defined as electrical activity of an alternating type recorded from the scalp surface after being picked up by metal electrodes and conductive media [4]. Inside the brain there are countless tiny electrical currents. These tiny currents are produced when neurons (brain cells) are activated. All these currents are generated all over the brain and set up a tiny electric potential field around the neurons [5]. Differences of electrical potentials are caused by summed postsynaptic graded potentials from pyramidal cells that create electrical dipoles between the body of the neuron (soma) and neural branches (apical dendrites). Brain electrical current consists mainly of Na+, K+, Ca++, and Cl- ions that are pumped through channels in neuron membranes in the direction caused by membrane potential. EEG measures the electric potential of many pyramidal neurons in the cerebral cortex. Only large populations of active neurons can generate electrical activity recordable on the scalp. Weak electrical signals detected by the scalp electrodes are massively amplified, and then stored to computer memory or displayed on paper [4].

EEG was discovered by the German neurologist Hans Berger in 1924 as an electrical phenomenon inside people's brains. He stated that weak electric currents generated in the brain can be recorded without opening the skull, and depicted graphically on a strip of paper [4]. EEG has been found to be a very powerful tool in the field of neurology and clinical neurophysiology due to the capability to reflect both the normal and abnormal electrical activity in the brain. In order to analyze an electroencephalogram, the descript-

tion of some elements such as frequency, amplitude, phase and wave shape are required. For the clinical study of EEG, frequency analysis is one of the most important methodologies [6]. Especially the bandwidth between 0.5 and 30 hertz contributed to the diagnosis of brain functions in the clinical field [7]. Berger also observed that the EEG, which displays the brain's electrical activity, changes in a consistent and recognizable way when the general status of the subject changes [4]. For example, from a state of relaxation to a state of alertness, or from a state of wakefulness to a state of sleep. Figure 1.1 shows the change in the EEG when going from a state of wakefulness (upper 2 waves) to a state of deep sleep (lower 2 waves).

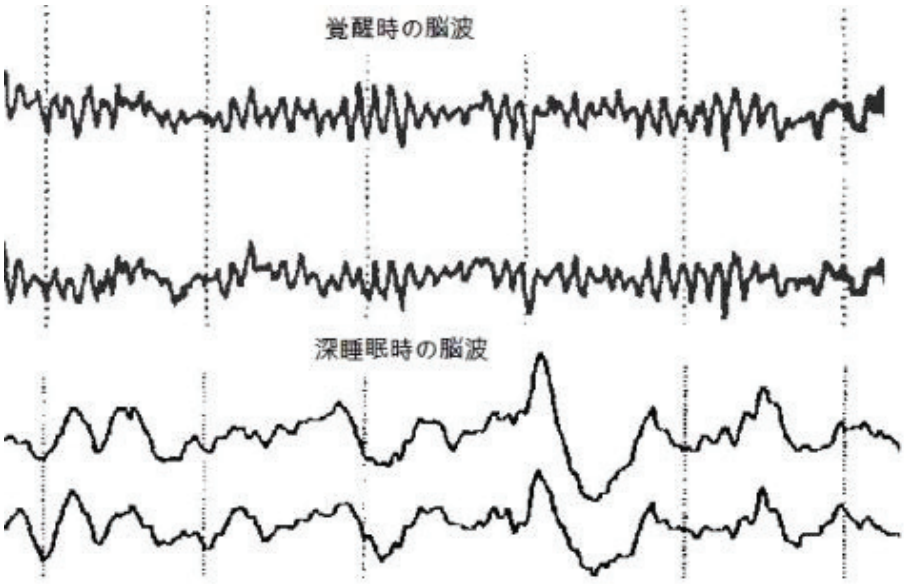

Figure 1.1: A change in the EEG due to sleep [7]. The above 2 waves represent a state of wakefulness; the lower 2 waves represent a state of deep sleep.

An EEG produces waveforms represented by a spectrum of frequencies. Routine interpretation of EEG involves bandwidths of frequencies that lie between 1 and 30 hertz [8]. Depending on the bandwidth (frequency range), the frequency has special characteristics, and a particular name is given. The four main frequency bandwidths used for analysis are the delta (δ) bandwidth, the theta (θ) bandwidth, the alpha (α) bandwidth, and the beta (β) bandwidth [6,8,9,10]. Each of these bandwidths has a specific frequency range. An overview of the frequency ranges of each bandwidth is shown in Table 1.1. Figure 1.2 shows the waveforms of the 4 major bandwidths. In addition to these 4 major bandwidths, there is also the gamma (γ) bandwidth, which has a frequency range of more than 30 hertz.

Table 1.1: The main frequency bandwidths in EEG [6,8,9,10].

Type of wave	Bandwidth name	frequency range
Slow wave	δ bandwidth	0.5–3.9 Hz
	θ bandwidth（medium slow wave）	4–7.9 Hz
	α bandwidth	8–13.9 Hz
Fast wave	β bandwidth (medium fast wave)	14–17.9 Hz
	β bandwidth	18–29.9 Hz
	γ bandwidth	30 Hz or higher

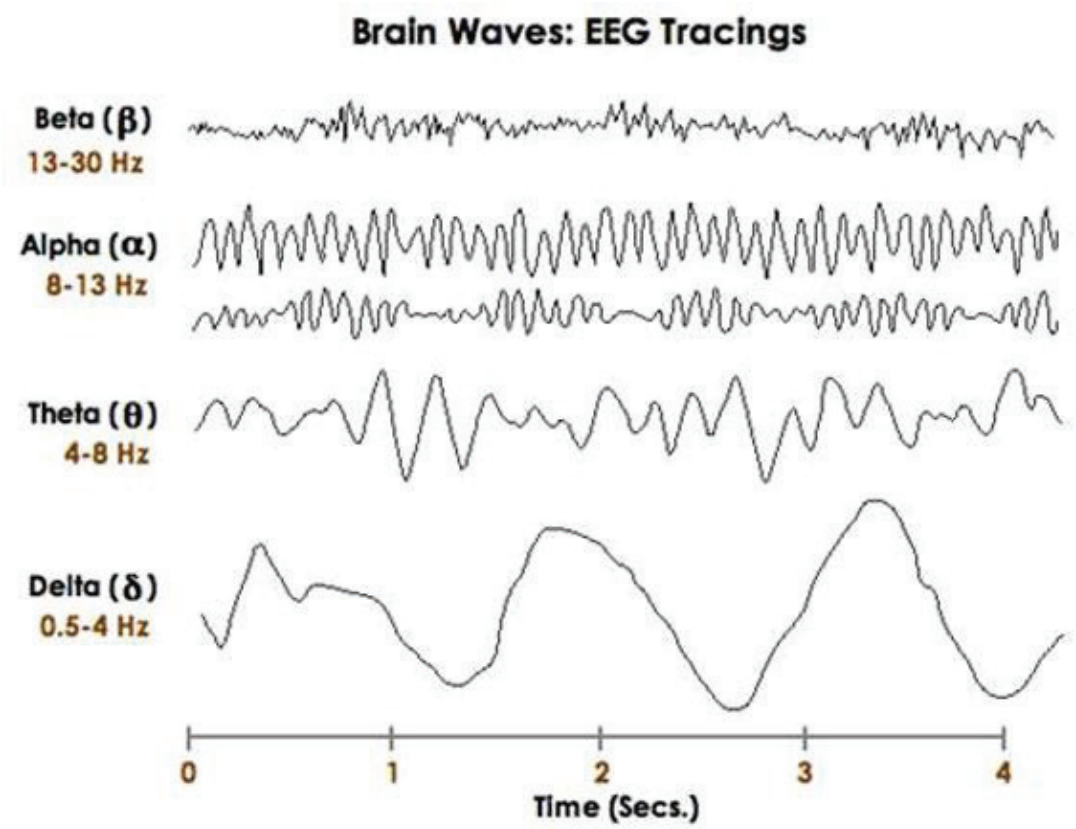

Figure 1.2: The δ bandwidth, θ bandwidth, α bandwidth, and β bandwidth in EEG [11].

1.2 The alpha rhythm

Alpha wave activity (also called the alpha rhythm) is the starting point to assess the background activity when interpreting an EEG. The alpha rhythm can for example be used as a criterion to decide whether or not an EEG is fast or slow [10]. As mentioned above, alpha waves have a frequency ranging from 8 to 13.9 hertz. The amplitude is mostly below 50 μV in adults [8,9,10]. The morphology of alpha waves on an EEG can be seen in figure 1.3 on the previous page. The normal alpha rhythm appears only in the electrodes that record the posterior regions of the brain, with the highest voltages in the occipital area. Alpha waves can be observed best during a state of relaxed wakefulness and often during periods of relative mental and physical inactivity [6,8]. There are cases where alpha wave activity has been evaluated in relation to cognitive and mental function [12]. One of the characteristics of the alpha rhythm is reactivity. The alpha rhythm usually only appears on an EEG after eye closure, and a decrease of the rhythm occurs as a response to eye opening [6,8]. Immediately after eye closure, the alpha frequency may be increased for a moment. This phenomenon is called the “alpha squeak effect” [6,8].

Because EEG changes according to the functional status of the brain, the scalp EEG is an important clinical tool for detecting and treating certain illnesses. Brain tumors, epilepsies, strokes, drug overdose, and severe head injury are some of the medical conditions that may appear in the spontaneous EEG [13]. These EEGs are considered to be abnormal. In addition, several mental illnesses may also be detected using EEG. In some elderly people, and in some individuals who suffer from mental disorders, the alpha rhythm can be observed in all, or almost all recording electrodes of the scalp. This phenomenon is called the “diffuse alpha pattern” and is considered to be an abnormal EEG [9]. In contrast to for example epileptiform discharges, the waves itself appearing on the EEG are not abnormal, but the observed pattern of the waves on the EEG is considered abnormal. It is known that the diffuse alpha pattern is visible in people with a small brain disorder and low brain function [9]. There have also been cases where the diffuse alpha wave pattern is observed in individuals in a comatose state (“alpha coma”) [14].

1.3 Neuropsychiatric disorders

This section gives a short description of some common neuropsychiatric disorders.

1.3.1 Depression

Depression is one of the most serious examples of a mood disorder. The concept mood refers to the internal emotional state of an individual. Mood disorders are a group of clinical conditions characterized by a disturbance of mood and a subjective experience of great distress [15]. A depressed mood shows loss of energy, interest and appetite, guilt feelings, and thoughts of death and suicide. Patients who are afflicted with major depressive episodes are said to have unipolar depression [15]. Unipolar depression is among the most common psychiatric disorders of adults. Mania is another example of a mood disorder, and sometimes depression occurs alternately with mania. Patients suffering from alternating depressive and manic episodes are said to have bipolar disorder [15].

1.3.2 Dementia

Dementia is a syndrome that consists of a decline in cognitive and intellectual abilities occurring in an awake and alert patient, which is severe enough to interfere significantly with work, social activities and relations with others [6]. Examples of disturbances in brain function are abstract thinking, memory, judgment, personality change, and so on. Dementia can be divided into cortical and subcortical dementia. Examples of cortical dementia are Alzheimer's Disease, Pick's disease, and Creutzfeldt–Jakob Disease. Huntington's disease is an example of subcortical dementia, and sometimes subcortical dementia occurs in Parkinson's disease [6].

1.3.3 Schizophrenia

Schizophrenia includes a variety of disorders that present somewhat similar behavioral symptoms. It comprises a group of disorders with heterogeneous etiologies, and it includes patients whose clinical presentations, treatment responses, and courses of illness are varied [15]. Bleuler named the disorder "schizophrenia", which means "split mindedness". Schizophrenia should not be confused with the disorder called "split personality" (recently called "multiple personality disorder"), which is a completely different mental disease [15]. Schizophrenia is characterized by a theoretical division between thought, emotion, and behavior. There is no laboratory test for Schizophrenia; the diagnosis of schizophrenia is based on psychiatric history and mental status examination. Some of the symptoms of Schizophrenia include delusions, catatonic behavior, hallucinations, and marked social withdrawal [15].

1.4 Epilepsy

Epilepsy is one of the most common neurological disorders, affecting 1% of the world's population (about 50 million people), and is characterized by epileptic seizures originating from excessive paroxysmal synchronous neuronal firing [16,17]. A clear definition of epilepsy, as well as criteria for the diagnosis of epilepsy were proposed by the International League Against Epilepsy (ILAE) in 2005: "Epilepsy is a persistent condition that causes epilepsy attacks and the resulting neurological organisms. It is a brain disorder characterized by physiologic, cognitive, psychological, and social consequences that requires at least one epileptic seizure to develop to be defined as epilepsy. It is the manifestation of transient features and symptoms caused by abnormally excessive or synchronous neuronal activity." [18]. A seizure lasting more than 30 minutes or several seizure episodes without regaining consciousness is called the 'status epilepticus'.

Epilepsy is categorized into two different types: primary generalized epilepsy and focal epilepsy [19]. In the same way, two main seizure types can be distinguished: primary generalized seizures and focal seizures. Generalized epilepsy is characterized by seizures involving the entire brain or large portions of the brain at the onset of the seizure. In focal epilepsy the seizures originate from a certain region in the brain (=epileptic focus) and may or may not spread over the brain during the seizure. The epileptic focus of the seizure might determine what symptoms occur, and could therefore be important to understand the cause of the disease and for therapy [19].

The pathogenesis of epilepsy is as of today still not fully understood. In as much as 70 % of people diagnosed with epilepsy, no specific cause can be determined [20]. Known causes include birth or head trauma, genetic inheritance, alcohol and drug abuse, and certain neurological and neuropsychiatric diseases.

To this day, there is still no complete cure for epilepsy, however epileptic seizures can be effectively controlled by medicines called Anti-Epileptic Drugs (AEDs) [20]. In addition, a ketogenic diet, and surgical removal of a small part of the brain that is causing the seizures could result in decrease or eliminate seizure occurrence. Because epilepsy is highly dynamic, techniques with the highest temporal resolution such as EEG are necessary for diagnosis. In recent years, research has reported that mild cognitive tasks such as an easy arithmetic question can suppress epileptic activity (afterdischarges) in the brain [21]. The latter study concluded that cognitive effort is a useful tactic to modify epileptic activity in the brain. The results of this study could possible lead to a better future treatment of epilepsy.

1.5 Objective and thesis outline

In this thesis, engineering theory and engineering methodology were applied to the medical field of clinical neurophysiology. The main purpose of this research is to explore the functional connectivity and changes in functional activity in the brain derived from EEG data, and to use wavelet-crosscorrelation analysis and network analysis based on graph theory in order to make the pathology clear in the diseased brain. Connectivity patterns, information transfer in the brain, and changes in brain activity were examined in healthy individuals, mental disorder patients and epilepsy patients. After constructing functional networks, the network spatial distribution was analyzed based on graph theory to further characterize the connectivity in the healthy brain and in the diseased brain. All analyses in this thesis were in the alpha bandwidth. One of the central questions is whether time series analysis in combination with network theory analysis can reveal how communication fails in neuropsychiatric and neurological disorders.

This thesis has two main studies, both of which are important for assessing the functional connectivity in the brain of patients suffering from mental diseases (chapter II) and individuals suffering from epilepsy (chapter III). These two studies are outlined individually in the following two chapters.

In Chapter II, the first goal of this thesis was to investigate and compare the functional connectivity in the brain between healthy individuals and individuals suffering from mental disorders. In some individuals, alpha waves appear in many regions of the brain, and this is considered abnormal electroencephalography (EEG). This phenomenon is known as diffuse alpha pattern. This study aims to extract and compare the features of the connectivity between the parts of the brain. The EEGs of healthy individuals and mental disorder patients (5 epochs per subject) with the diffuse alpha pattern were analyzed using wavelet–crosscorrelation analysis.

In Chapter III, not only the functional connectivity, but also the connection configuration (the topology) of the brain network was analyzed based on graph theory. In contrast to chapter II, this chapter focuses on individuals suffering from epilepsy, a disorder where proper diagnosis requires the highest possible temporal resolution. EEG is therefore used to aid in the diagnosis of epilepsy. Before performing graph theoretical analysis, five epochs per healthy subject, and ten epochs (during epileptiform discharge and non-discharge) per epilepsy patient were selected and analyzed using wavelet–crosscorrelation analysis. The measures calculated using graph theoretical analysis were the clustering coefficient, characteristic path length, small-worldness, and nodal betweenness centrality.

Chapter IV, the final chapter, provides a global summary of the two separate studies, and an overall conclusion.

Chapter Ⅱ

Comparing the Features of the Diffuse Alpha Pattern with the Normal Alpha Pattern using Wavelet-crosscorrelation Analysis

2.1 Introduction

Many studies have shown that neurophysiological and neuroimaging techniques could to be useful for the assessment of clinical pathologies. It has been shown that Electroencephalography (EEG) may aid in the diagnosis of neuropsychiatric diseases. Abnormalities in EEG have indeed been observed in individuals with mental disorders [22]. Previous research has reported that quantitative frequency analysis of EEG data is useful as a supplement to diagnosis for adult psychiatric diseases [3]. Other studies have suggested that quantitative EEG analysis could be used as a biomarker in disorders such as Parkinson's disease [23].

Among frequency analysis, alpha waves are a popular research topic. Normally, alpha waves have a frequency ranging from 8 to 13.9 Hz, and can be seen the most clearly in healthy individuals in the occipital region of the brain during the closing of the eyes [6,8]. Berger made the unexpected observation that when subjects opened their eyes, the EEG oscillations in the alpha band decreased in amplitude or disappeared completely (the "Berger effect") [24]. Alpha waves play an important role in cognitive processing. It has been found that alpha peak frequency in posterior regions increases with increasing cognitive demands [25]. Alpha wave activity with high amplitude has been observed in patients with Alzheimer's disease [26]. This implies that it may be possible that an abnormality in the appearance of alpha waves in the EEG could be an indication of an abnormal EEG. Another study has found that a disruption of electrical oscillations at rest is linearly correlated with neurological deficits. Alpha synchrony is suggested to be a specific biomarker of neurological function in patients with brain lesions [27]. An increased variability of anterior EEG in the alpha band was found to be possibly a characteristic feature for depression, and this could suggest that anterior EEG alpha asymmetry is a trait marker for depression [28]. All of these studies indicate that conducting research on alpha waves is important and useful.

There are cases where alpha waves do not only appear in the occipital region, but also continuously in all regions of the brain. This phenomenon, where alpha waves appear in all or nearly all electrodes, is called the "diffuse alpha pattern", and is regarded as a type of abnormal EEG [9]. The diffuse alpha pattern has been observed in the EEG of individuals during states of unconsciousness [29], as well as in some individuals suffering from mental disorders.

Research has been carried out that extracts and quantifies the features of the alpha activity and the connectivity between different parts of the brain. It was suggested that mild cognitive impairment patients have a higher degree of functional connectivity between hemispheres and in hemispheres during working memory task [30]. The alpha bandwidth may be the characteristic bandwidth in distinguishing mild cognitive impairment patients from healthy individuals during working memory tasks [31].

In the present study, the objective was to investigate the connectivity in the brain of individuals who have the normal alpha pattern, as well as individuals who have the diffuse alpha pattern. The alpha activity was evaluated, and, by using a method called Wavelet–crosscorrelation analysis, it was abstracted how the connectivity in the alpha band between the parts of the brain is different between individuals with the normal alpha pattern and individuals with the diffuse alpha pattern.

In addition, the following question was asked: To what extent does the brain work differently in individuals where the diffuse alpha pattern can be observed in the EEG, as compared to individuals whose EEG show the normal alpha pattern? For this reason, Wavelet–crosscorrelation analysis was used to visualize the correlation pattern in the brain, and compare the connectivity between the brain of normal alpha pattern individuals and diffuse alpha pattern individuals. It can be hypothesized that the connectivity strength between the parts in the brain might differ between these two groups of subjects.

The novelty of this study is abstracting the alpha band to visualize and investigate the correlation pattern and connectivity strength in the brain. This study is mainly based on the use of Wavelet–crosscorrelation analysis, however in addition, a different correlation measure, Phase Locking Value, will also be conducted.

2.2 Methods

2.2.1 Subjects and selection of the EEG data

The EEG data used in this research was measured and collected in the Matsumoto Clinic and the University of Hyogo. EEG data was obtained by scalp recordings from 10 healthy subjects (5 males and 5 females; mean age: 24.40 ± 2.46 years), and 10 individuals suffering from various neuropsychiatric disorders (5 males and 5 females; mean age: 54.80 ± 10.43 years). The EEG of the healthy individuals was recorded at the University of Hyogo, and the EEG of the patients was recorded at the Matsumoto Clinic. The healthy individuals were adults whose EEG showed no abnormalities. Alpha activity could be observed in the occipital area. The subjects with neuropsychiatric disorders were medicated with psychoactive drugs, and abnormalities could be observed in the EEG. The diffuse alpha pattern appeared prominently in all of the 10 patients. The objective of this study was to investigate and compare the connectivity in the brain of individuals who have the normal alpha pattern, and individuals who have the diffuse alpha pattern. For this reason, 10 healthy subjects whose EEGs did not show the diffuse alpha pattern, and 10 neuropsychiatric disorder patients whose EEG showed the diffuse alpha pattern were selected for this study. The healthy subjects' information can be seen in table 2.1, and the patients' information can be seen in table 2.2.

Table 2.1: Healthy subject profile (mean age: 24.40±2.46 years).

Subject number	Age [years]	Gender	Number of epochs
1	21	Female	5
2	27	Female	5
3	23	Male	5
4	24	Female	5
5	25	Male	5
6	22	Male	5
7	23	Female	5
8	30	Female	5
9	25	Male	5
10	24	Male	5

Table 2.2: Patient profile (mean age: 54.80±10.43 years).

Patient number	Age [years]	Gender	Disorder	Number of epochs
1	58	Female	Schizophrenia	5
2	40	Female	Low IQ/Depression	5
3	50	Male	Depression	5
4	55	Male	Neurosis	5
5	56	Female	Insomnia	5
6	70	Male	Dementia	5
7	54	Male	Depression	5
8	64	Female	Schizophrenia	5
9	66	Male	Hypochondria	5
10	35	Female	Neurosis/ Depression	5

The EEG of all subjects was measured during a state of relaxation while the eyes were closed, and there was no sound at the time of recording. The recording of scalp voltage fields was obtained by means of multiple electrodes placed in standardized positions relative to head landmarks. In this research, scalp electrodes were placed according to the International 10–20 electrode positions system. The system was adopted in 1958 and standardized physical placement and designations of electrodes on the scalp. The head is divided into proportional distances from prominent skull landmarks (nasion, inion, preauricular points) to provide appropriate coverage of all regions of the brain. The label 10–20 indicates the proportional distance in percentage between ears and nose where

points for electrodes are chosen [4]. A total of 19 electrode channels were used for recording. The placement of the electrodes according to the International 10–20 electrode positions can be seen in figure 2.1.

Electrode placements are labeled according to adjacent brain regions: Fp (frontal pole), F (frontal), C (central), T (temporal), and O (occipital). The letters are accompanied by odd numbers on the left side of the head and with even numbers on the right side (see figure 2.1).

The 19 electrode channels were:

Fp1 and Fp2 (frontal pole),
F3 and F4 (frontal),
C3 and C4 (central),
P3 and P4 (parietal),
O1 and O2 (occipital),
F7 and F8 (anterior temporal),
T3 and T4 (temporal),
T5 and T6 (posterior temporal),
Fz, Cz, and Pz (the z–line).

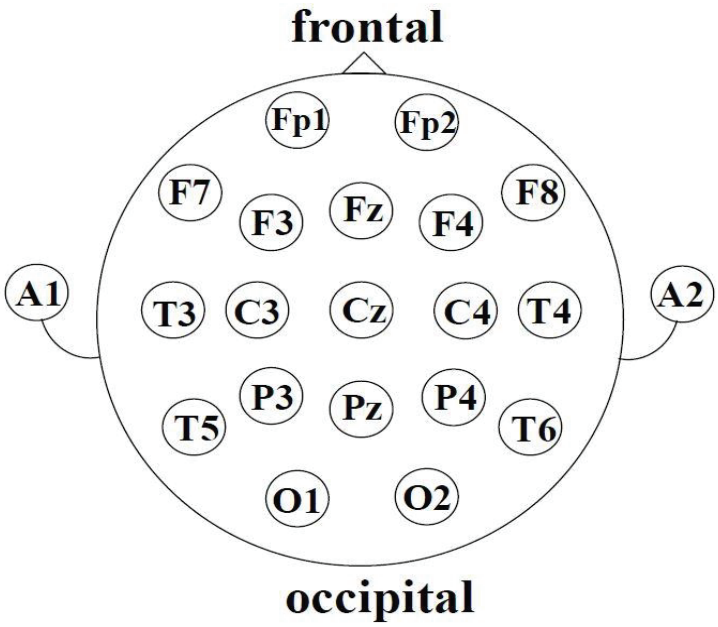

Figure 2.1: Electrode placement according to the International electrode positions system. [32]

The 19 electrodes read the signal from the head surface; amplifiers bring the microvolt signals into the range where they can be digitalized accurately; a converter changes signals from analog to digital form; and a personal computer stores and displays the obtained data [9].

An electroencephalogram is an analog signal, therefore in cases where quantitative analysis is applied, the EEG signals must be digitized so that they can be processed by a digital computer. The EEG signal must be processed in such a way that the random variable (the potential as a function of time) will have only 1 set of discrete values at a set of discrete time instances [6]. In order to do this analog–to–digital (AD) conversion, a method called 'sampling' was used. Sampling is the process of obtaining a sequence of instantaneous values of a wave at regular or intermittent time intervals [6]. In general, an EEG signal is sampled at equal time intervals (Δt), thus transforming the continuous signal into a set of data with different values separated by intervals Δt. The sampling frequency f_s can be defined as the number of times that was sampled in a certain time period [33]. The choice of the sampling frequency is based on the 'sampling theorem'. The sampling theorem theoretically shows how large the sampling frequency must be to be able to accurately express the nature of the original analog waveform [34]. The theorem states that no information about the original continuous time signal is lost when the sampling frequency f_s is equal to or greater than twice the highest frequency component of the signal. The highest frequency component of the signal is called the Nyquist frequency (f_m) [35]. The relation between f_s and f_m is shown in equation 2.1.

$$f_s \geq 2f_m \tag{2.1}$$

In this study, time segments (epochs) of 2 seconds long were analyzed for each subject, and the number of sampling points in one epoch was 1000, therefore the sampling frequency was 500 Hz. A bandpass filter was set between 0.5 Hz and 30.0 Hz.
All subjects provided informed consent, and the study protocol was approved by the Ethics Committee of the Graduate School of Applied Informatics, University of Hyogo.

2.2.2 Analysis methods

In order to abstract the measured EEG data, the software Vital Tracer (developed by Kissei Comtec Company) was used. This software allows to visualize and analyze EEG data, as well as to abstract the EEG data to numerical data. A method called Wavelet–crosscorrelation analysis (see section 2.2.2.5) was used to analyze non-stationary EEG data, and to obtain both wavelet power spectra and Wavelet Crosscorrelation Coefficients (WCC values). WCC values are a measure of functional connectivity between distant brain regions. In other words, Wavelet–crosscorrelation analysis makes it possible to obtain the correlations between time series from different brain areas. In this study, the WCC values were calculated in the entire alpha bandwidth (8–13.9 Hz). The programming language Matlab R2017b (developed by Mathworks) was used in order to

calculate the WCC values from the abstracted numerical EEG data. In addition, the functional connectivity patterns were visualized in brain graphs. In order to statistically compare the obtained WCC values between individuals with the normal alpha pattern and individuals with the diffuse alpha pattern, the software IBM SPSS Statistics 24 was used (see section 2.2.5).

Analyzing low values does not provide a high reliability, therefore low amplitudes were excluded from our analysis.

Various analysis methods such as the Fourier Transform, Wavelet Transform, Crosscorrelation analysis, Correlation analysis, and Wavelet-crosscorrelation analysis are explained below.

2.2.2.1 Fourier Transform

Frequency analysis is a method that can quantify the extent of the frequency components of an EEG. Performing a frequency analysis makes it possible to investigate the size of each frequency. It is for example possible to investigate at which frequency the waveform with the highest amplitude occurs during task concentration, or during sleep. A Fourier Transform (FT) is one of the methods that can be used to analyze the frequency components of a waveform, and therefore obtain a power spectrum. Calculating a power spectrum is a common method of EEG quantification [36]. A power spectrum is a function of the frequency (in Hz), and it gives the distribution of the squared amplitude of different frequency components [6].

An FT does not provide information about the time domain of the signal. Performing an FT is sufficient for signals in which the parameters remain constant over time (=stationary signals). However, if a signal contains frequency components that emerge and vanish within certain time intervals, both time and frequency localization are required [37]. Such signals, where the parameters change over time, are called non–stationary signals. Sometimes it is necessary to investigate how the frequency changes at each point in time (time–frequency analysis). The FT only indicates that a particular frequency component is present in the analysis window, but does not give its temporal position in that window. Many biological signals, including waveforms, often do not conform to the stationary state. In general, EEG signals can only be considered stationary during relatively short time periods (epochs) [6]. Therefore, non–stationary analysis is required. A wavelet transform is one example of a method to analyze non–stationary signals. This method makes it possible to decompose signals that contain a number of frequencies and that have rapidly changing components [38].

2.2.2.2 Wavelet Transform

In order to compensate for the lack of time information of the Fourier Transform, a method called wavelet transform was used in this study to obtain 2–second wavelet power spectra in the alpha band in five epochs for each electrode. The wavelet spectra were compared between the healthy subjects and patients. Using this method, it becomes possible to conduct spectrum analysis in a broad frequency range without losing time information [37]. To do time–frequency analysis, it is necessary to choose an appropriate time window. The Wavelet Transform of a signal can be calculated by projecting the signal onto a basic wavelet. This tiny wave is called the mother wavelet (*g(t)*), and is very important in wavelet analysis. Any function can be used as the mother wavelet if it satisfies the condition for acceptance. The condition for acceptance C_g is shown in equation 2.2, where ω represents the frequency. For a certain function to be able to become the mother wave, the function must be able to vibrate, and must have a fast decline towards zero. Furthermore, the integral of the wavelet must be equal to zero [39].

$$C_g = \int_{-\infty}^{\infty} \frac{|\hat{g}(\omega)|^2}{|\omega|} d\omega < \infty \tag{2.2}$$

In this dissertation, a Gaussian wavelet (Gabor function) was used as the mother wavelet (equation 2.3), where the constant Ω is given by 2π [39,40]. It was chosen because it is suitable for time–frequency analysis, and because the non–orthogonal wavelets can offer numerically–stable reconstruction if the scale factor is close to 1 and the shift constant is close to 0 [41]. The Gaussian wavelet has one of the lowest values for the time-frequency resolution product. In other words, it has one of the least spreads in in the time domain for a given spread in the frequency domain [37,38].

$$g(t) = e^{-\frac{t^2}{2}}(e^{j\Omega t} - e^{-\frac{\Omega^2}{2}}) \tag{2.3}$$

The length of the Gaussian mother wavelet varies according to the frequency, and was therefore set to m. The mother wavelet was employed for the 2-second EEG epoch from $-m$ to $1000+m$ (figure 2.2). The mother wavelet shifts every two milliseconds along the 2-second epoch. The area outside of the epoch was considered zero. Due to convolution of the mother wavelet with the EEG epoch, the edge effect occurs, therefore data outside of 2000-*m* milliseconds was excluded from our next analysis (Wavelet–crosscorrelation analysis). In addition, not all data within the 2000-*m* milliseconds was adopted in the next analysis. Because analyzing low values does not provide high reliability, we set a threshold value for wavelet spectral values. Wavelet spectral values below 10 percent

compared to the maximum value of the wavelet power spectrum were also excluded from the next analysis.

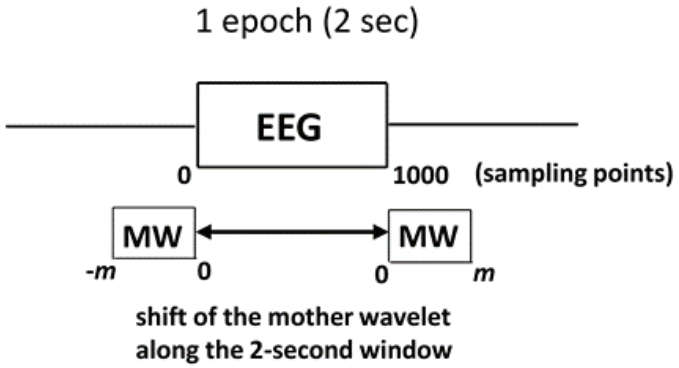

Figure 2.2: Projection of a Gabor mother wavelet. The mother wavelet (MW) shifts every two milliseconds along the two-second epoch from –*m* to 1000+*m*; *m*= the length of the mother wavelet. [42]

By making the mother wavelet expandable and contractable, the time information is saved when conducting frequency analysis [39]. The wavelet transform $W_x\ (a,b)$ of a signal $x(t)$ is calculated in equation 2.4 [38], where a is the scaling parameter which changes the flexibility of the mother wavelet; b is the parameter that shifts the mother wavelet, and t represents the time. By shifting these parameters on the original signal $x(t)$, time–frequency analysis becomes possible.

$$W_x(a,b) = \int_{-\infty}^{\infty} \overline{\frac{1}{\sqrt{|a|}} g\left(\frac{t-b}{a}\right)} x(t)\, dt \qquad (2.4)$$

The transformed coefficients a and b are mapped on a two–dimensional plane. This is called a scalogram or a wavelet power spectrum. The absolute value ABS used on the scalogram is shown in equation 2.5, where R^2 is the real part, and I^2 is the imaginary part of the formula.

$$ABS = \sqrt{R^2 + I^2} \qquad (2.5)$$

If a reverse Wavelet Transform is used, the original signal $x(t)$ can be recovered. The reverse wavelet transform is calculated in equation 2.6. C_g shows the condition for which the formula becomes valid.

$$x(t) = \frac{1}{C_g} \iint_{\mathrm{R}^2} W_x(a,b) \frac{1}{\sqrt{|a|}} g\left(\frac{t-b}{a}\right) \frac{dadb}{a^2} \qquad (2.6)$$

However, because of the uncertainty principle of Heisenberg, there is a restriction to the time and frequency resolution of a wavelet transform [34]. The Wavelet Transform uses short windows at high frequencies and long windows at low frequencies, which results in the time resolution being good at high frequencies and frequency resolution being good at low frequencies [38]. In order to compensate for this demerit, it is for example possible to perform an FT at a very short time interval to analyze the frequency components of the waveform. An FT has the same time resolution and frequency resolution everywhere [36].

In the Wavelet Transform, there is a relation between the uncertainty of time and the uncertainty of frequency. This relation is shown in equation 2.7 [39], where Δt is the time resolution, and Δf is the frequency resolution. If the time resolution is increased, the frequency resolution will decrease. Vice versa, if the frequency resolution is increased, the time resolution will decrease. This trade–off between frequency and time resolution is called the uncertainty principle of Heisenberg [39].

$$\Delta t \times \Delta f \geq \frac{1}{2} \tag{2.7}$$

As is displayed in equation 2.8, the frequency resolution Δf is the smallest frequency unit that can be measured in an EEG. T represents the measuring time. In EEG analysis, overlapping of data must be avoided. Data that have a lower frequency than this frequency resolution are too close to the frequency values of other data, and will cause the data to be considered the same. Therefore, data with lower frequencies than the frequency resolution need to be left out by means of a low–pass filter [6].

$$\Delta f = \frac{1}{T} \tag{2.8}$$

The time resolution Δt is displayed in equation 2.9 by means of the Nyquist frequency f_m and the sampling frequency f_s. The time resolution is the smallest time interval that can be measured in an EEG. Even if data is measured with a shorter time interval than the time resolution, the data will overlap and has no meaning.

$$\Delta t = \frac{fs}{fm} \tag{2.9}$$

As mentioned above, an FT has the same time resolution and frequency resolution everywhere, but a wavelet transform has a trade–off between time and frequency resolution. In other words, for a wavelet transform, both a high time resolution and a high frequency resolution at the same time is not possible.

2.2.2.3 Crosscorrelation analysis

Crosscorrelation analysis enables the degree of waveform similarity between 2 different time–series to be determined [37]. It provides a quantitative measure of the relatedness of 2 signals, usually from different electrodes. It can also reveal common components that occur at the same moment in time, or at a constant delay [38]. The Crosscorrelation function of 2 time–series is expressed by equation 2.10, where *x(t)* and *y(t)* are the values of the 2 signals *x* and *y*, and τ is the time–lag of *x(t)* with respect to *y(t)* [38,40]. In this case, *x(t)* is the signal to be evaluated, and *y(t)* is the reference for the Crosscorrelation.

$$C_{\mathrm{xy}}(\tau) = \lim_{T\to\infty} \frac{1}{2T} \int_{-T}^{T} x(t)y(t+\tau)dt \qquad (2.10)$$

By conducting Crosscorrelation analysis between scalp electrodes, it is possible to abstract the functional connectivity, as well as the propagation speed and the propagation direction of the EEG signals inside the brain. However, Crosscorrelation analysis is not appropriate for non–stationary signals [38].

2.2.2.4 Correlation analysis

Correlation analysis is a method that displays how much the nature and shape of 2 signals resemble at different frequencies. The correlation values range from 0 to 1, with 0 being the minimum value and 1 the maximum value. The closer the correlation value is to 1, the more the 2 signals are the same in terms of shape and nature. The closer the value is to 0, the more the 2 signals are different in terms of shape and nature [43]. Performing Correlation analysis is useful in order to know the functional connectivity between the electrodes of the brain [43]. The correlation values can be derived from the power spectrum density function of a signal, and from the cross–spectrum density function between 2 signals. The power spectrum density function $S_{x,x}(f)$ of the signal *x(t)* is derived in equation 2.11.

$$S_{x,x}(f) = \int_{-\infty}^{\infty} R_{xx}(\tau)e^{-j2\pi f\tau}d\tau \qquad (2.11)$$

The cross-spectrum density function $S_{x,y}(f)$ between the signals *x(t)* and *y(t)* is derived in equation 2.12.

$$S_{x,y}(f) = \int_{-\infty}^{\infty} R_{xy}(\tau)e^{-j2\pi f\tau}d\tau \qquad (2.12)$$

When making *G(f)* the one–way spectrum and *S(f)* the two–way spectrum, $f > 0$ and the actual spectrum becomes equation 2.13.

$$G(f) = 2S(f) = 2\int_{-\infty}^{\infty} R(\tau)e^{-j2\pi f\tau}d\tau \tag{2.13}$$

The correlation values are represented as $\gamma^2_{x,y}(f)$ and are derived in equation 2.14.

$$\gamma^2{}_{x,y}(f) = \frac{\left|G_{xy}(f)\right|^2}{G_{xx}(f)G_{yy}(f)}, \quad 0 \le \gamma^2_{xy}(f) \le 1 \tag{2.14}$$

2.2.2.5 Wavelet–crosscorrelation analysis

We used Wavelet–crosscorrelation analysis in order to calculate Wavelet–crosscorrelation Coefficients (=WCC) between all 19 electrodes. It is a method that, while maintaining time information, makes it possible to investigate and visualize the correlation of signals (neuronal activity) between distant brain areas at various frequencies [38]. It therefore becomes possible to know how strong the functional connectivity is between the different areas in the brain for a wide range of frequencies. Calculating the time lag (TL) between two signals, and thus obtaining information about the propagation of neuronal activity in the brain is also possible [44]. It is a combination of the above mentioned methods Wavelet Transform and Crosscorrelation analysis. Like Correlation analysis, it displays how much the nature and shape of two signals resemble each other at different frequencies. WCC values therefore range from 0 to 1. The closer the WCC value is to 1, the more the two signals are similar in terms of shape and nature; the closer the value is to 0, the more different the two signals. As opposed to crosscorrelation analysis, Wavelet–crosscorrelation analysis is a powerful tool to analyze non–stationary data, for example signals that have rapidly changing components and transient changes, such as EEGs that have sudden interictal epileptiform discharges [38,44]. The wavelet–crosscorrelation function $WC_{x,y}(a,\tau)$ is defined as [38]

$$WC_{x,y}(a,\tau) = \lim_{T\to\infty}\frac{1}{2T}\int_{-T}^{T}\overline{W_x(b,a)}W_y(b+\tau,a)\,db\,, \tag{2.15}$$

where *T* represents the period, *a* the scaling parameter, *b* the parameter that shifts the mother wavelet, and τ the time-lag in the wavelet space. $WC_{x,y}(a,\tau)$ is complex-valued and consists of a real part $RWC_{x,y}(a,\tau)$ and an imaginary part $IWC_{x,y}(a,\tau)$.

$RWC_{x,y}(a,\tau)$ can be used to express the strength of the correlation between two signals x and y. $\overline{W_x(b,a)}$ represents the complex conjugate. The wavelet–crosscorrelation coefficient $WR_{xy}(a,\tau)$ from the real part of the wavelet–crosscorrelation function $RWC_{x,y}(a,\tau)$ is [38]

$$WR_{x,y}(a,\tau) = \frac{\left|RWC_{x,y}\ (a,\tau)\right|}{\sqrt{RWC_x(a,0)RWC_y(a,0)}}\ . \tag{2.16}$$

2.2.3 Data processing protocol

In this study, for each healthy individual and for each patient's measured EEG, five artifact-free epochs of 2 seconds were carefully selected for analysis by visual inspection (in total 50 epochs for all healthy subjects, and 50 epochs for all patients). All epochs were selected separate on the time course of the EEG (see figure 2.3). After abstracting the EEG data by means of Vital Tracer, the numerical data was run in an original Matlab program to obtain wavelet spectra and WCC values in the alpha band. The WCC values were analyzed for 27 frequency scales, with the lowest frequency at 8.06 Hz, and the highest at 13.89 Hz. The 27 frequency scales are shown in table 2.3. The objective of this study was to compare the functional connectivity between healthy subjects and mental disorder patients, therefore several epochs were selected repeatedly at random and epoch data were averaged in order to achieve statistically significant comparison.

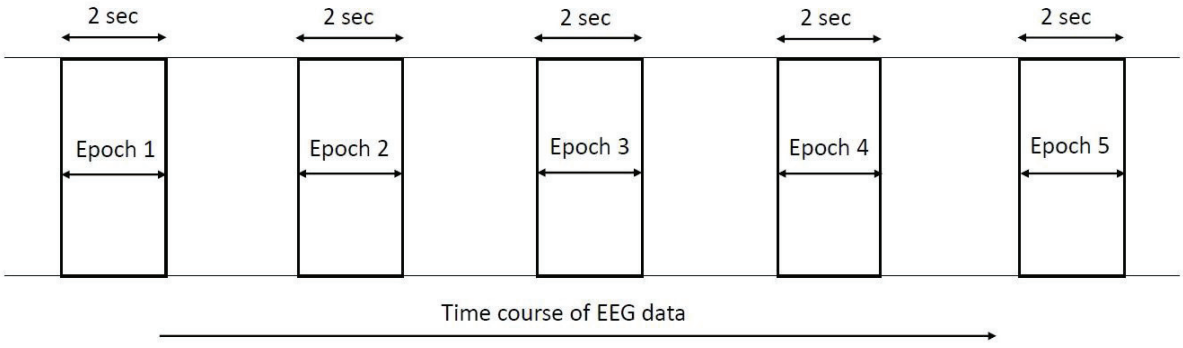

Figure 2.3: Selection of separate time segments (epochs) on the time course of the EEG data.

Table 2.3: Wavelet frequency scale numbers and frequency values of the alpha bandwidth. The frequency scales in the alpha bandwidth are shown in the red frame.

Scale Number	Scale Frequency	Scale Number	Scale Frequency	Scale Number	Scale Frequency	Scale Number	Scale Frequency
1	250	17	27.778	33	14.706	49	10
2	166.67	18	26.316	34	14.286	50	9.8039
3	125	19	25	35	13.889	51	9.6154
4	100	20	23.81	36	13.514	52	9.434
5	83.333	21	22.727	37	13.158	53	9.2593
6	71.429	22	21.739	38	12.821	54	9.0909
7	62.5	23	20.833	39	12.5	55	8.9286
8	55.556	24	20	40	12.195	56	8.7719
9	50	25	19.231	41	11.905	57	8.6207
10	45.455	26	18.519	42	11.628	58	8.4746
11	41.667	27	17.857	43	11.364	59	8.3333
12	38.462	28	17.241	44	11.111	60	8.1967
13	35.714	29	16.667	45	10.87	61	8.0645
14	33.333	30	16.129	46	10.638	62	7.9365
15	31.25	31	15.625	47	10.417	63	7.8125
16	29.412	32	15.152	48	10.204	64	7.6923

First, for each electrode for all epochs of all subjects, the frequency at which the highest wavelet spectral value occurs was calculated and statistically analyzed to compare between healthy individuals and individuals with the diffuse alpha pattern.

Next, the WCC values between all electrodes were averaged over all epochs and all healthy subjects/all patients, and visualized in a brain graph using an original program of the software Tcl/Tk. The brain graphs were then compared between the individuals with the normal alpha pattern and individuals with the diffuse alpha pattern. A threshold was set for the WCC values: any values below 0.3 were not included in the analysis because low values may not be meaningful. Each line in the brain graph corresponds to a WCC value (a functional connection) between an electrode channel. The 19 electrode channels correspond to circles in the brain graph. 19 channels means a maximum of 171 pair combinations are possible. A WCC threshold was set over all brain graphs to reveal the strongest correlation strengths in each graph. Choosing low threshold values would give rise to too many connections, resulting in difficult visual interpretation of each graph.

In addition, we compared WCC values between the normal alpha pattern subjects and diffuse alpha pattern subjects in specific orientations in the brain: the coronal and sagittal orientations. These were further divided into 2 sub-orientations: the medial coronal and lateral coronal orientations; and the medial sagittal and lateral sagittal orientations. All 4 sub-categories are shown in figure 2.4. WCC values were cut out in a specific orientation using an original program of Matlab R2016b. The WCC values of each orientation were then averaged over all epochs and all healthy subjects/all patients, visualized in brain graphs, and statistically compared between healthy subjects and patients. In order to reveal the strongest connections between the electrodes, the WCC values were given a different threshold in each orientation.

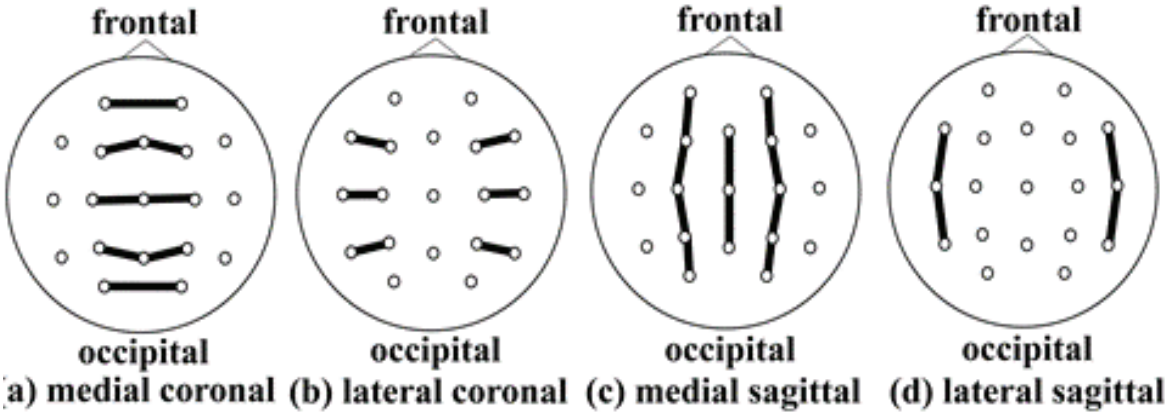

Figure 2.4: The coronal and sagittal orientations of the brain. These are further divided into the medial coronal (a), lateral coronal (b), medial sagittal (c), and lateral sagittal (d) orientations. [42]

The general overview of the data analysis and data processing protocol is shown in figure 2.5.

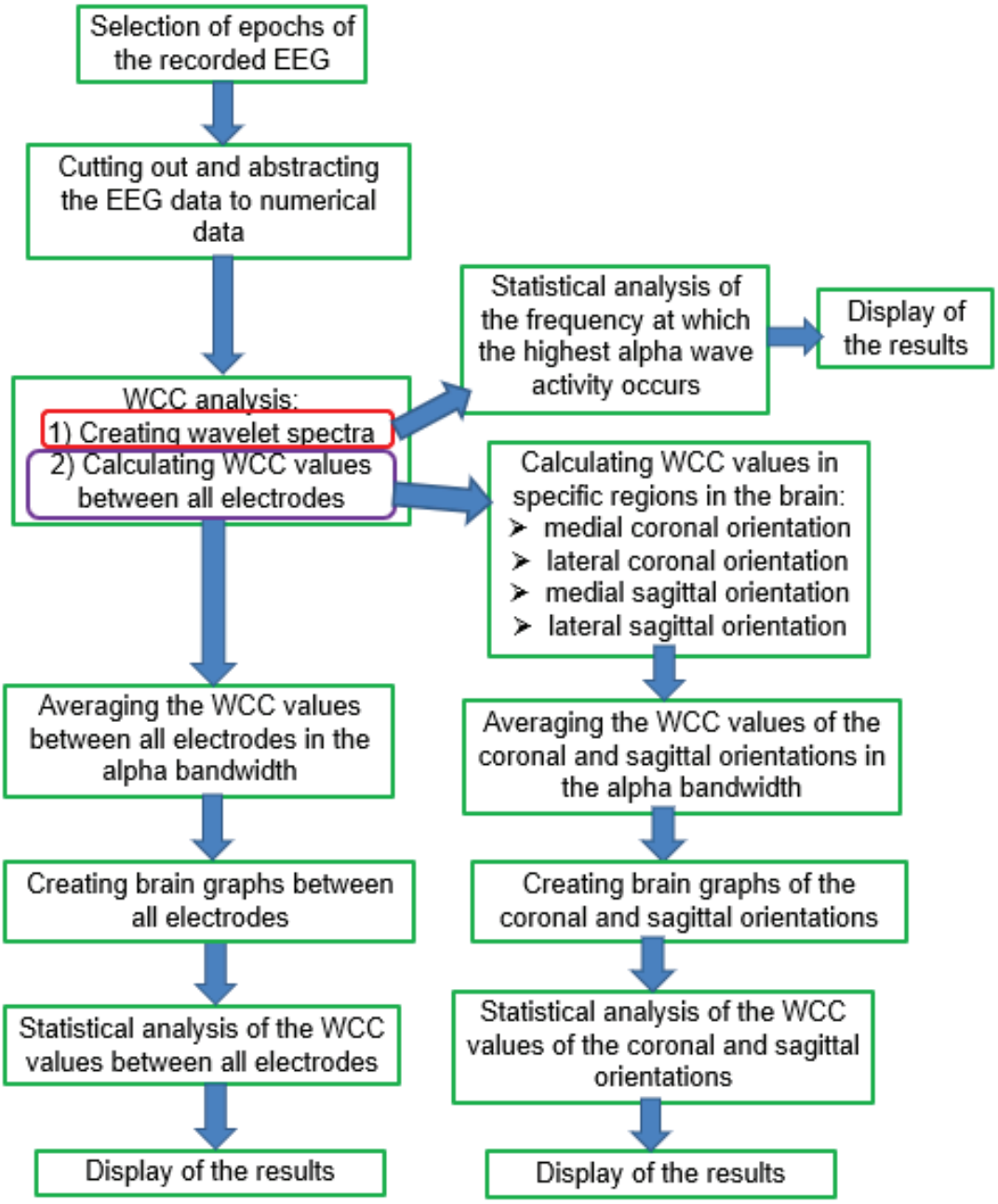

Figure 2.5: General overview of the data analyzing and data processing protocol.

2.2.4 Phase Locking Value

Phase Locking (PL) is a method that reveals to what extent the phase difference synchronizes between two signals. In other words, it quantifies the stability of the phase difference between the two signals in a predefined frequency range [45]. The merit of calculating the Phase Locking Value (PLV) is that it is a measure completely independent of the amplitude of signals, and therefore can be valuable to compare the obtained results of Phase Locking with Wavelet-crosscorrelation analysis. A PLV close to 1 shows that if time elapses, the phase difference between two signals doesn't change much (strong phase

synchrony). When the PLV value is close to 0, the phase difference between two signals changes considerably in function of time (weak phase synchrony). To calculate PLV, it is first necessary to calculate the phase of the signals from the coefficients of their wavelet transform at the chosen frequency. The phase difference between two signals *x* and *y* at frequency *f* and time *t* can be derived from the angles of their wavelet coefficients (equation 2.17) [45]:

$$\exp\left(\mathrm{j}\left(\varphi_y(f,t)-\varphi_x(f,t)\right)\right)=\frac{W_x(t,f)\overline{W_y(t,f)}}{\left|W_x(t,f)W_y(t,f)\right|} \tag{2.17}$$

where φ represents the phase.

The stability of the phase difference across the epochs is quantified by a Phase Locking Value (PLV) in equation 2.18 [45]:

$$\mathrm{PLV}(f,t)=\left|\frac{1}{N_{epoch}}\cdot\sum_{epoch=1}^{N_{epoch}}\exp\left(j(\varphi_{y,epoch}(f,t)-\varphi_{x,epoch}(f,t))\right)\right| \tag{2.18}$$

where *N* shows the number of epochs of one subject.

The PLV derived from each subject was computed in the alpha band and averaged using an original program of MATLAB 2016b. PLV was calculated and averaged over all epochs and all healthy subjects/patients. Because phase synchrony could be prominent in the medial areas in the brain, PLV was in addition calculated and averaged along the medial coronal and medial sagittal orientations. PLV is considered to reflect the functional connectivity between brain regions [45].

2.2.5 Statistical analysis

All statistical analyses in this study were performed using SPSS Statistics 24. Statistical tests can be applied to confirm whether or not the obtained differences between the results are valid and reliable or not. Parametric tests are tests where the data have a normal distribution, and the variance is distributed equally [46]. Examples of parametric tests are the Student's t–test, the χ2–test, and the one–way ANOVA. Non–parametric tests are tests where the data do not have a normal distribution, and where the variance is not distributed equally. In this study 2 parametric tests were used: the Student's t–test, and the one–way ANOVA (Analysis Of Variance). The t–test was used to investigate whether

or not the difference between 2 averages is significant. The one–way ANOVA was used to test whether or not the difference between 3 or more averages is significant. Furthermore, in the case of comparing 3 or more averages, Bonferrroni corrections were used. Using Bonferroni corrections allows us to know where exactly the difference is between 3 or more averages [47]. Performing a t-test or a one-way ANOVA allows to compute values of probability p.

The mean frequencies at which the highest spectral activity occurs between the healthy subjects and patients with the diffuse alpha pattern were statistically compared using the t-test.

To directly compare the difference of the mean WCC values over the entire functional network between healthy subjects and patients, the t-test was used on all 171 WCC values.

As for the coronal and sagittal orientations in the brain, the mean WCC values were statistically compared between the healthy individuals and the patients using the one-way ANOVA with Bonferroni corrections on the medial coronal orientation, the lateral coronal orientation, the medial sagittal orientation, and the lateral sagittal orientation.

The mean PLV value was statistically compared between all healthy subjects and all patients using the Student's t-test on all 171 channel pair combinations, and in the medial coronal and medial sagittal orientations. In addition to the t-test, the Rayleigh test was used to analyze the circular dispersion of the phase in the brain. The Rayleigh test can be used to statistically analyze whether or not samples are drawn from a uniform distribution [48]. The test was performed between all epochs of the healthy subjects, and between all epochs of the patients.

2.3 Results

2.3.1 EEGs

Figure 2.6 shows the EEG of a healthy subject (figure 2.6a), and a neuropsychiatric disorder patient with the diffuse alpha pattern (figure 2.6b). In the healthy subject's EEG, alpha waves mainly appeared in the occipital region of the brain (electrodes O1 and O2) during eyes closed. This is the normal alpha pattern. In the patient's EEG, alpha waves prominently appear in many regions of the brain (almost all electrodes). This is the diffuse alpha pattern.

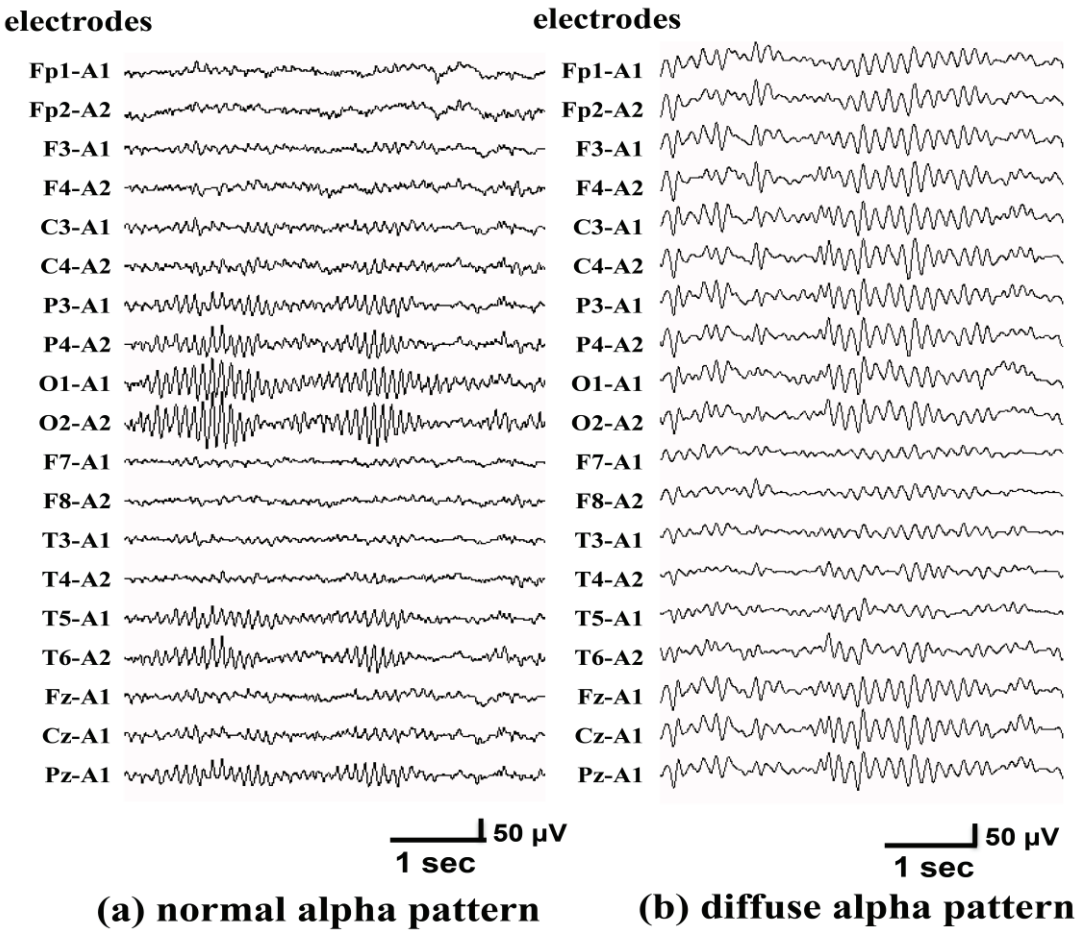

Figure 2.6: EEG of an epoch of a healthy subject (a), and a patient with the diffuse alpha pattern (b). In the healthy subject's EEG, alpha waves appear only in O1 and O2 (normal situation); in the patient's EEG, alpha waves appear in many electrodes (diffuse alpha pattern). [from 42]

2.3.2 Wavelet spectra

Figure 2.7 shows the wavelet spectra during 2 seconds of a representative example of a healthy subject with the normal pattern (figure 2.7a) and a patient with the diffuse alpha pattern (figure 2.7b). The wavelet spectra are shown at all 19 electrodes, according to the International 10–20 electrode positions system. The abscissa shows the time in seconds, and the ordinate shows the frequency in hertz. The color bar represents the lowest and the highest spectral value for all electrodes. In the healthy subject, high spectral alpha wave activity mainly appeared in O1 and O2. In the patient, high spectral activity widely appeared in electrodes Fp1, Fp2, F3, Fz, F4, C3, Cz, C4, T3, and T4.

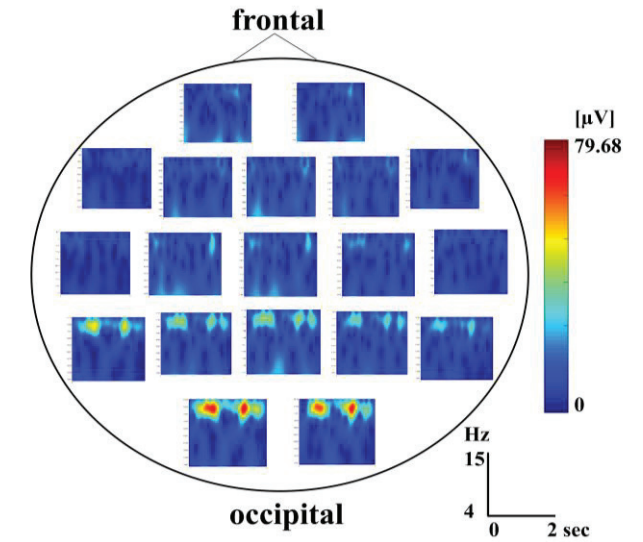

(a) Healthy subject (normal alpha pattern)

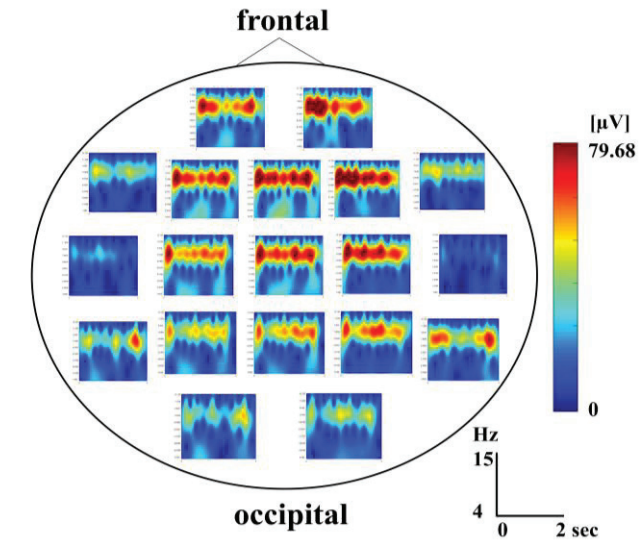

(b) Patient (diffuse alpha pattern)

Figure 2.7: Wavelet spectra at all electrodes of a healthy subject with the normal alpha pattern (a) and a patient with the diffuse alpha pattern (b). The abscissa shows the time in seconds, and the ordinate shows the frequency in Hz. The color bar on the right of the figure represents the lowest and the highest spectral value for all 19 electrodes. [42]

Figure 2.8a shows the wavelet power spectra at electrode F4 of a representative example of a healthy subject, and figure 2.8b shows the wavelet power spectra at F4 of a representative example of a patient with the diffuse alpha pattern. It can be observed that the spectral activity in the alpha bandwidth (8–13.9 Hz) in the patient is much higher than in the healthy individual.

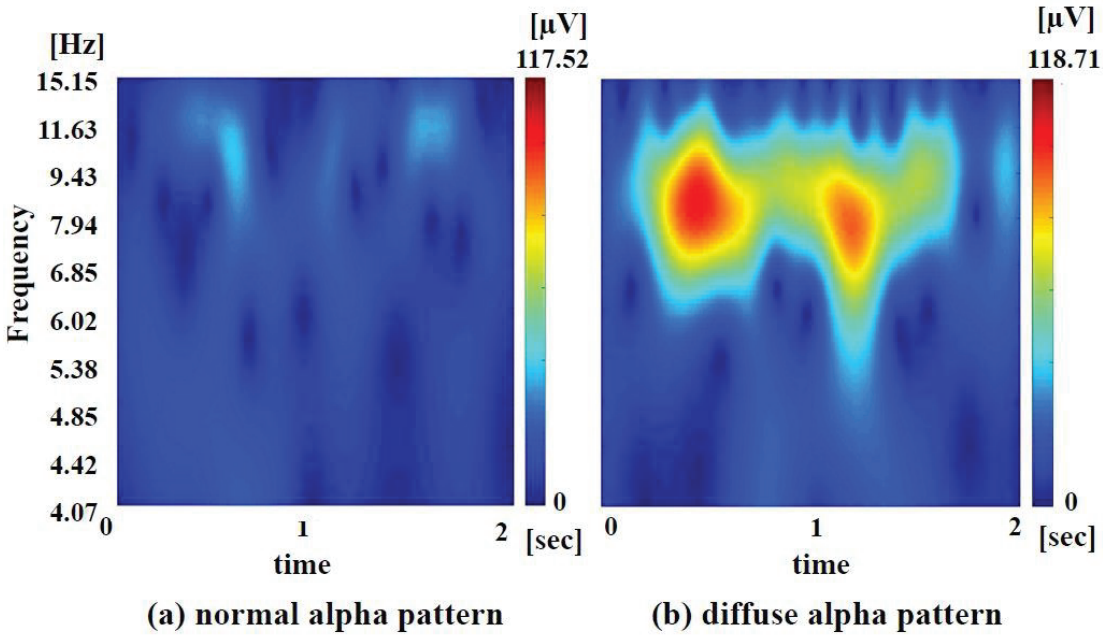

Figure 2.8: Wavelet spectra at the F4 electrode of a subject with the normal alpha pattern (a) and a subject with the diffuse alpha pattern (b). The abscissa shows the time in seconds, the ordinate shows the frequency in Hz. The highest alpha wave spectral activity is shown above the color bar.

Figure 2.9a shows the wavelet power spectra at electrode O2 of a representative example of a healthy subject, and figure 2.9b shows the wavelet power spectra at O2 of a representative example of a patient with the diffuse alpha pattern. The spectral activity in the alpha bandwidth in the patient is higher than in the healthy individual. In addition, the peak of the wavelet spectra in the alpha bandwidth at O2 in the healthy individual occurs at a higher frequency than in the patient.

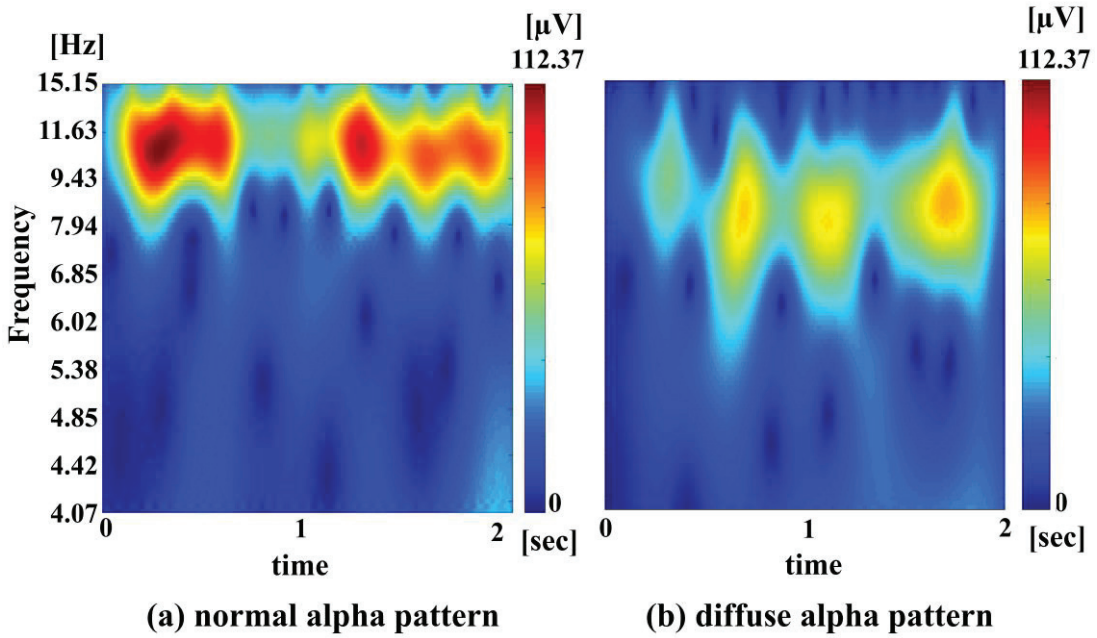

Figure 2.9: Wavelet spectra at the O2 electrode of a subject with the normal alpha pattern (a) and a subject with the diffuse alpha pattern (b). The abscissa shows the time in seconds, the ordinate shows the frequency in Hz. The highest alpha wave spectral activity is shown above the color bar. [42]

Both figures 2.8 and 2.9 indicate that the spectral activity in the alpha bandwidth of a patient with the diffuse alpha pattern occurs at a lower frequency than compared with a healthy subject. The peak of the wavelet spectra in a healthy subject seems to occur at a higher frequency. Figure 2.10 shows a statistical comparison of the average frequency value at the peak of the wavelet spectra in the alpha band between healthy subjects and patients. The ordinate shows the total average frequency value of all 19 electrodes. The highest wavelet power spectra in the alpha band of the patients with the diffuse alpha pattern occur significantly at a lower frequency than the highest wavelet spectra in the alpha band of healthy individuals with the normal alpha pattern ($p<0.001$).

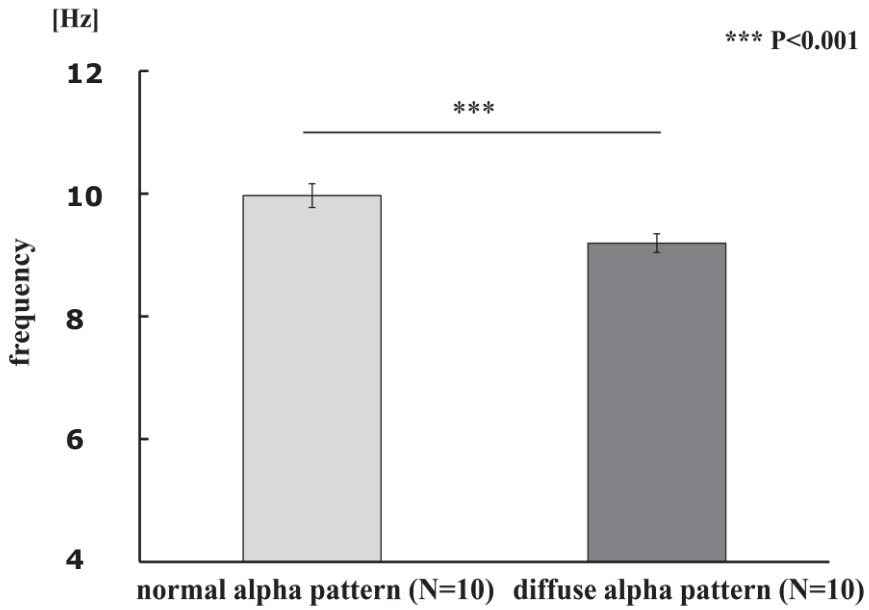

Figure 2.10: The average frequency value of all electrodes at the peak of the wavelet spectra in the alpha band. The light gray bar represents the total average of all electrodes of all healthy subjects (normal alpha pattern), the dark grey bar the total average of all electrodes of all patients (diffuse alpha pattern). N means the number of subjects; the number of electrodes is 19. [42]

2.3.3 WCC comparison between all brain regions

Figure 2.11 shows brain graphs that plot the mean WCC values of all 5 epochs of all 10 healthy subjects (figure 2.11a) and of all 5 epochs of all 10 patients with the diffuse alpha pattern (figure 2.11b) in the alpha bandwidth. Blue displays $0.85 \leqq WCC < 0.88$, green displays $0.88 \leqq WCC < 0.91$, and red displays $0.91 \leqq WCC \leqq 1.00$. The WCC values between all electrodes of the patients with the diffuse alpha pattern is visibly higher than the WCC values between all electrodes of healthy individuals with the normal alpha pattern. In other words, the functional connectivity in the patients with the diffuse alpha pattern is stronger and more global than compared with the healthy subjects. In healthy individuals, the functional connectivity is more local; the strongest functional connections were seen in the occipital region and in the frontal region.

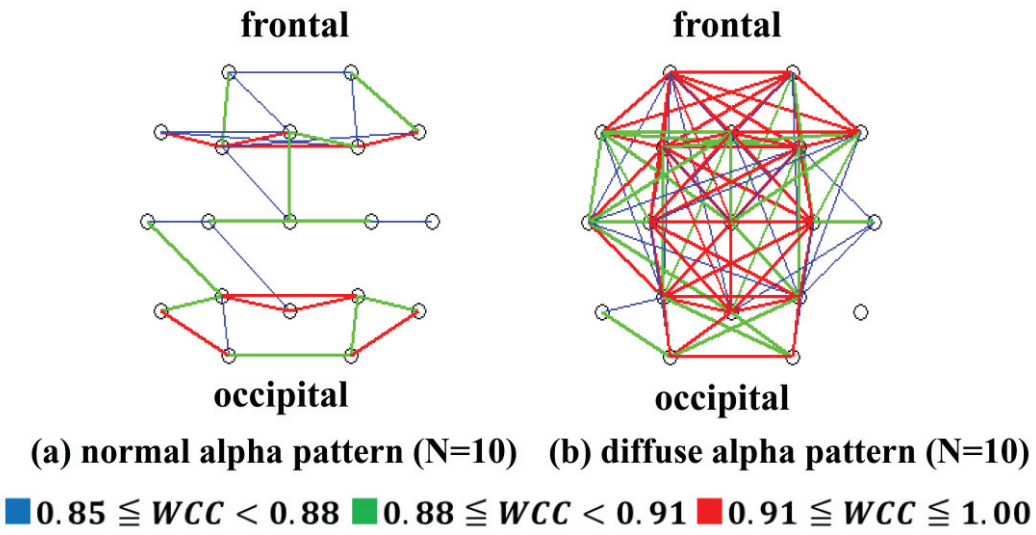

Figure 2.11: Brain graphs of the mean of the WCC values of all 10 healthy subjects (normal alpha pattern) of all 5 epochs for all 27 frequency scales of the alpha bandwidth (a), and the mean of the WCC values of all 10 patients (diffuse alpha pattern) of all epochs for all 27 frequency scales of the alpha bandwidth (b). Blue displays 0.85≦WCC<0.88, green displays 0.88≦WCC<0.91, and red displays 0.91≦WCC≦1. [42]

Figure 2.12 shows the mean WCC values of all epochs of all 10 healthy subjects, and the mean WCC value of all epochs of all 10 patients at 5 separate frequencies: (a) frequency scale 37 (13.51 Hz), (b) 40 (12.5 Hz), (c) 45 (11.1 Hz), (d) 50 (10 Hz), and (e) frequency scale 59 (8.48 Hz). Blue displays 0.85≦WCC<0.88, green displays 0.88≦WCC<0.91, and red displays 0.91≦WCC≦1. Similar to figure 2.11, it can be observed that the WCC values of the patients are higher than the WCC values of the healthy individuals. It can be seen that in the brain of patients with the diffuse alpha pattern, the WCC values between all 19 electrodes in the alpha bandwidth increases as the frequency decreases. In other words, the functional connectivity in the patients' brain seems to be stronger in the alpha 1 bandwidth (8.06–10.87 Hz) than in the alpha 2 bandwidth (11.1–13.89 Hz).

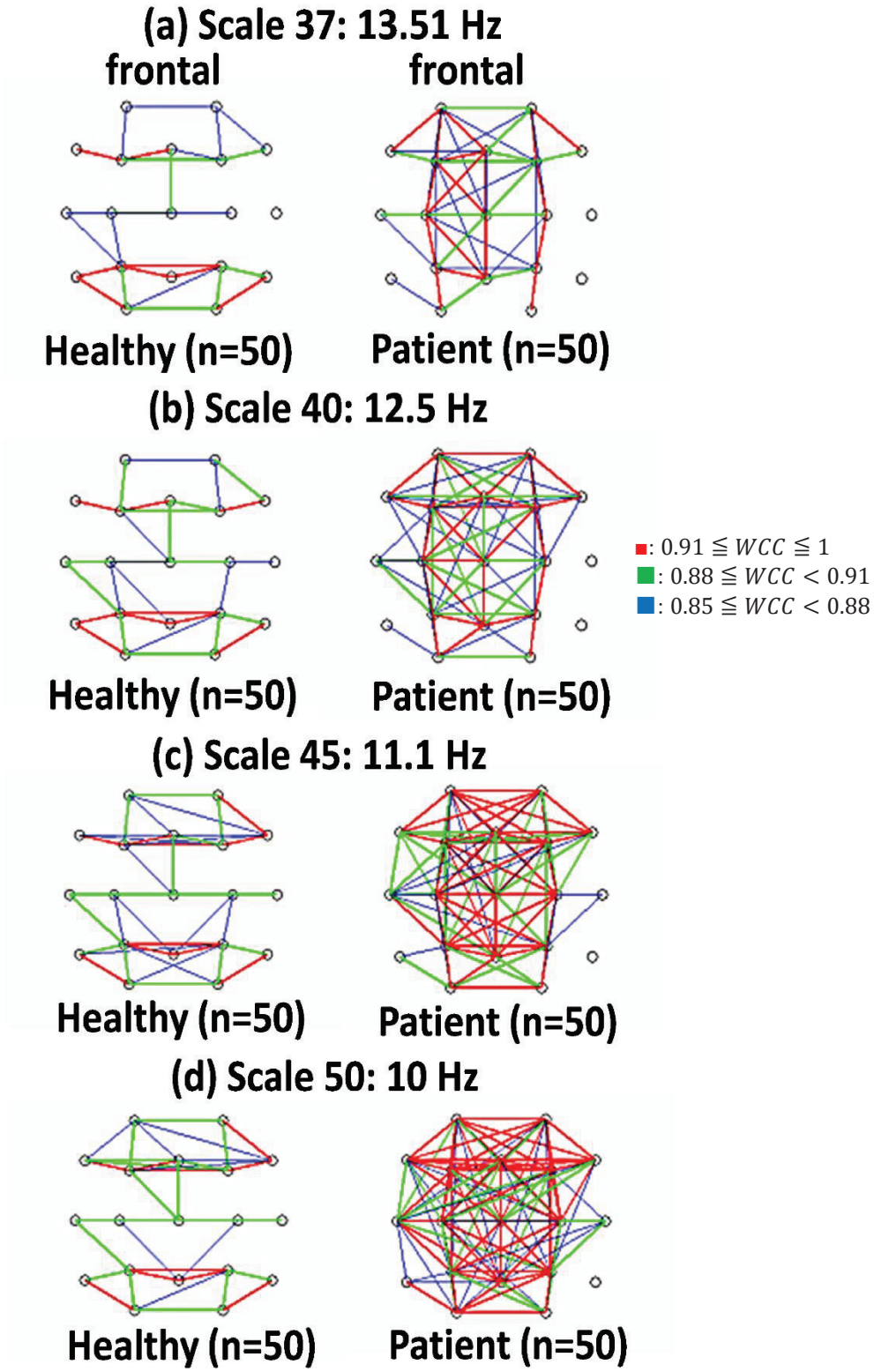

Figure 2.12: Display of the total average of the WCC values of all 10 healthy subjects (right) and all 10 patients (left) in a map using Tcl/Tk. The WCC maps are displayed at frequency scales (a) 37, (b) 40, (c) 45, (d) 50, and (e) 59. Blue displays 0.85≦WCC<0.88, green displays 0.88≦WCC<0.91, and red displays 0.91≦WCC≦1.

Figure 2.13 shows the mean of the WCC values (50 epochs) between all 19 electrodes of all 10 healthy subjects, as well as the mean of the WCC values (50 epochs) between all 19 electrodes of all 10 patients in the alpha bandwidth. The mean WCC value in the patients with the diffuse alpha pattern is significantly higher than the mean WCC value in the brain of healthy individuals with the normal alpha pattern ($p<0.001$).

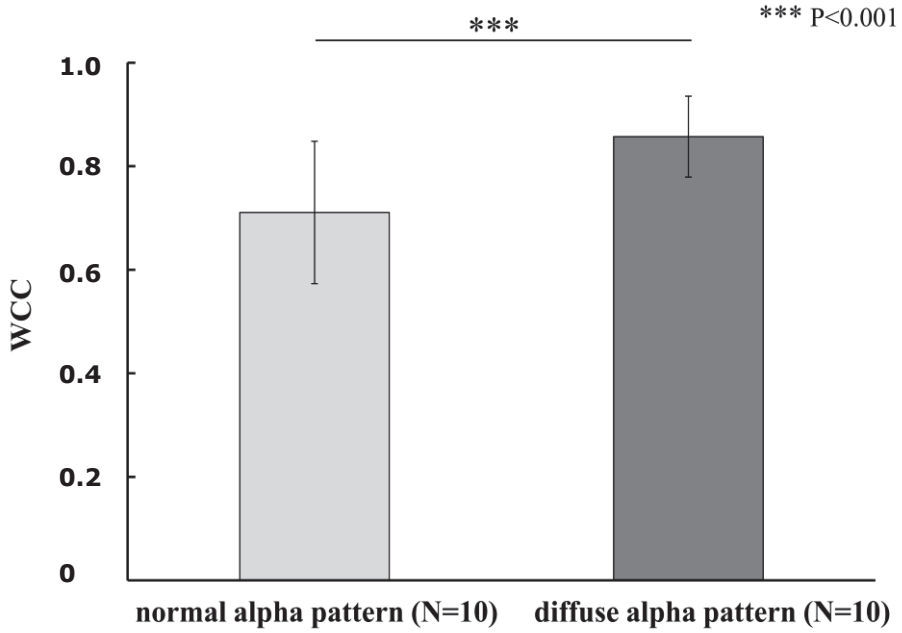

Figure 2.13: Comparison of the mean of the WCC value between all electrodes of all 10 healthy subjects (normal alpha pattern) with all 10 patients (diffuse alpha pattern) in the alpha bandwidth. [42]

Figure 2.14 shows the total average of the WCC values between all 19 electrodes of all 10 healthy individuals and all 10 patients for the frequency scales 37 (13.51 Hz), 40 (12.5 Hz), 45 (11.1 Hz), 50 (10 Hz), and 59 (8.48 Hz). The WCC value for each subject at each frequency represents the mean of the WCC values between all 19 electrodes (the mean of all 171 channel pair combinations). It can be seen that for each of the frequency scales, the WCC values of the patients with the diffuse alpha pattern are significantly higher ($p<0.001$). In addition, in the lowest frequency scale (8.48 Hz), and at 10 Hz, the mean WCC value in the brain of individuals with the diffuse alpha pattern is significantly higher ($p<0.05$) than the WCC value at frequency scale 37 (13.51 Hz).

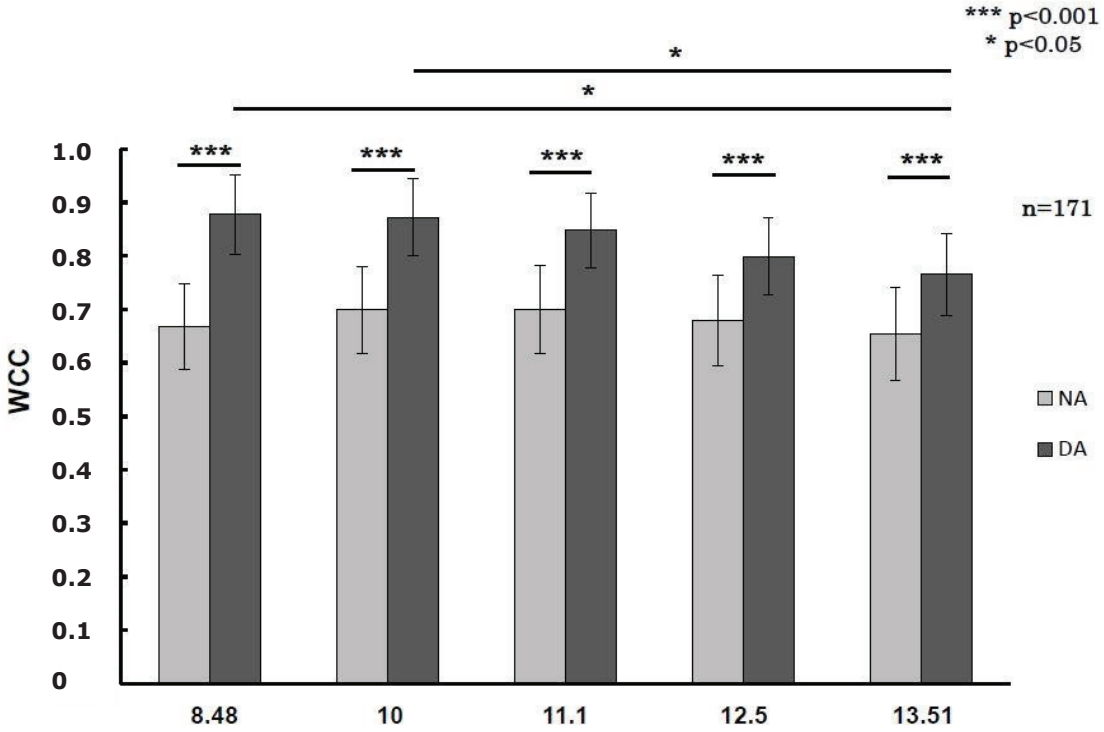

Figure 2.14: Total average of the WCC values of all 10 healthy subjects (light gray bars) and all 10 patients (dark gray bars) for 5 different frequency scales. The ordinate shows the WCC values, the abscissa the frequency scale in Hz. NA= Normal Alpha pattern, DA= Diffuse Alpha pattern.

2.3.4 WCC comparison along the coronal and sagittal orientations

Figure 2.15 shows the brain graphs of the coronal and sagittal orientations of the brain of the healthy subjects (figure 2.15A) and patients with the diffuse alpha pattern (figure 2.15B). Figure 2.15A and 2.15B represent the mean WCC values along the medial coronal orientation in (a); the mean WCC values along the lateral coronal orientation in (b); the mean WCC values along the medial sagittal orientation in (c); and the mean WCC values along the lateral sagittal orientation of the brain in (d). In order to reveal the strongest connections between the electrodes, the WCC values were given a different threshold in each orientation. For the coronal orientation, blue displays $0.88 \leqq WCC < 0.91$, green displays $0.91 \leqq WCC < 0.94$, and red displays $0.94 \leqq WCC \leqq 1.00$; for the sagittal orientation, blue displays $0.80 \leqq WCC < 0.85$, green displays $0.85 \leqq WCC < 0.90$, and red displays $0.90 \leqq WCC \leqq 1.00$. For both the coronal and sagittal orientations, it can be visibly observed that the WCC values of the patients are higher than the WCC values of the healthy individuals.

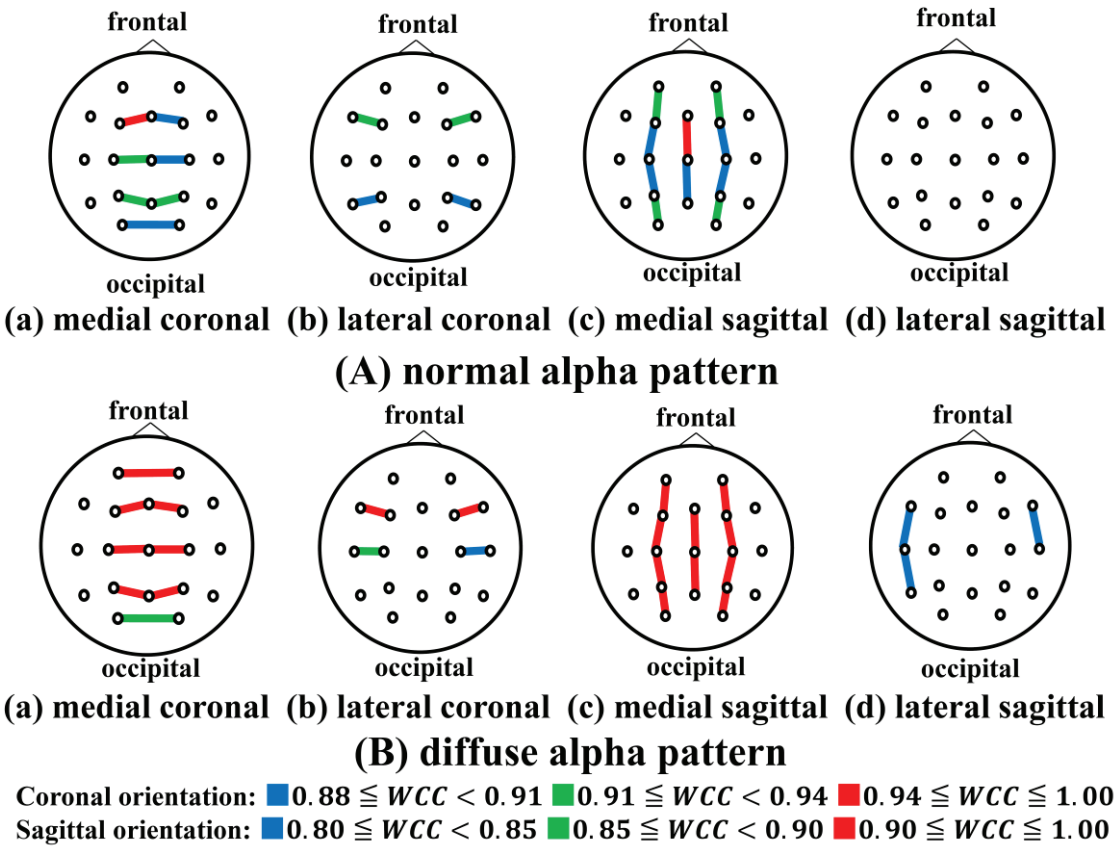

Figure 2.15: Brain graphs of the coronal and sagittal orientations of the brain of the healthy subjects (upper row, N=10) and patients with diffuse alpha pattern (lower row, N=10). (a) represents the WCC of the medial coronal orientation, (b) is the lateral coronal orientation, (c) is the medial sagittal orientation, and (d) represents the lateral sagittal orientation of the brain. For the coronal orientation, blue displays 0.88≦WCC<0.91, green displays 0.91≦WCC<0.94, and red displays 0.94≦WCC≦1.00; for the sagittal orientation, blue displays 0.80≦WCC<0.85, green displays 0.85≦WCC<0.90, and red displays 0.90≦WCC≦1.00. [42]

Figure 2.16 shows the average of the WCC values of all 10 healthy subjects (normal alpha pattern), and the average of the WCC values of all 10 patients (diffuse alpha pattern) for the different orientations in the brain. The abscissa shows the orientation, the ordinate shows the WCC values. It can be observed that for the medial coronal ($p<0.01$), the medial sagittal ($p<0.001$), and the lateral sagittal ($p<0.05$) orientations of the brain, the average of the WCC values of the patients with the diffuse alpha pattern is significantly higher than the average of the WCC values of the healthy subjects. In all subjects, the average of the WCC values of the lateral sagittal orientation was the lowest ($p<0.001$/ $p<0.01$). In the healthy individuals, the average of the WCC values along the medial coronal orientation is higher than the average of the WCC values in the medial sagittal orientation ($p<0.05$). As for the patients, the average of the WCC values in the medial coronal orientation is higher than the average of the WCC values in the lateral coronal orientation ($p<0.05$).

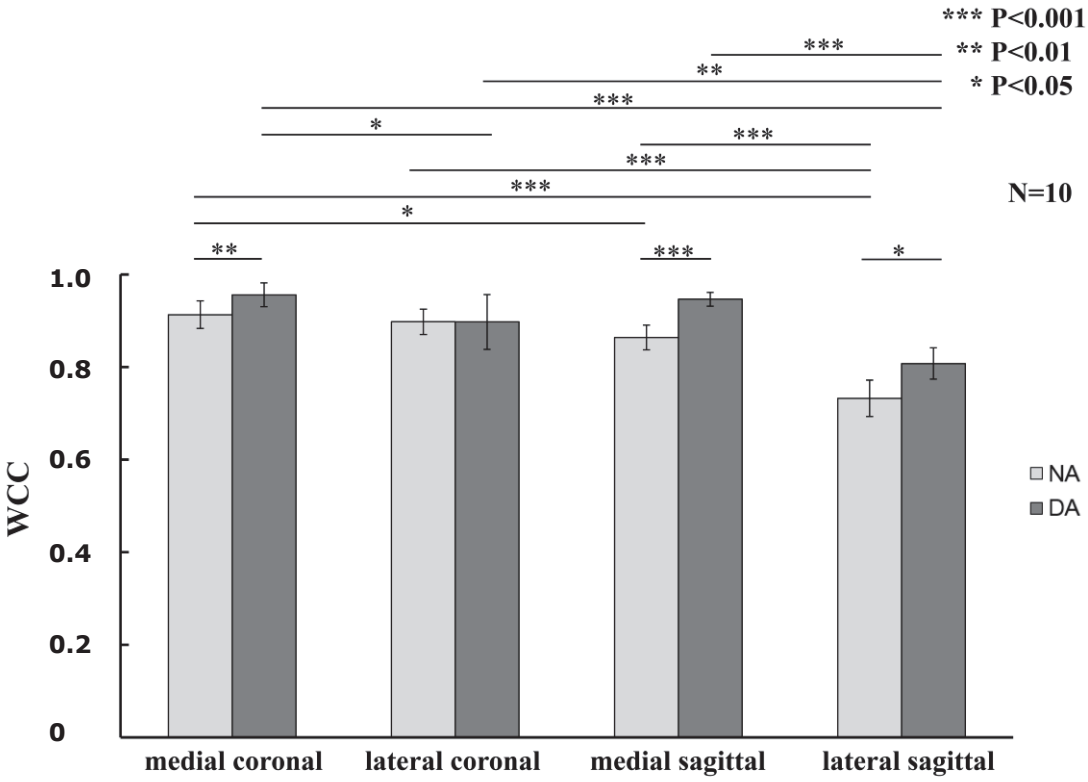

Figure 2.16: Mean of the WCC values in the alpha bandwidth of all 10 healthy subjects (NA=normal alpha pattern), and the average of the WCC values of all 10 patients (DA=diffuse alpha pattern) for 4 different orientations in the brain: the medial coronal, the lateral coronal, the medial sagittal, and the lateral sagittal orientations. The WCC values represent the mean value between the electrodes in each of these four orientations. [42]

2.3.5 PLV comparison

Figure 2.17 shows the total average of the PLV between all 19 electrodes, the medial coronal, and the medial sagittal of all 10 healthy subjects (normal alpha pattern), and all 10 patients (diffuse alpha pattern) in the alpha bandwidth. The abscissa shows the orientation, the ordinate shows the PLV values. The upper line bars and asterisks show the results of the t-test; the asterisks just above the bar graphs show the results of the Rayleigh test. We can observe that in all three cases, the average PLV values of the subjects with the diffuse alpha pattern is higher than the average PLV values of the healthy individuals. These results are significant between all electrodes ($p<0.01$), and along the medial sagittal orientation ($p<0.001$). In the patients, between all electrodes and along the medial sagittal orientation, the dispersion of the phase is polarized ($p<0.05$).

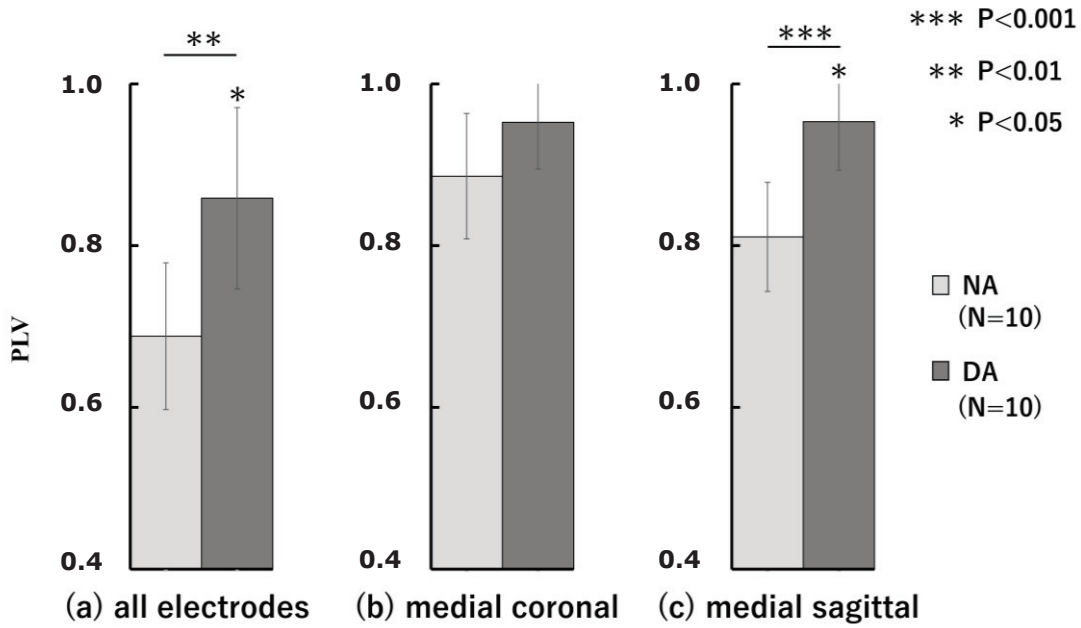

Figure 2.17: Comparison of the average of the PLV value in the alpha bandwidth between all electrodes (a), the medial coronal orientation (b), and the medial sagittal orientation (c) of all 10 healthy subjects (NA=normal alpha pattern) with all 10 patients (DA=diffuse alpha pattern). The lower asterisks above the bar graphs show the results of the Rayleigh test. [42]

2.4 Discussion

In the present study, the normal alpha pattern with the diffuse alpha pattern was compared, and how the connectivity in the brain differs between these 2 patterns was investigated. It was found that the connectivity in the brain of individuals with the diffuse alpha pattern is stronger than in individuals without the diffuse alpha pattern. This finding may be explained by hypothesizing that the connectivity in the brain in individuals with the diffuse alpha pattern needs to be stronger in order for the communication in the brain to work sufficiently.

2.4.1 Wavelet spectra

It is common that alpha waves in healthy individuals have the highest alpha spectral activity (the highest voltage) in the occipital region of the brain. Previous research reported that in some individuals, alpha activity in the brain increases with age [6]. In addition, there have been reports that alpha activity occurs at a higher frequency in healthy individuals, and occurs at a lower frequency in elderly people [9]. In the present research, the distribution of the alpha activity and the frequency at which the highest alpha activity occurred was different between the individuals with the normal alpha pattern and the individuals with the diffuse alpha pattern. Observing a map of wavelet spectra could be helpful for doctors to intuitively understand the distribution of the spectral activity in the alpha band.

2.4.2 WCC comparison between all brain regions

The results in this study statistically confirm that the WCC values between all the electrodes at all frequencies were significantly higher in the individuals with the diffuse pattern than the WCC values of the healthy subjects. In previous research, it was found that Wavelet–crosscorrelation analysis can help reveal and visualize the dynamic changes of brain conditions [37,38]. Calculating WCC values allows to visualize the connectivity in the human brain, as well as the communication between the brain regions which cannot be seen by means of EEG alone. It allows easy comparison of the brain function between individuals with the normal alpha pattern and individuals with the diffuse alpha pattern. Investigating the connectivity in the brain can be useful to diagnose mental diseases.

Several studies have been carried out on the connectivity in the brain of people with abnormal EEG and mental diseases. There is evidence that individuals suffering from dementia such as Alzheimer's disease, might have altered functional brain connectivity patterns when compared to healthy individuals [49]. Another study revealed that in people

with Alzheimer disease, the connectivity in the brain, as well as the small world property of the brain is altered [50]. The latter study suggests that there is a disrupted organization of functional brain networks in people suffering from Alzheimer's disease. It has been reported that depression is a mental illness that presents alterations in functional brain connectivity [51]. In addition, another study revealed that there may be an increase in brain functional connectivity in individuals suffering from depression [52]. A relation can be found between dementia and depression: some dementia patients have symptoms of depression [15].

The results described in 2.3.3 suggest that in healthy individuals, communication may occur either in only the occipital area; or either in only the frontal area of the brain. In the patients with the diffuse alpha pattern, it could be the case that communication in the brain is only possible if all regions of the brain are actively involved [53]. This might be due to inefficiency in the connectivity in the brain of the patients. In the brain of healthy individuals, it could be that communication in the brain occurs at a relatively low level of connectivity. Communication in the brain of healthy individuals may be more efficient from a time perspective than patients with the diffuse alpha pattern. In other words, it may take longer for information to spread in the brain of the mental disorder patients.

Studies about connectivity between specific brain regions have also been conducted. Auditory connectivity via the corpus callosum has been reported to be responsible for the interplay of right and left speech-relevant brain regions [54]. It appears that there is a significantly increased effective connectivity in the gamma band from the right to the left secondary auditory cortex during conscious perception of left ear stimuli [54]. However, it remains unknown in which direction the interhemispheric communication is realized. Another study has reported that the functional connectivity of the human brain changes in several regions in the brain of individuals suffering from mesial temporal lobe epilepsy. An increased functional connectivity was found in the medial temporal lobe, the frontal lobe, and between the parietal and frontal lobes [55]. Another study has suggested that in cognitive impairment patients, the connectivity between hemispheres is stronger than the intra-hemispheric connectivity [31]. This latter study also revealed that these patients display greater connectivity than healthy individuals, and suggests that the patients mobilize a compensatory mechanism to maintain the processing effectiveness while the processing efficiency is reduced [31].

2.4.3 WCC comparison along the coronal and sagittal orientations

In the present study, it was observed that along the sagittal orientation, the functional connectivity between the occipital and the frontal areas of the brain in the patients is strong, especially in the medial area. Along the coronal orientation, the functional connectivity between the right and left hemispheres of the brain was strong in the medial

area. A similar trend of inefficiency may be concluded for the communication between the frontal and occipital areas of the brain via the parietal area.

2.5 Limitation of this study

The present study has a limitation. There is a large gap in age difference between the healthy individuals with the normal alpha pattern and the neuropsychiatric disorder patients with the diffuse alpha pattern, therefore there is a possibility that the observed results could be due to the age difference. In a future study, it may be advisable to measure the EEG of older healthy individuals, close to the age of the patients.

2.6 Conclusion

The results reported in 2.3 are in line with previous studies revealing altered connectivity in people with abnormalities and diseases in their brain. The increased connectivity found in our results suggest that in mental disorder patients with the diffuse alpha pattern, the communication in the brain in general, as well as the communication between the left and right hemispheres via the parietal area may not be efficient.

Conflict of interest: The author declares no competing financial interests.

Ethical approval: All procedures performed in studies involving human participants were in accordance with the ethical standards of the Ethics Committee of the Graduate School of Applied Informatics of the University of Hyogo at which the studies were conducted (IRB approval number UHGSAI-2018-9).

Informed consent: Informed consent was obtained from all individual participants included in the study.

Chapter Ⅲ

Graph Theoretical Analysis of Interictal EEG Data in Epilepsy Patients during Epileptiform Discharge and Non-discharge

3.1 Introduction

EEG and other neuroimaging techniques have been suggested to be useful as a supplement for the diagnosis of neuropsychiatric diseases. Previous research has suggested that quantitative EEG analysis could be used as a biomarker in diseases such as autism and absence epilepsy [56]. Several studies have reported that electroencephalography (EEG) could be an important tool for the diagnosis of epilepsy and to study epilepsy processes [17,57–59]. The EEG of epilepsy patients during non-epileptic seizures is characterized by the appearance of epileptiform discharges and is referred to as interictal EEG [58,59]. While the detection of interictal epileptiform discharges in EEG is important for diagnosis, it has been reported that around 10% of epileptic patients never show discharges [17,57]. These studies suggest that diagnosing epilepsy with high sensitivity is still difficult. It has been reported that synchronization between EEG time series from different brain regions differs between epilepsy patients and healthy subjects in the interictal state [17]. This latter study concluded that functional connectivity may help in the diagnosis of epilepsy.

Functional connectivity in the brain is defined as the statistical interdependencies between signals of brain activity recorded from distant brain regions by neuroimaging techniques [60,61]. These interdependencies between time series are considered to reflect the functional interactions between different brain areas, and can be derived from various analysis methods [1]. Characterization and quantification of the functional connectivity in the human brain may help reveal changes in neuronal activity and connection patterns between brain areas, and allow us to understand how these changes give rise to disturbances in brain function [62]. Mizuno-Matsumoto et al. [38] reported that a method called wavelet–crosscorrelation analysis of MEG data could help visualize the initiation and propagation of epileptiform activity in the brain of epilepsy patients. Previous work suggested that focal lesions caused by brain tumors disturb not only the localized brain function, but also the widespread functional connectivity between brain areas [63]. Brain disorders may not only be related to a dysfunction of a certain brain area, but also to the way brain areas are functionally connected [64]. Brain function seems to be dependent on the spatial distribution (the topology) of the functional connections.

In modern neuroscience, a new method using graph theory has been proposed to characterize and quantify the topology of the brain as a network. The brain can be considered a complex anatomical or functional network of neurons, neuron populations, or brain regions [1,65,66]. A graph is an abstract mathematical representation of a real-life network. In graph theory, the nodes of a network are referred to as vertices, and the

connections (links) between these nodes as edges [67]. Watts and Strogatz have discovered that other than regularly connected networks and completely randomly connected networks, there is a class of networks called “small-world” networks [68]. Small-world networks have many local connections (high clustering) between nodes, and a few random long-distance connections (short path lengths) between nodes. A small-world network is considered to be an optimal network, and many types of real-life networks have been shown to have small-world properties [67,69]. A lot of research has revealed small-world topology in anatomical and functional networks of the brain in animals and in humans. Studies based on MRI found a small-world configuration in both the anatomical network [65] and the functional network [70] of the human brain. Previous work based on EEG revealed small-world properties in the brain functional networks of healthy individuals. These studies revealed a loss of optimal brain function due to a loss of small-world topology in the brain network of Schizophrenia [71] and Alzheimer [61] patients, and suggested that network measures may aid in the diagnosis of neuropsychiatric diseases. Studies based on fMRI found altered small-world topology in epilepsy patients compared to healthy adults [55,72]. Another study based on intracranial electrocorticographic recordings in epilepsy patients found different network topologies during the ictal, preictal, and postictal periods [19].

Using wavelet-crosscorrelation analysis and graph theoretical analysis of scalp recorded EEG, the present study aimed to examine whether or not the functional connectivity and the small-world properties of the brain network of healthy individuals differ from epilepsy patients. While previous studies used fMRI recordings and graph theory to examine the network topology of healthy adults and epilepsy patients [55,72], in this paper the focus is on scalp EEG recordings, which have a high temporal resolution suitable for analyzing rapidly changing brain signals. The second purpose of this study was to examine the interictal period of the EEG of the epilepsy patients, and compare the functional connectivity and the small-worldness of the brain network between during epileptiform discharge and during non- discharge. A study based on MRI found that not only the small-world topology, but also the centrality of the brain network of patients with Alzheimer’s disease is different from healthy individuals [73]. Following this latter study, lastly the present study aimed to examine whether or not the nodal betweenness centrality of the brain network differs between healthy subjects and epilepsy patients, and between during discharge and during non-discharge in the interictal period.

3.2 Methods

3.2.1 Subjects and selection of the EEG data

The EEG data used in this study was measured and collected in the Matsumoto Clinic and the University of Hyogo. EEG data was obtained by scalp recordings from the same 10 healthy subjects as the previous study in chapter II (5 males and 5 females; mean age: 24.40 ± 2.46 years), and 10 individuals who were diagnosed with epilepsy (4 males and 6 females; mean age: 41.30 ± 14.44 years). There is an age difference between the healthy subjects and patients, but based on previous studies, the functional network of the brain shows differences between children and healthy adults [74], and between healthy adults and elderly individuals [75]. Another study based on EEG divided healthy adults in 3 age groups, and showed a different brain functional network only between young adults (ages 16-45), middle-aged adults (ages 50-70), and elderly people (age >70) [76]. In our study, the possibility that the age difference could affect the results to some degree cannot be excluded, however based on these studies, this possible influence might be minimal.

All 10 epilepsy patients suffered from generalized epilepsy, therefore no epileptic focus was present in any of the patients' brains. The EEG of the patients was recorded at the Matsumoto Clinic. Table 3.1 shows the medical diagnosis of each patient. Epileptiform discharges could be observed in each patient's EEG. The EEGs of all subjects were measured during resting-state with eyes closed, and there was no sound at the time of recording. To record the EEG data, scalp electrodes (19 channels) were placed according to the International 10–20 electrode positions system (see figure 2.1 in chapter 2).

Table 3.1: Patient profile (mean age: 41.30±14.44 years). [32]

Patient number	Age [years]	Gender	Type of epilepsy
1	32	Male	Autonomic seizure
2	61	Female	Grand mal
3	52	Female	Autonomic seizure
4	48	Female	Grand mal
5	25	Female	Grand mal
6	59	Male	Grand mal
7	56	Female	Grand mal
8	34	Male	Autonomic seizure
9	23	Male	Autonomic seizure
10	33	Female	Autonomic seizure

In this study, epochs of 2 seconds long were analyzed for each subject, and the number of sampling points in one epoch was 1000, therefore the sampling frequency was 500 Hz. A bandpass filter was set between 0.5 Hz and 30.0 Hz.

This research was approved by the Ethics Committee of the Graduate School of Applied Informatics of the University of Hyogo (UHGSAI-2018-9). All subjects agreed to be measured and gave written informed consent.

3.2.2 Analysis methods

Similar to the study in chapter II, Vital Tracer was used to abstract the measured EEG data, and all selected epochs were analyzed by means of Wavelet–crosscorrelation analysis to derive wavelet power spectra and WCC values. In the current study, the WCC values were calculated in two separate parts in the alpha bandwidth: the alpha 1 bandwidth (8.06–10.87 Hz), and the alpha 2 bandwidth (11.1–13.89 Hz). Matlab R2018b was used in order to calculate the WCC values from the abstracted numerical EEG data. The correlation strengths were visualized in brain graphs using TcL/Tk to reveal functional connectivity patterns. High reliability cannot be obtained by analyzing low values, therefore low amplitudes were excluded from the analysis. For the next step, a correlation matrix was constructed, and network analysis based on graph theory was used to obtain network parameters in order to further quantify the connectivity patterns and information flow in the brain.

In order to statistically compare the obtained WCC values and network parameters between healthy individuals and individuals suffering from epilepsy, the software IBM SPSS Statistics 24 was used.

The basis of Graph Theory, and various measures of graph theoretical analysis are explained below.

3.2.2.1 Graph theoretical analysis: basic concepts

The analysis of networks can be applied to many sciences: sociology, biology, neurology [69]. Networks consist of nodes and links, which form connections between nodes, and can mathematically be described as graphs [67]. In Graph Theory, graphs are characterized by vertices (nodes), and edges (links) which connect vertices [67]. An example of a graph is shown in figure 3.1.

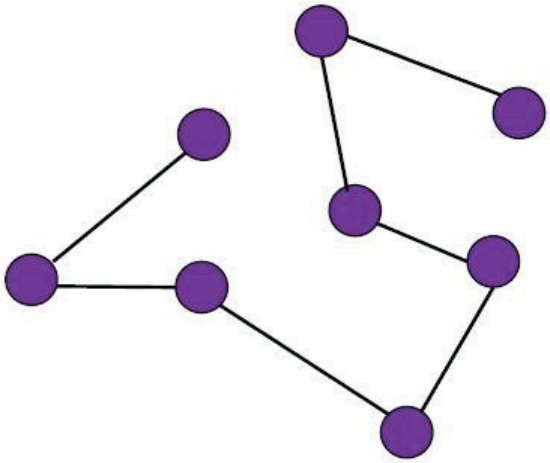

Figure 3.1: An example of a graph with vertices (purple spheres) and edges (lines).

A key measure in Graph Theory is the degree of a vertex, often represented with the symbol *k* [67]. The degree *k* of a vertex *i* is the number of edges *i* has to other vertices [67].

3.2.2.2 Graph theoretical analysis: global measures

As mentioned in introduction, graph theory is a relatively new method to characterize the properties of a network. Networks are characterized by several parameters that can quantify the network topology. Two of the most commonly calculated global measures are the Clustering coefficient *C* and the characteristic Path Length *L*.

The local clustering coefficient C_i of vertex *i* with degree k_i (the number of links departing from vertex *i*) is defined as the ratio of the number of existing edges (e_i) between neighbor vertices of *i*, and the maximum possible number of edges between neighbor vertices of *i* [66]. C_i is defined in equation 3.1. The Clustering coefficient indicates to what extent neighbors connected to a given vertex are also connected to each other [66,67,77]. C_i is between 0 and 1. $C_i = 0$ if none of the neighbors of vertex *i* connect to each other. $C_i = 1$ if the neighbors of *i* all link to each other.

$$C_i = \frac{2e_i}{k_i(k_i - 1)} \tag{3.1}$$

To obtain the mean *C* of a graph with *N* vertices, C_i is averaged over all vertices. *C* is defined in equation 3.2 [66,67,77].

$$C = \frac{1}{N}\sum_{i=1}^{N} C_i \tag{3.2}$$

C can be considered a global measure of the segregation (specialization) of the entire network, and indicates the local interconnectedness and cliquishness within the network [77]. There is an alternative definition of the clustering coefficient of a network based on transitivity (equation 3.3) [78].

$$C^{\Delta} = \frac{3\ X\ the\ number\ of\ triangles}{number\ of\ paths\ of\ length\ 2} \tag{3.3}$$

To evaluate the properties of a real-life network, *C* must be compared to the clustering coefficient estimated in a random network with the same number of vertices, edges, and degree distribution of the network of interest [79,80]. The normalized Clustering coefficient γ is the ratio between the Clustering coefficient *C* of the actual network, and C_{rand}, the Clustering coefficient of the corresponding surrogate random network that has the same number of vertices, edges and degree distribution as the actual network [70,79,80]. γ is defined in equation 3.4.

$$\gamma = \frac{C}{C_{rand}} \tag{3.4}$$

The shortest path length or distance $d_{i,j}$ between two vertices *i* and *j* is the minimum number of edges that have to be traveled to go from *i* to *j* (equation 3.5) [66].

$$d_{i,j} = \sum_{a_{u,v} \in g_{i \leftrightarrow j}} a_{u,v} \tag{3.5}$$

Where $a_{u,v}$ is the connection status between vertices *u* and *v*, and $g_{i \leftrightarrow j}$ is the shortest path between *i* and *j*.

The characteristic Path Length *L* is the mean of the path lengths between all possible pairs of vertices in the graph [66,67,77]. *L* is defined in equation 3.6.

$$L = \frac{1}{N(N-1)} \sum_{i,j \in N, i \neq j} d_{i,j} \tag{3.6}$$

The characteristic path length can be considered a global measure of the integration of the entire network, and indicates how easy it is to transport information in the network [66,77]. The normalized characteristic path length λ is the ratio between the characteristic Path length *L* of the actual network, and L_{rand}, the characteristic Path Length of the corresponding surrogate random network that has the same number of vertices, edges and degree distribution as the actual network [70,79,80]. λ is defined in equation 3.7.

$$\lambda = \frac{L}{L_{rand}} \tag{3.7}$$

Several types of networks exist. In regular networks, all edges in the graph are connected in an orderly manner. In random networks, all edges in the graph are completely randomly connected. The Watz-Strogatz model (figure 3.2) found the existence of a class of networks called 'Small-world' networks in between regular and random networks [67,68]. In Small-world networks many edges are regularly connected, and only few edges are randomly connected. It is possible for regular networks to evolve into Small-world networks and eventually into random networks by increasing p, the probability of randomly rewiring an edge in the graph (see figure 3.2). Regular networks are characterized by both a high Clustering coefficient and a high (long) characteristic Path Length, resulting in good local connectedness (specialization). On the other hand, random networks have both low clustering and very short path length, resulting in good global connectedness [67,68]. A small-world network has a high C close to a regular network, but a very small L close to that of a random network. In other words, small-world networks combine good local connectedness (segregation) with good global connectedness (integration) [68].

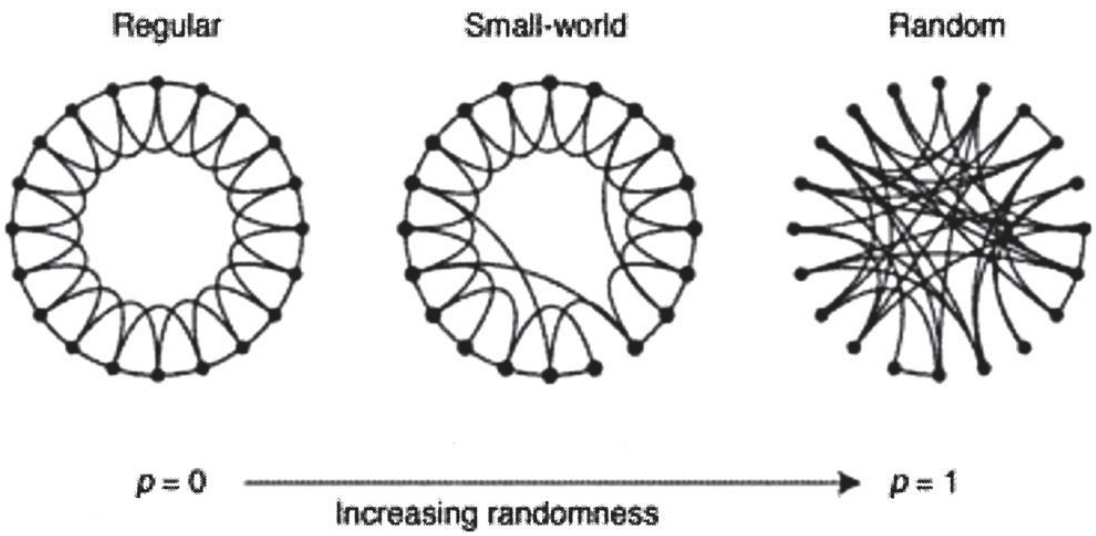

Figure 3.2: The random rewiring procedure of the Watts-Strogatz model. As the probability of rewiring p increases, the network evolves from regular, to Small-world, to random [81].

These properties of small-world networks present an attractive model for brain functional connectivity, as the brain supports both segregated/specialized information processing and integrated information processing [80].

Some studies have suggested to combine the above defined measures γ and λ of Small-worldness into one measure. The index of Small-worldness σ is defined as the ratio of the normalized Clustering coefficient divided by the normalized characteristic Path Length. σ is defined in equation 3.8.

$$\sigma = \frac{\gamma}{\lambda} \tag{3.8}$$

As in Small-world networks the Clustering coefficient C is much higher than C_{rand} of the corresponding random network, the normalized clustering coefficient $\gamma >> 1$. The characteristic Path Length L of a Small-world network is almost as low as the L_{rand} of the corresponding random network, therefore the normalized characteristic Path Length $\lambda \geq 1$. Consequently, a certain network is considered a small-world network if $\sigma > 1$ [70,78,80].

3.2.2.3 Graph theoretical analysis: nodal measures

A common nodal measure is the nodal betweenness centrality B_i. The betweenness centrality B_i of vertex i is the ratio between all shortest paths between vertices j and k that run through i, divided by all shortest paths between j and k [66,75,82]. B_i is defined in equation 3.9.

$$B_i = \sum_{j,k \in N, j \neq k} \frac{n_{j,k}(i)}{n_{j,k}} \tag{3.9}$$

$n_{j,k}$ represents all shortest paths between vertices j and k. B_i is an index of the relative importance of a vertex in the network, and also reflects the consequences of a loss of a certain vertex [66].

The normalized betweenness centrality b_i of a vertex is the ratio of the nodal Betweenness Centrality B_i divided by the average betweenness centrality of all the vertices of the network B [73,75,82]. b_i is defined in equation 3.7. b_i is a measure that captures the influence of a vertex over information flow between other vertices in the network, and can be considered 'hubs' (= vertices with high degree) [66,77].

$$b_i = \frac{B_i}{B} \tag{3.10}$$

3.2.3 Data processing protocol

Similar to the previous study of this dissertation, for each healthy individual's measured EEG, five artifact-free epochs of 2 seconds were carefully selected for analysis by visual inspection (in total 50 epochs). For each epilepsy patient's measured EEG, five artifact-free 2-second-epochs that had epileptiform discharge (in total 50 epochs), and five artifact-free 2-second-periods that showed no discharge (in total 50 epochs) were selected and carefully distinguished by careful visual inspection. All epochs were selected separate on the time course of the EEG (see figure 2.3 in chapter II). Within each patient's interictal EEG, the epileptiform discharge epochs and non-discharge epochs were selected with a time difference of 1 to 3 minutes from each other on the time course of the EEG. In this paper, we did not investigate the time course of the EEG, but following previous studies, we distinguished and selected several discharge and non-discharge epochs repeatedly per subject [16,17]. The selected epochs were then averaged in order to achieve reliable statistical comparison of network measures between during discharge and during non-discharge, as well as between healthy subjects and patients. After abstracting the EEG data by means of Vital Tracer, the numerical data was run in an original Matlab program to obtain wavelet spectra and WCC values in the alpha 1 bandwidth and alpha 2 bandwidth. The WCC values were analyzed for 10 frequency scales in the alpha 1 bandwidth (lowest frequency at 8.06 Hz, and highest frequency at 10.87 Hz), and 17 frequency scales in the alpha 2 bandwidth (lowest frequency at 11.1 Hz, and highest frequency at 13.89 Hz). The objective of this study was to compare the brain network topology between healthy subjects and epilepsy patients, and between epileptiform discharge and non-discharge. For this reason, the normal EEG epochs and discharge and non-discharge epochs were selected repeatedly at random and the epoch data were averaged in order to achieve statistically significant comparison.

The WCC values were calculated between all 19 electrode channels (171 channel pair connections were possible). Each functional interaction between an electrode pair corresponds to 1 WCC value. The calculated WCC values were constructed into a functional brain network by using a Tcl/TK program. In the constructed functional brain graphs, the vertices represent the electrode channels, and the edges correspond to the functional interactions (WCC values) between the electrodes. An interaction between 2 vertices was considered an edge only if the WCC value is above a certain threshold, otherwise no edge was shown. Choosing low threshold values would give rise to too many edges, resulting in difficult visual interpretation of each graph. A WCC threshold of 0.8 was therefore fixed over all graphs to reveal the strongest correlation strengths in each graph.

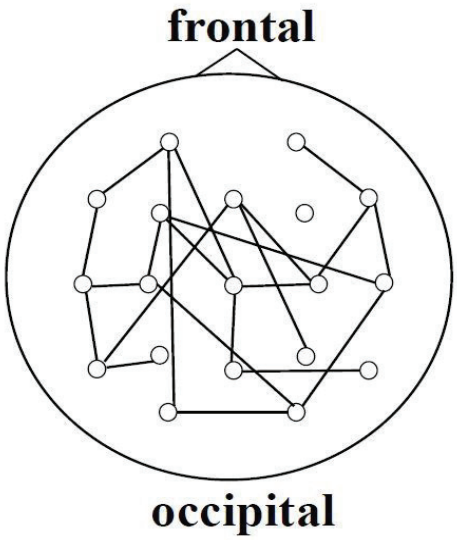

Figure 3.3: An example of a graphical representation of a functional brain network. The vertices (circles) of the graph correspond to the electrodes, and the edges (lines) of the graph represent the WCC values between the electrodes. [32]

Using an original program of Matlab R2017b, the calculated 171 WCC values were first converted to square 19x19 correlation matrices. Correlation matrices are also referred to as connectivity matrices, or adjacency matrix. The rows and columns of each correlation matrix represented the electrode channels, and the entries represented the WCC values. An example of a correlation matrix of a healthy individual is shown in figure 3.4. The color bar on the left represents the strength of the WCC values. Yellow color indicates the highest WCC values, dark blue color shows the lowest WCC values.

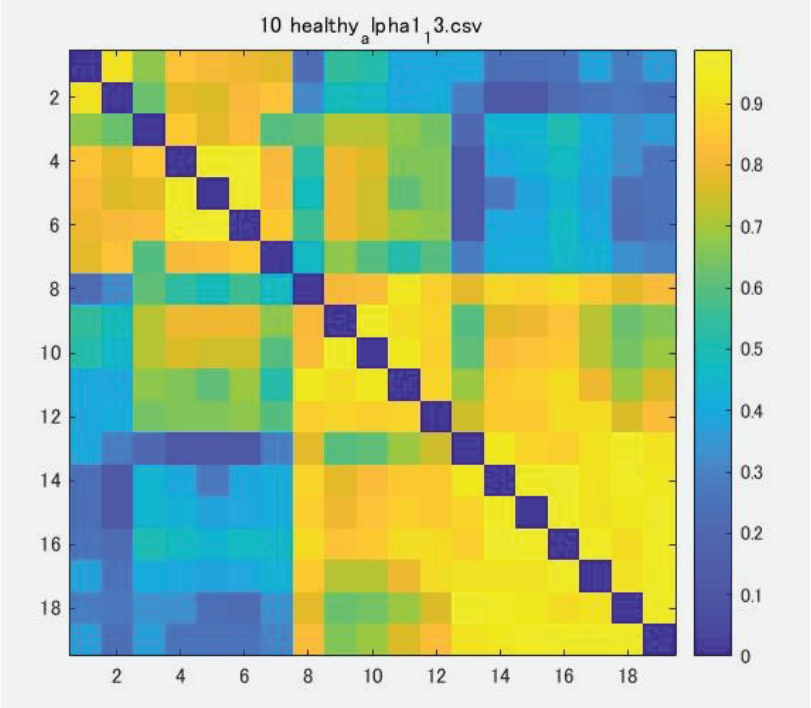

Figure 3.4: An example of a 19x19 correlation (connectivity) matrix. The color bar on the left represents the strength of the WCC values.

To compute the network parameters γ, λ, and σ, we input the correlation matrices in the Matlab toolbox GRETNA. In order to define the presence or absence of edges between the vertices, the correlation matrix was thresholded into a binary matrix by using the sparsity threshold method. An edge was present if the correlation value was above the threshold (value 1), otherwise an edge was absent (value 0). Density (also referred to as sparsity) is defined as the number of existing edges in the network divided by the maximum number of edges possible in the network [73,82,83]. Sparsity can be expressed as a percentage (for example 15 %) or as a decimal number (for example 0.15). The higher the sparsity ratio, the more the vertices of a network are connected by edges (see figure 3.5). The meaning of a sparsity threshold in this study is that the strongest WCC values were chosen by GRETNA as edge sparsity. For example, a sparsity threshold of 10 % means that 10 % of all possible edges in the network are shown in the graph, and that these edges represent the strongest WCC values. Setting a sparsity threshold ensures that all graphs of all subjects have the same number of edges and degree distribution, and that alterations in the topology are solely reflected by differences in network measures between healthy subjects and patients [61,84]. If graphs between the healthy subjects and patients had different edges, alterations in the topological organization could be due to differences in number of edges or degree distributions.

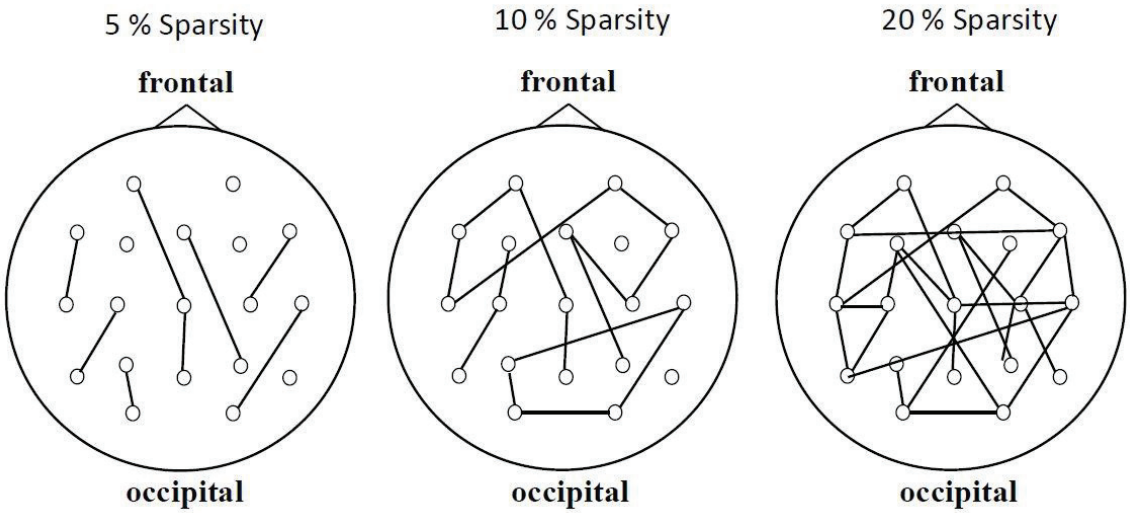

Figure 3.5: Illustration of the meaning of sparsity (density). The higher the sparsity, the more edges are shown in the graph.

In the present study, a range of connectivity sparsity thresholds (10 to 40 %) was used with an increment of 0.01, and the network analysis was repeated at each sparsity threshold value. This range of sparsity thresholds was chosen to avoid non-significant or spurious connections between vertices [75]. Low sparsity thresholds guarantee that edges with high correlation strengths (stronger, significant connections) remain, which may be more meaningful for our analysis [72,77].

In order to compute γ and λ, GRETNA is able to generate surrogate random networks with the same number of vertices, edges, and degree distributions as the actual networks. Vertices completely disconnected from the graph are an infinite number of paths separated from the other vertices, therefore in the computing of λ, the distance $d_{i,j}$ of disconnected vertices is infinite. For this reason, disconnected vertices were excluded while calculating L and λ in our analysis. Graphs with sparsity thresholds lower than 10 % were not calculated, therefore the number of disconnected vertices was kept at a minimum.

B_i was calculated using GRETNA. To investigate the nodal characteristics of each vertex, a fixed sparsity threshold of 30% was chosen because this threshold value ensures all vertices are included in the functional networks and the number of false positive paths are minimized, and may optimize interregional correlation strengths and therefore be biologically plausible [73,80,82]. An original Matlab program was used to visualize the B_i values of all vertices in a brain graph. To define the hubs of the network, the normalized betweenness centrality b_i was computed for each vertex [73,75,82]. Following previous studies, vertices with values of b_i >1.5 were defined as hubs [73,82].

3.2.4 Statistical analysis

In this study, to directly compare the difference of the mean WCC values over the entire functional network between healthy subjects and epilepsy patients during epileptiform discharge and during non-discharge, one way-ANOVA with Bonferroni corrections was used on all 171 WCC values.

The calculated network measures γ, λ, and σ were first averaged over all sparsity threshold values. ANOVA with Bonferroni corrections was used on all 50 epochs to statistically compare the difference of the network parameters over the entire functional network between healthy individuals and epilepsy patients during discharge and during non-discharge.

As for the nodal Betweenness Centrality, ANOVA with Bonferroni corrections was used at a 30% sparsity threshold value to compare the brain regions (electrodes) with the highest b_i.

3.3 Results

3.3.1 EEGs

Figure 3.7a shows the EEG of a healthy subject. Alpha waves mainly appeared in the occipital region of the brain (electrodes O1 and O2) during eyes closed (normal situation). Figures 3.7b and 3.7c show the interictal EEG of a patient at the time of epileptiform discharge, and during of non-discharge, respectively. Epileptiform discharges (theta bursts) sometimes prominently appeared in the interictal EEG of epilepsy patients over many channels.

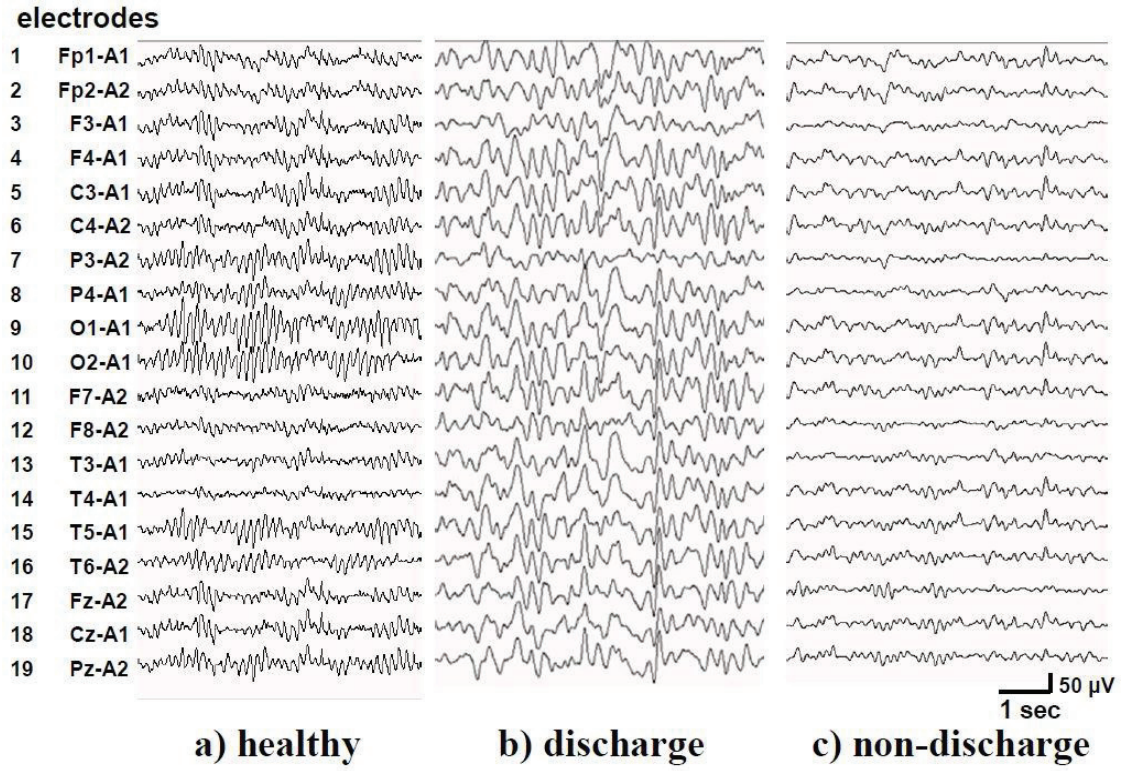

Figure 3.7: EEG of an epoch of a) a healthy individual; b) a patient during epileptiform discharge; and c) a patient during non-discharge. During discharge, theta bursts are visible. [32]

3.3.2 Wavelet spectra

Figure 3.8 shows the mean wavelet spectra of the mean of all 50 2-second epochs of the healthy subjects (figure 3.8a), the patients at the time of epileptiform discharge (figure 3.8b), and at the time of non-epileptiform discharge (figure 3.8c). The wavelet spectra are shown at all 19 electrodes according to the International 10–20 electrode positions. The abscissa shows the time in seconds, and the ordinate shows the frequency in Hz. The color

bar represents the lowest and the highest spectral value for all electrodes. In the healthy subjects, high spectral activity only appeared in O1 and O2. In the patient during discharge, very high spectral activity widely appeared in many electrodes. At the time of non-discharge, high spectral activity appeared in some electrodes.

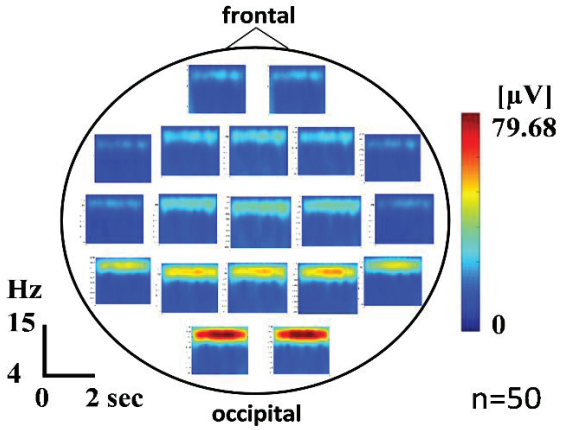

(a) Healthy subject

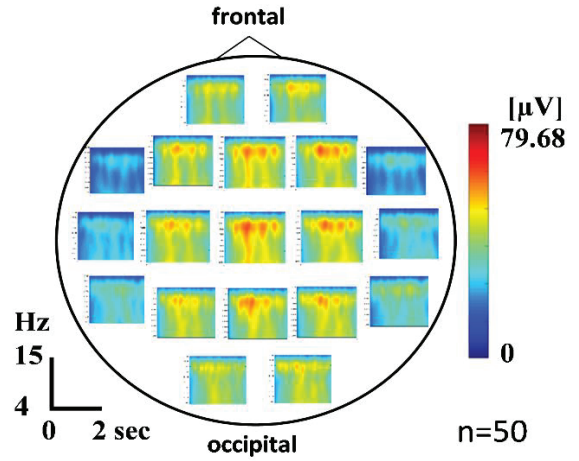

(b) Discharge

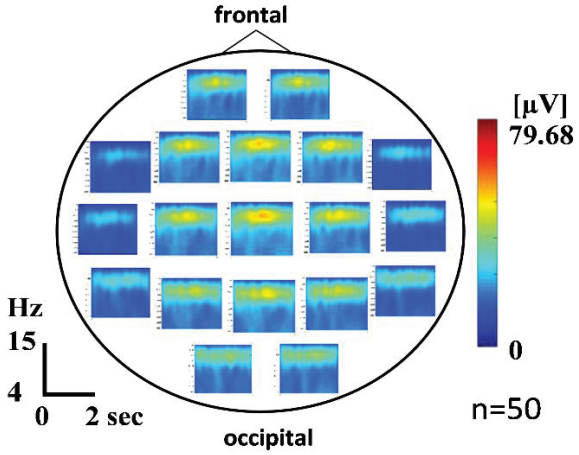

(c) Non-discharge

Figure 3.8: Mean wavelet spectra at all electrodes of the healthy individuals (a), the patients at the time of discharge (b) and at the time of non-epileptiform discharge (c). The color bar on the right of the figure represents the lowest and the highest spectral value for all 19 electrodes [32].

3.3.3 Wavelet-crosscorrelation analysis

Figure 3.9 shows brain graphs that plot the mean WCC values of all 50 epochs of all healthy subjects (figure 3.9a), and all patients during epileptiform discharge (figure 3.9b), and at the time of non-discharge (figure 3.9c) in the alpha 1 bandwidth. The WCC values of the healthy subjects were the highest (the correlation was the strongest) in the frontal and occipital areas of the brain. In the patients, during both discharge and non-discharge, the strongest connections were seen in the left central and left parietal areas of the brain. Figure 3.10 shows brain graphs that plot the mean WCC values of all 50 epochs of all healthy subjects (figure 3.10a), and all patients during discharge (figure 3.10b), and at the time of non-discharge (figure 3.10c) in the alpha 2 bandwidth. Similar to the alpha 1 band, the WCC values of the healthy subjects were the highest (the correlation was the strongest) in the frontal and occipital areas of the brain. In the patients, both at the time of discharge and non-discharge, the strongest connections were seen in the left central and left frontal areas of the brain.

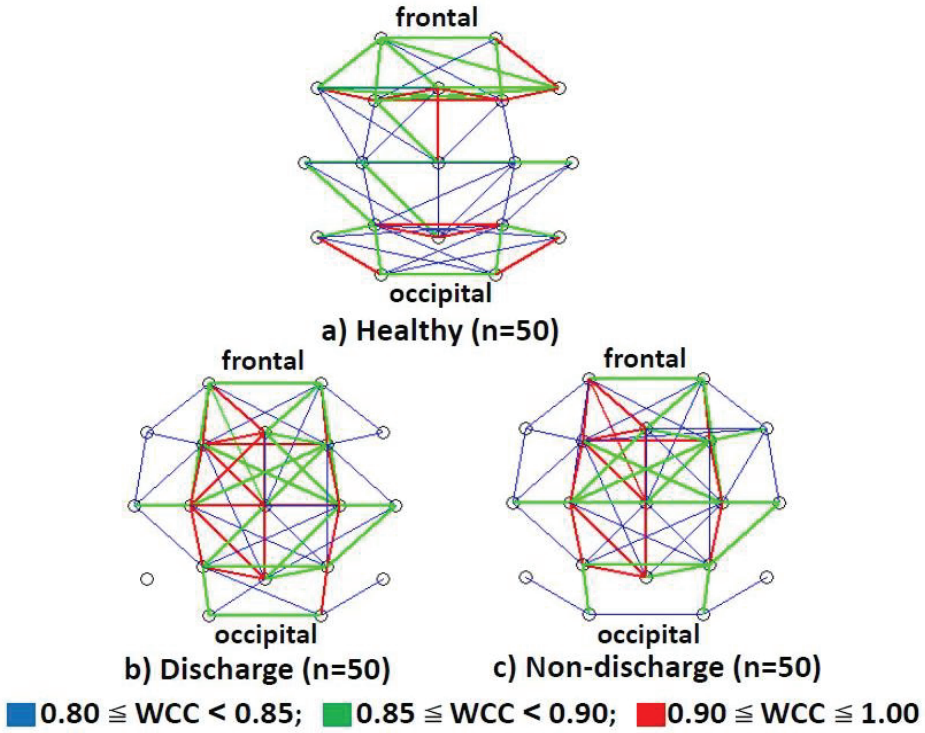

Figure 3.9: Brain graphs of the mean WCC values in the alpha 1 band of all 50 epochs of all healthy subjects (a), of all patients at the time of discharge (b), and non-discharge (c). Blue displays 0.80≦WCC<0.85, green displays 0.85≦WCC<0.90, and red displays 0.90≦WCC≦1.00. [32]

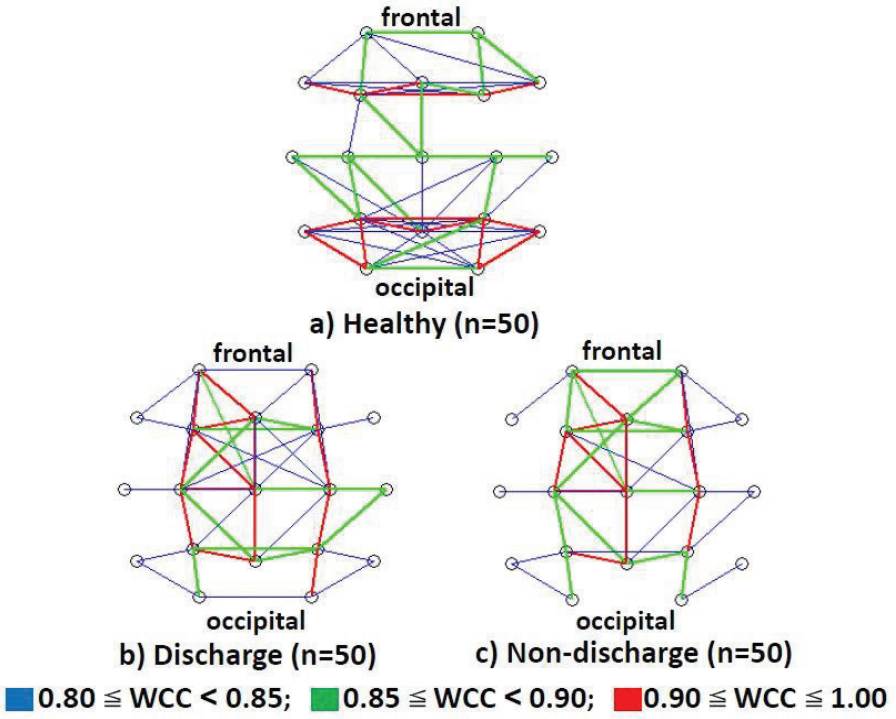

Figure 3.10: Brain graphs of the mean WCC values in the alpha 2 band of all 50 epochs of all healthy subjects (a), of all patients at the time of discharge (b), and non-discharge (c). Blue displays 0.80≦WCC<0.85, green displays 0.85≦WCC<0.90, and red displays 0.90≦WCC≦1.00.

Figure 3.11 shows the mean WCC value between all 19 electrodes of all epochs of the healthy controls, and the mean WCC value between all 19 electrodes of all epochs of the epilepsy patients (during discharge and non-discharge) in the alpha 1 bandwidth. The mean WCC value in the patients at the time of both discharge ($p<0.001$) and non-discharge ($p<0.01$) was significantly higher than the mean WCC value in the brain of healthy individuals. Figure 3.12 shows the mean WCC value between all 19 electrodes of all epochs of the healthy controls, and the mean WCC value between all 19 electrodes of all epochs of the epilepsy patients (during discharge and non-discharge) in the alpha 2 bandwidth. The mean WCC value in the patients at the time of discharge was slightly higher than the mean WCC value in the brain of healthy individuals and slightly higher than during non-discharge, but these differences are non-significant.

Figure 3.13 shows the WCC values averaged over 5 epochs for each individual subject in the alpha 1 band, and figure 3.14 shows the WCC values averaged for each subject in the alpha 2 band. In the alpha 1 band as well as in the alpha 2 band, for both healthy subjects and patients, significant individual differences are visible.

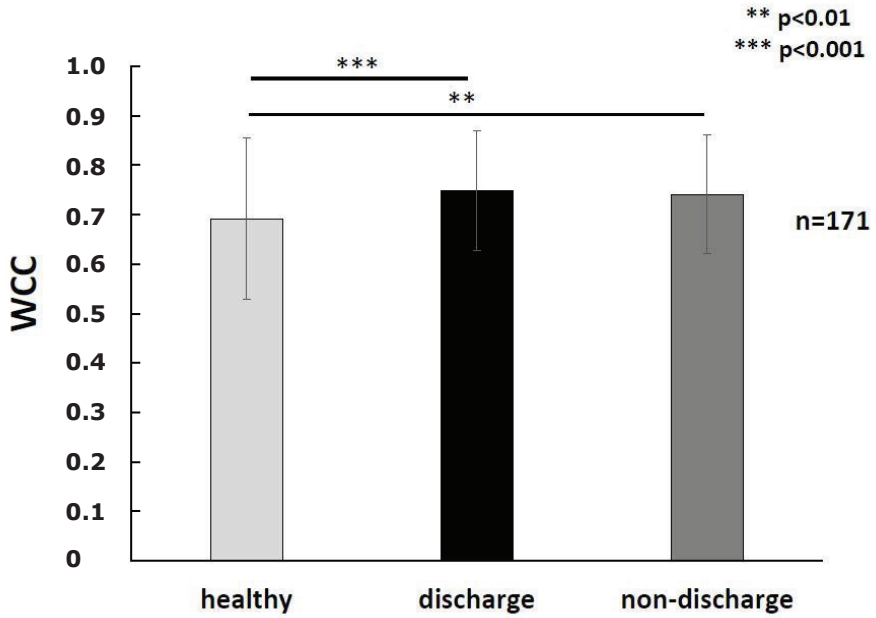

Figure 3.11: The mean WCC value between all 19 electrodes of all 50 epochs in the alpha 1 bandwidth for all healthy subjects, and all epilepsy patients during discharge and non-discharge. [32]

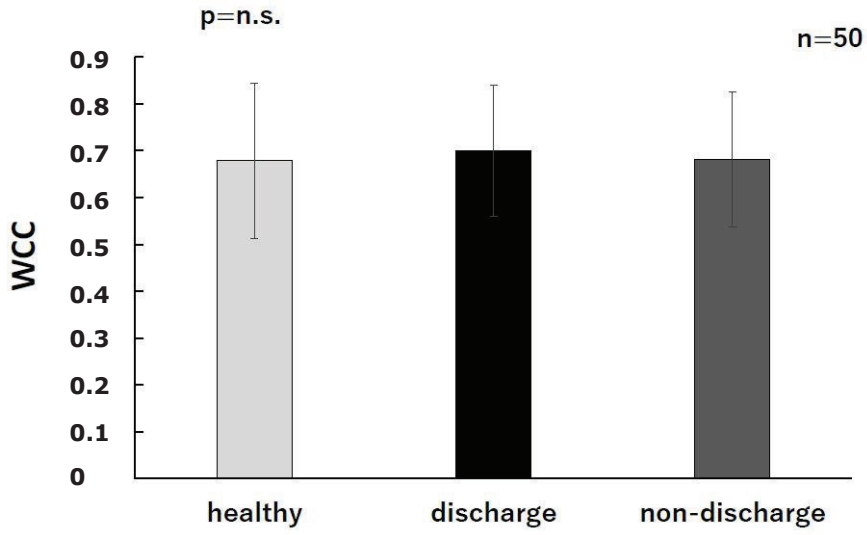

Figure 3.12: The mean WCC value between all 19 electrodes of all 50 epochs in the alpha 2 bandwidth for all healthy subjects, and all epilepsy patients during discharge and non-discharge.

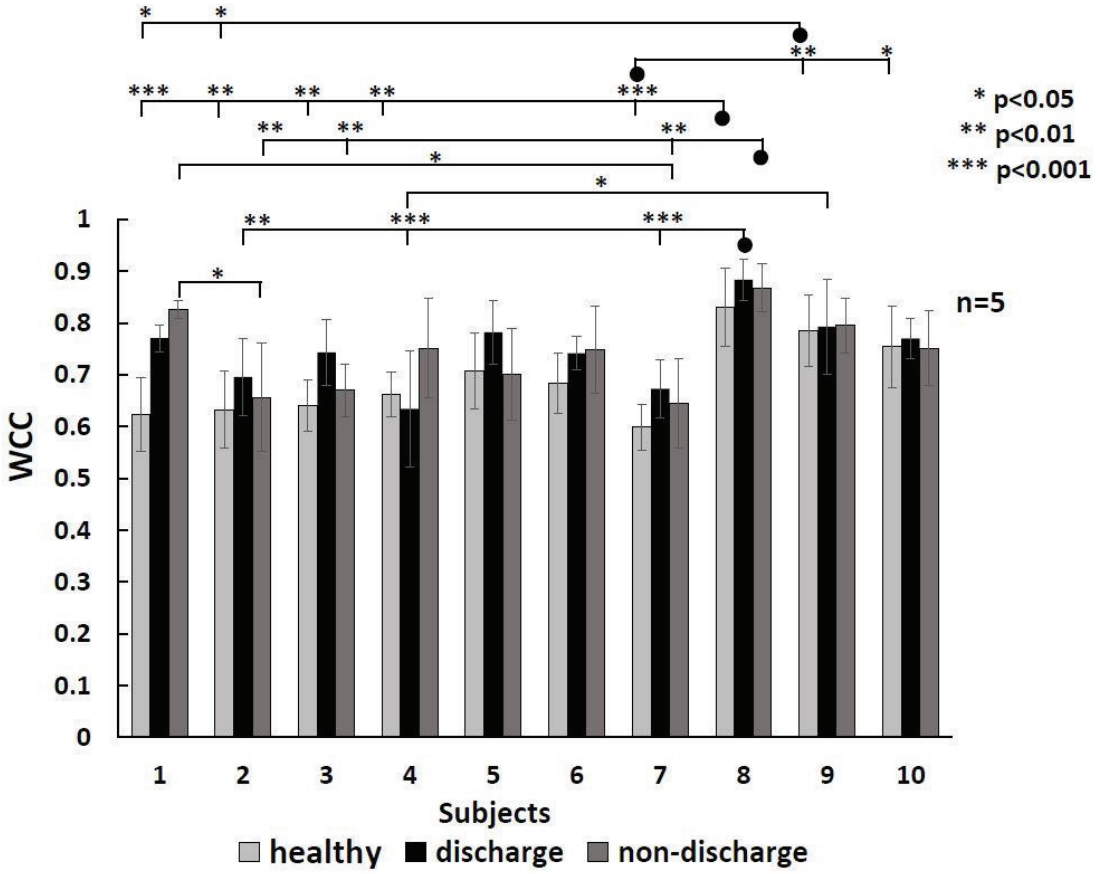

Figure 3.13: WCC values for each individual subject in the alpha 1 band.

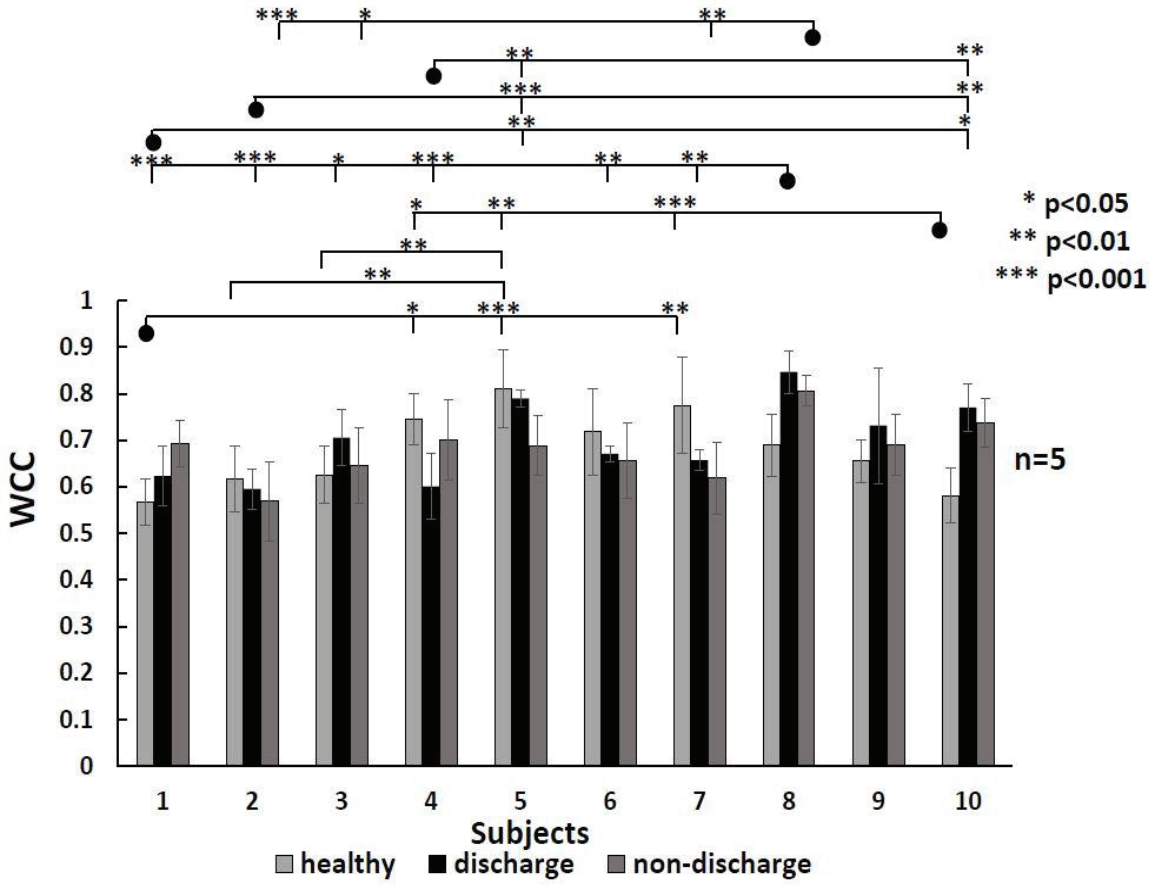

Figure 3.14: WCC values for each dividual subject in the alpha 2 band.

3.3.4 Graph theoretical analysis

3.3.4.1 Global measures

Figure 3.15 shows the comparison of the mean normalized clustering coefficient γ of all 50 epochs (averaged over all sparsity thresholds) among the healthy subjects, the patients during discharge and during non-discharge in the alpha 1 bandwidth. Significantly lower mean γ values were seen in the patients during both discharge and non-discharge compared to the healthy subjects ($p<0.001$). Figure 3.16 shows the mean normalized characteristic path length λ of all epochs for all thresholds in the alpha 1 bandwidth. The mean λ values of the brain network of the patients at the time of both discharge and non-discharge ($p<0.001$) were significantly lower than the mean λ value of the brain network of the healthy subjects. Figure 3.17 shows the comparison of the mean small-worldness σ of all epochs and thresholds in the alpha 1 bandwidth. Significantly lower mean σ values were observed in the brain network of the patients during both discharge and non-discharge than in the healthy subjects ($p<0.01$).

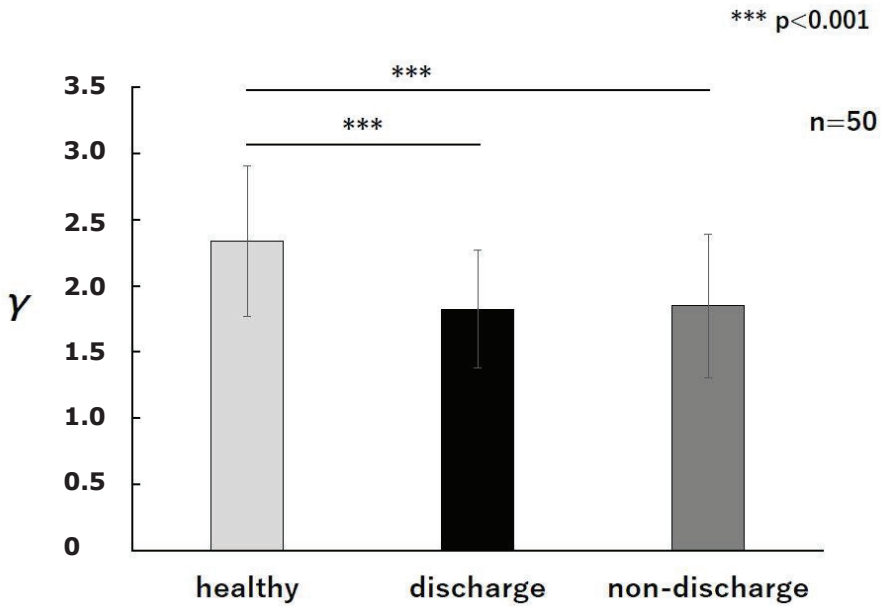

Figure 3.15: The mean value of the global network index γ of all 50 epochs in the alpha 1 band for the healthy subjects, and the patients during discharge and non-discharge. γ was averaged over all sparsity thresholds (10% to 40%). [32]

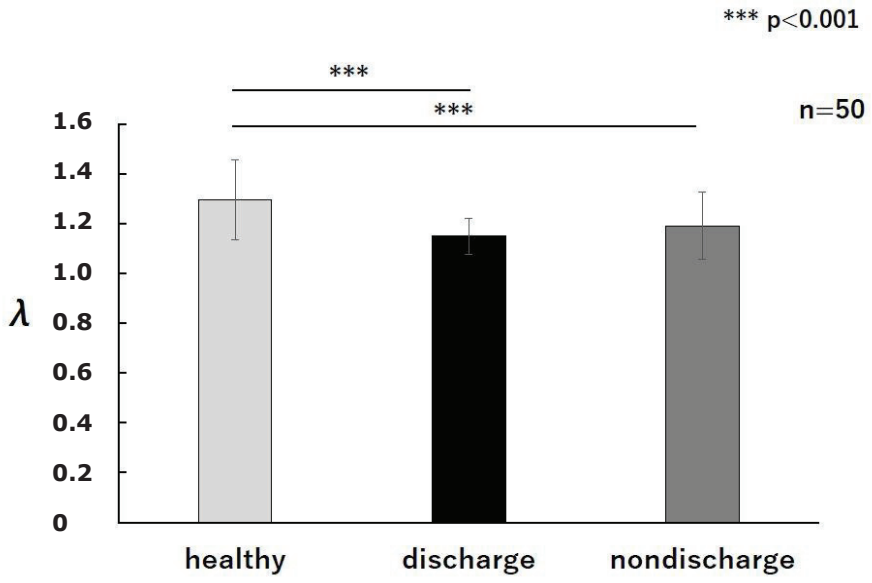

Figure 3.16: The mean value of the global network metric λ of all 50 epochs in the alpha 1 band for the healthy subjects, and the patients during discharge and non-discharge. λ was averaged over all sparsity thresholds (10% to 40%). [32]

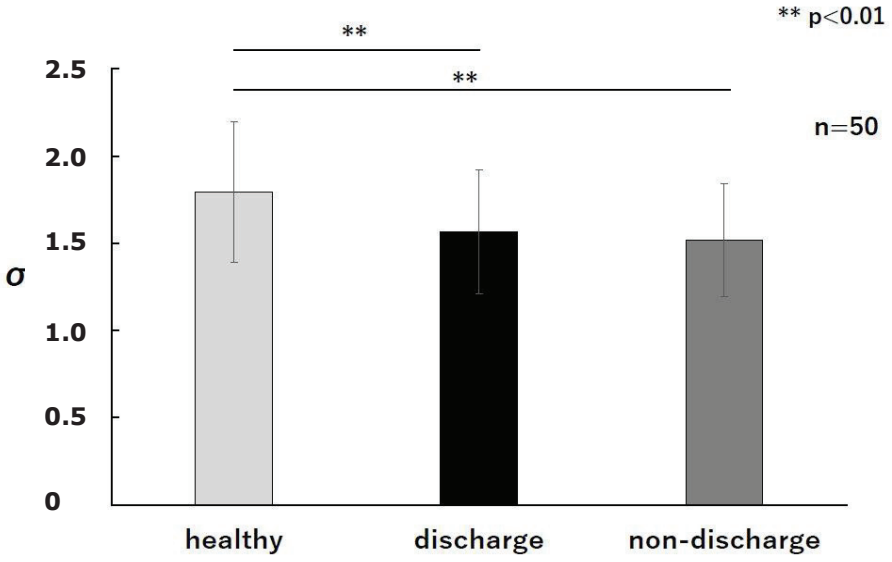

Figure 3.17: The mean value of the global network measure σ of all 50 epochs in the alpha 1 band for the healthy subjects, and the patients during discharge and non-discharge. σ was averaged over all sparsity thresholds (10% to 40%). [32]

Figures 3.18, 3.19, and 3.20 show the change of network indices γ, λ, and σ, depending on the threshold in the alpha 1 band. As described in methods, a range of sparsity thresholds between 0.1 and 0.4 with an increment of 0.01 were calculated, meaning 31 values of γ, 31 values of λ, and 31 values of σ were computed. A common trend was seen for all three measures: the values of γ, λ, and σ decreased with higher edge density (in other words lower WCC threshold) in the alpha 1 band. This decrease occurred for both healthy subjects and patients, both during discharge and non-discharge.

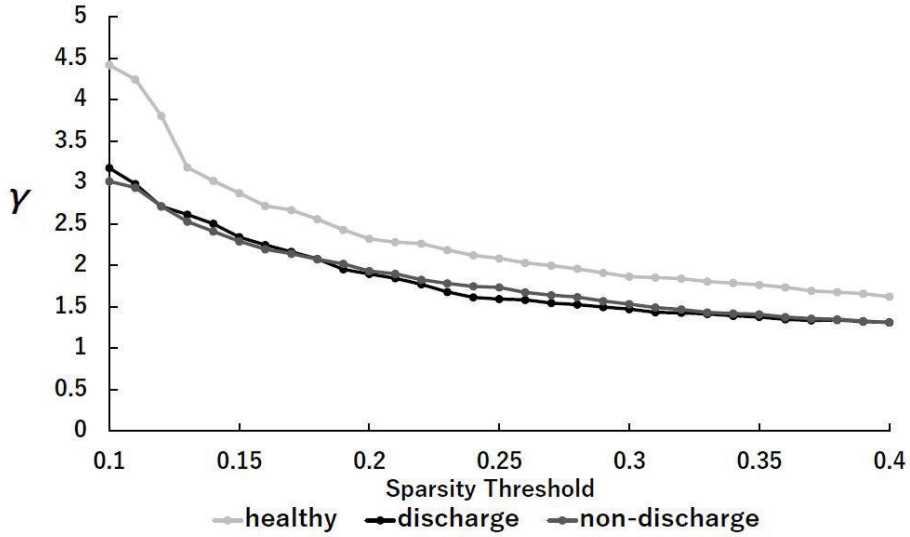

Figure 3.18: Change of γ depending on the sparsity threshold in the alpha 1 band. [32]

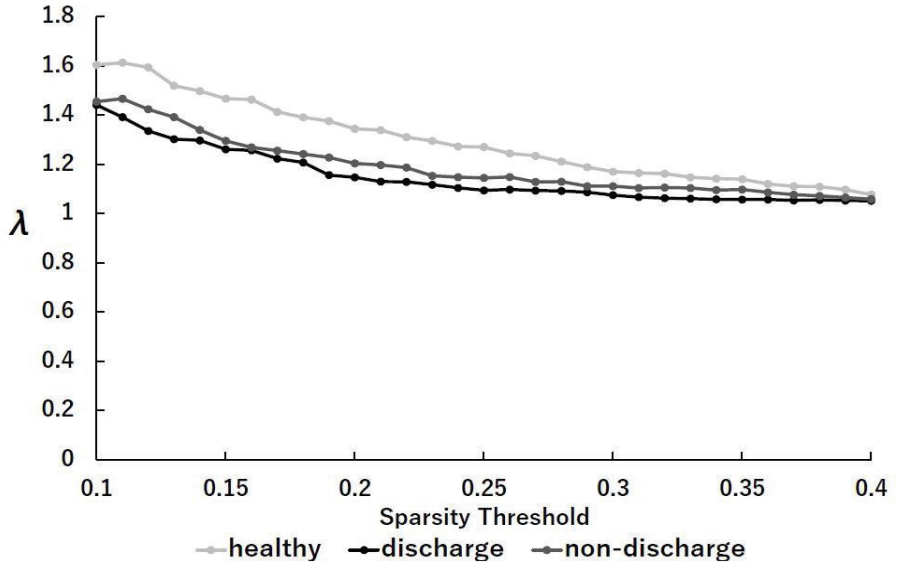

Figure 3.19: Change of λ depending on the sparsity threshold in the alpha 1 band. [32]

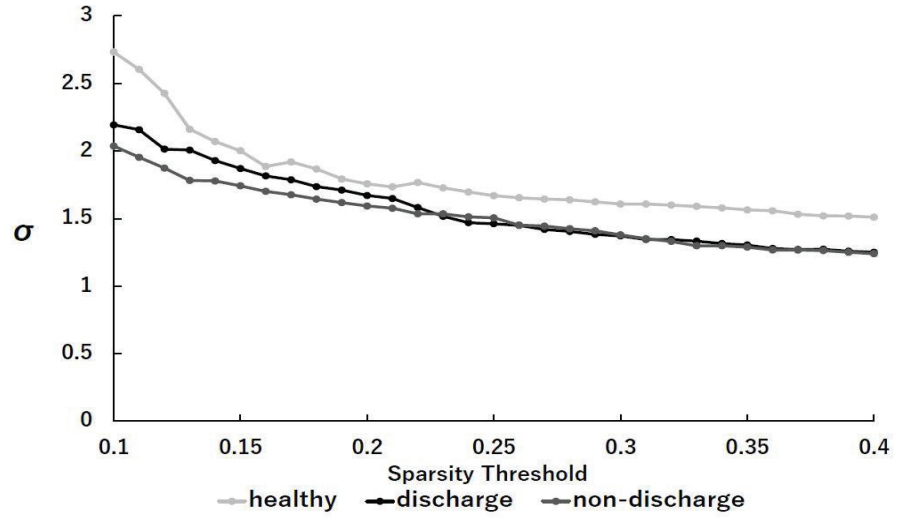

Figure 3.20: Change of σ depending on the sparsity threshold in the alpha 1 band. [32]

Figure 3.21 shows the comparison of the mean normalized clustering coefficient γ of all 50 epochs (averaged over all sparsity thresholds) among the healthy subjects, the patients during discharge and during non-discharge in the alpha 2 bandwidth. Significantly lower mean γ values were seen in the patients during both discharge ($p<0.01$) and non-discharge ($p<0.05$) compared to the healthy subjects. Figure 3.22 shows the mean normalized characteristic path length λ of all epochs for all thresholds in the alpha 2 bandwidth. The mean λ values of the brain network of the patients at the time of both discharge ($p<0.001$) and non-discharge ($p<0.01$) were significantly lower than the mean λ value of the brain network of the healthy subjects. Figure 3.23 shows the comparison of the mean small-worldness σ of all epochs and thresholds in the alpha 2 bandwidth. Lower mean σ values were observed in the brain network of the patients during both discharge and non-discharge than in the healthy subjects, though as opposed to the alpha 1 band, this difference was not significant.

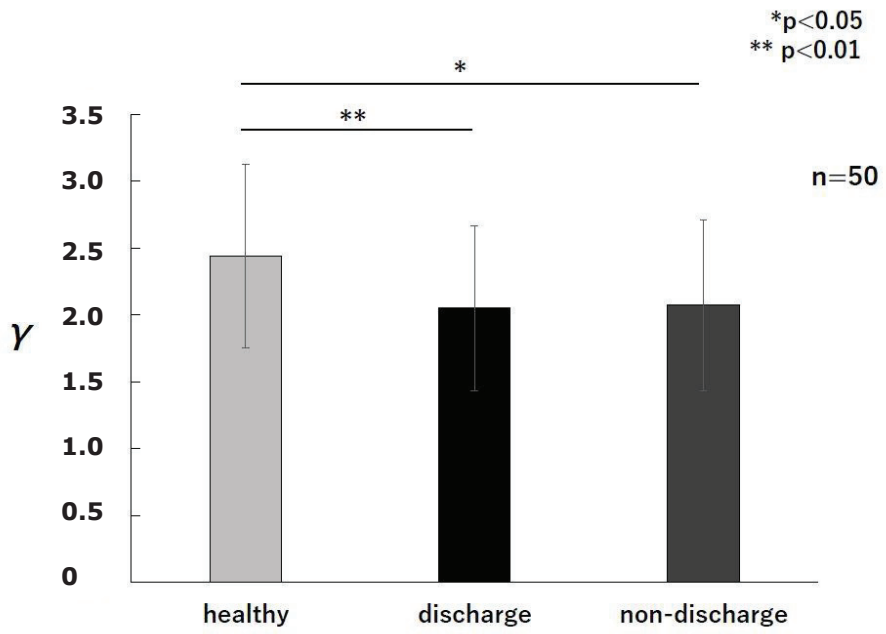

Figure 3.21: The mean value of the global network measure γ of all 50 epochs in the alpha 2 band for the healthy subjects, and the patients during discharge and non-discharge. γ was averaged over all sparsity thresholds (10% to 40%).

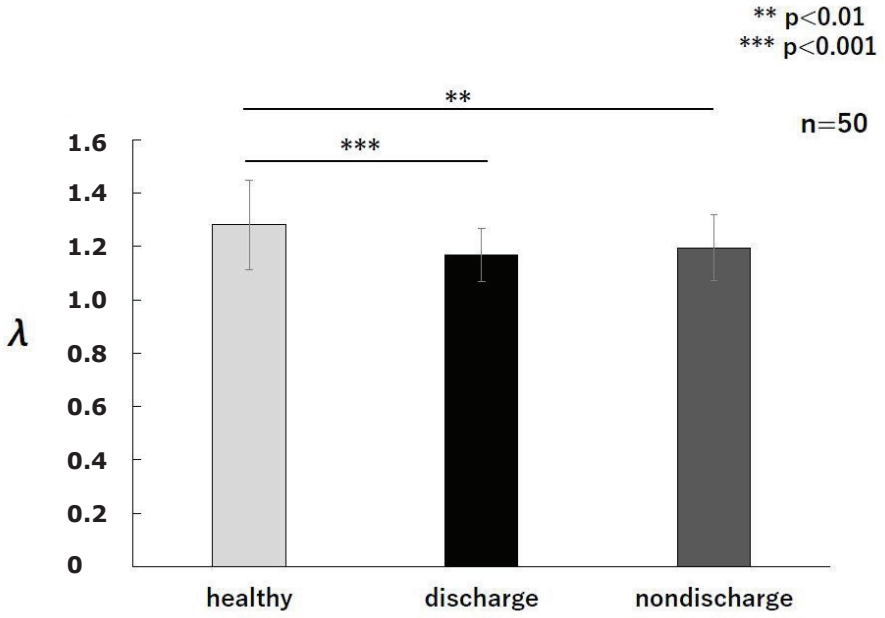

Figure 3.22: The mean value of the global network index λ of all 50 epochs in the alpha 2 band for the healthy subjects, and the patients during discharge and non-discharge. λ was averaged over all sparsity thresholds (10% to 40%).

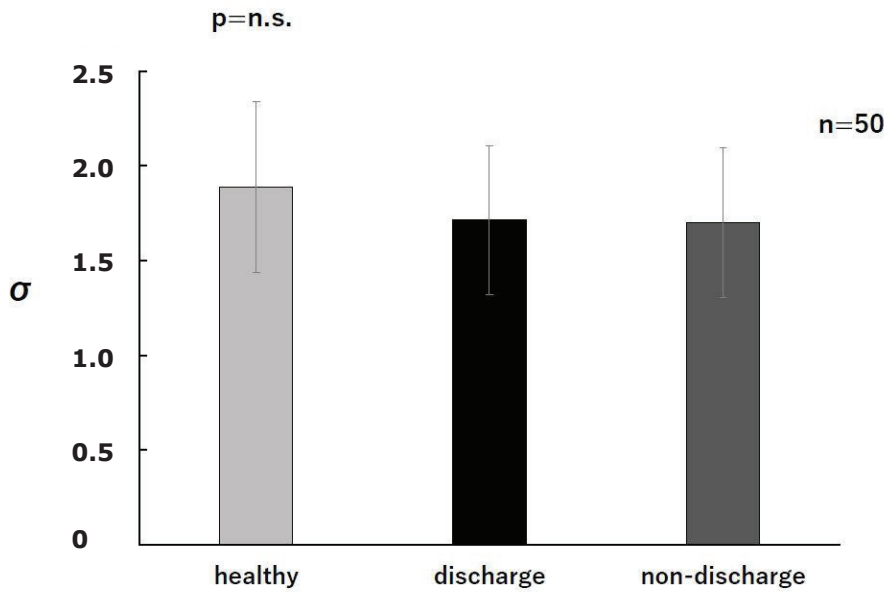

Figure 3.23: The mean value of the global network measure σ of all 50 epochs in the alpha 2 band for the healthy subjects, and the patients during discharge and non-discharge. σ was averaged over all sparsity thresholds (10% to 40%).

Figures 3.24, 3.25, and 3.26 show the change of network indices γ, λ, and σ, depending on the threshold in the alpha 2 band. Similar to the alpha 1 band, the value of all three measures γ, λ, and σ decreased with higher sparsity threshold in the alpha 2 band. This decrease occurred for both healthy subjects and patients, both during discharge and non-discharge.

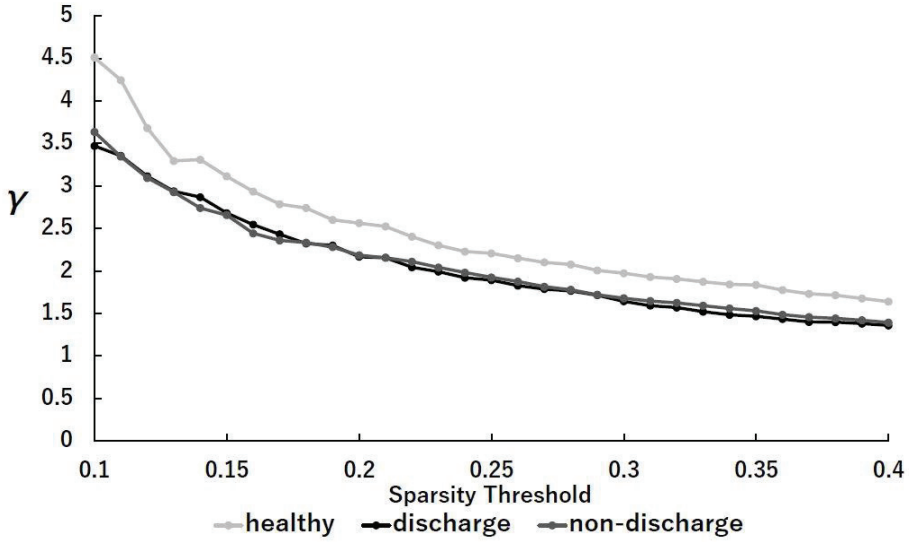

Figure 3.24: Change of γ depending on the sparsity threshold in the alpha 2 band.

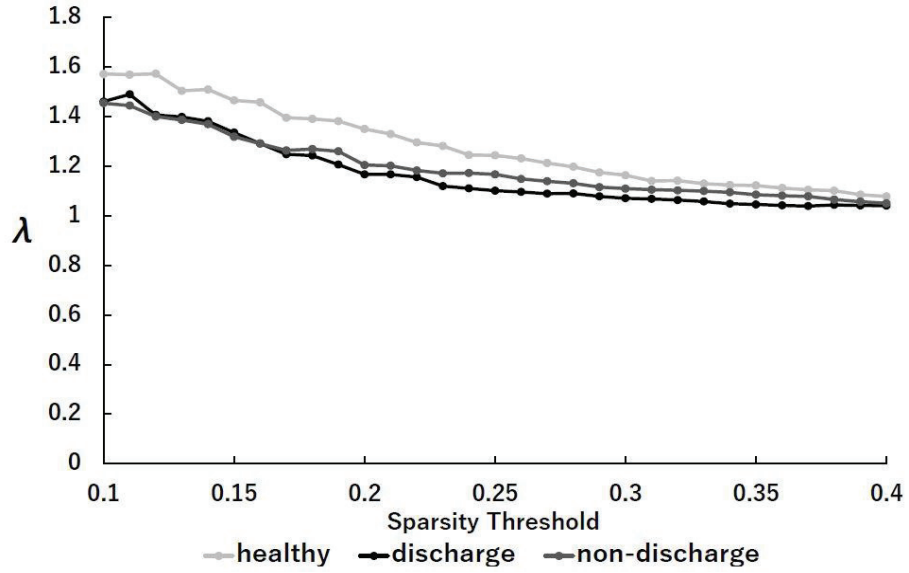

Figure 3.25: Change of λ depending on the sparsity threshold in the alpha 2 band.

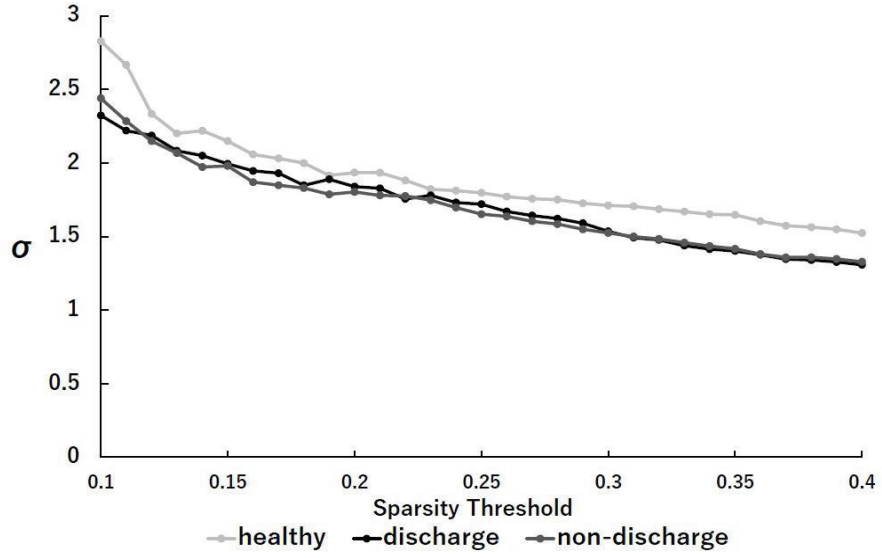

Figure 3.26: Change of σ depending on the sparsity threshold in the alpha 2 band.

Figure 3.27 shows the σ values averaged over 5 epochs for each individual subject in the alpha 1 band, and figure 3.28 shows the σ values averaged for each subject in the alpha 2 band. In the alpha 1 band, for both healthy subjects and patients, non-significant individual differences are visible. In the alpha 2 band, individual differences are visible between the patients.

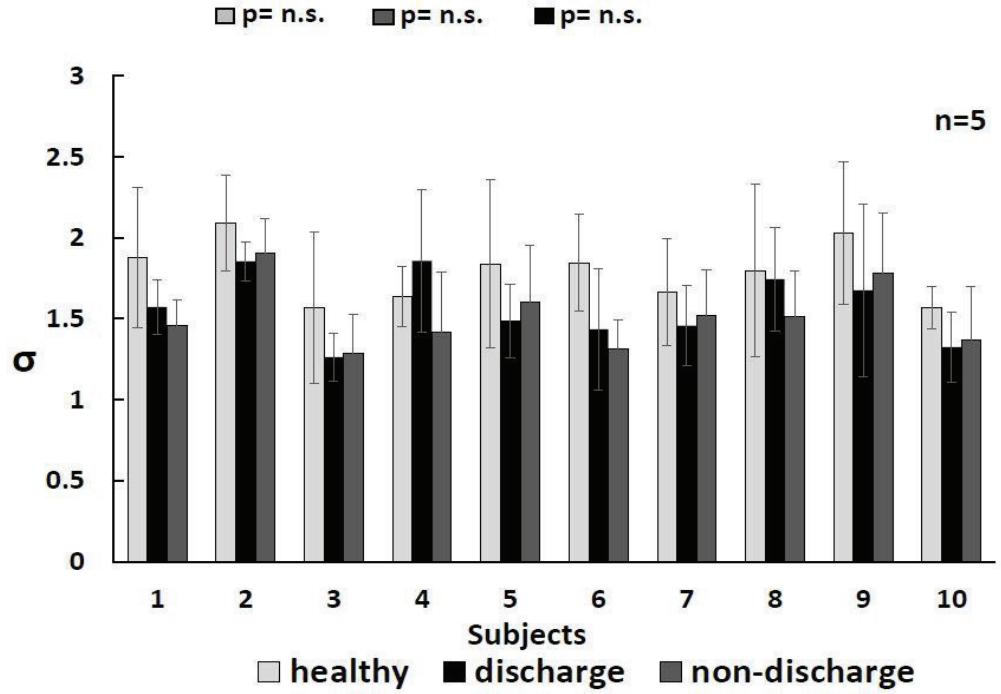

Figure 3.27: σ values for each individual subject in the alpha 1 band.

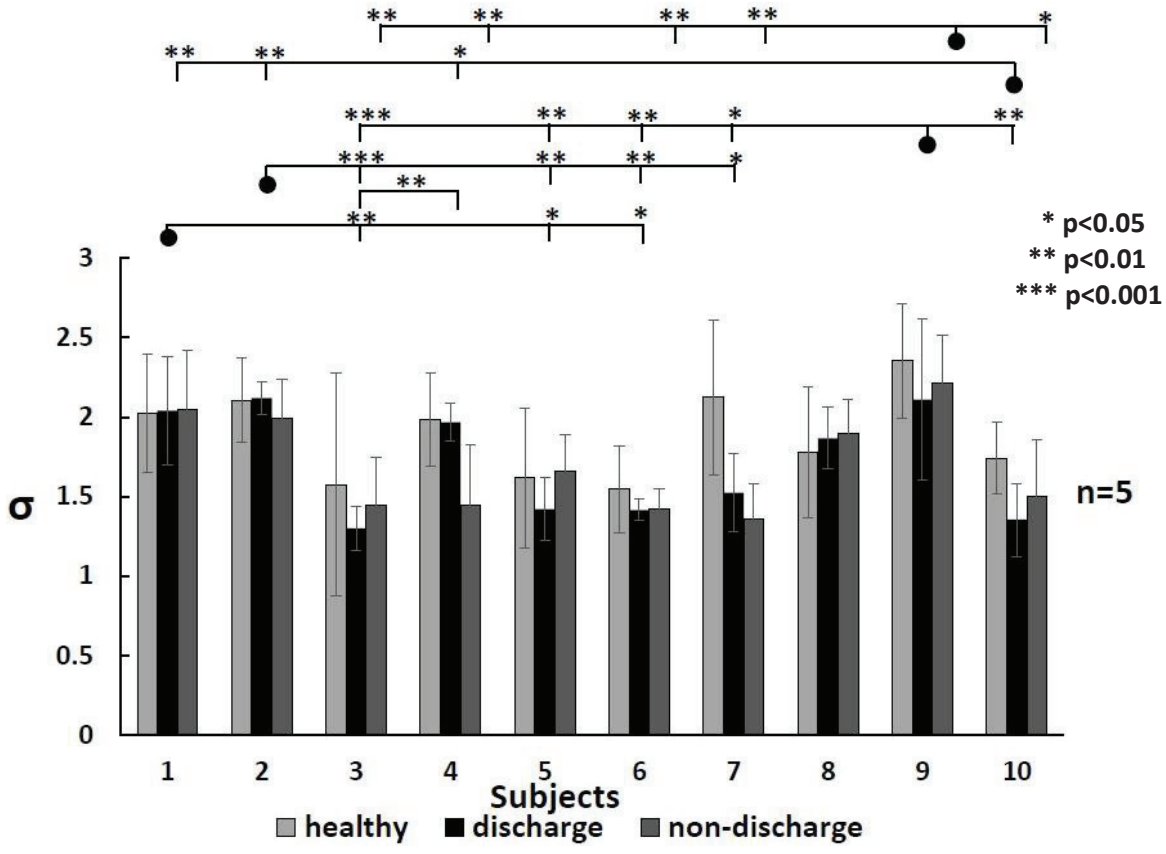

Figure 3.28: σ values for each individual subject in the alpha 2 band.

3.3.4.2 Nodal measures

Figure 3.29 shows the distribution of the nodal betweenness centrality B_i of all healthy subjects (figure 3.29a), of all patients during epileptiform discharge (figure 3.29b), and of all patients during non-discharge (figure 3.29c) in the alpha 1 bandwidth. The color bar on the right shows the values of B_i. In addition, the size of the nodes is proportional to the size of B_i. In the healthy subjects and the patients during non-discharge, high centralities were found in the left, middle, and right central and parietal areas. On the other hand, during discharge, high centrality was observed mainly in the right central area, and there was no high centrality in the middle area. Figure 3.30 shows the distribution of the nodal betweenness centrality B_i of all healthy subjects (figure 3.30a), of all patients during epileptiform discharge (figure 3.30b), and of all patients during non-discharge (figure 3.30c) in the alpha 2 bandwidth. The results in the alpha 2 band differ somewhat from the alpha 1 band. In the healthy subjects and the patients during non-discharge, high centralities were found in the left, middle, and right central areas. The right parietal area showed lower centrality, and the left frontal area showed higher centrality in the healthy subjects than during non-discharge. During discharge, the highest centralities were observed mainly in the right and left central and parietal areas, and there was medium centrality in the middle area.

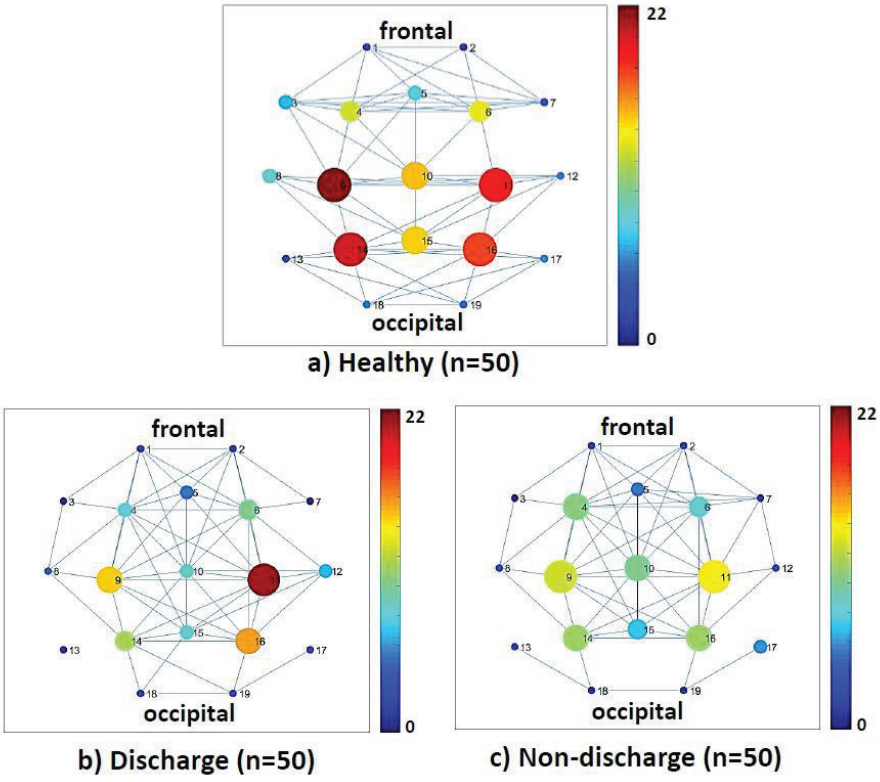

Figure 3.29: Nodal betweenness centrality B_i of all 19 vertices in the alpha 1 bandwidth, represented in a brain graph. The color bar on the right shows the value of B_i. [32]

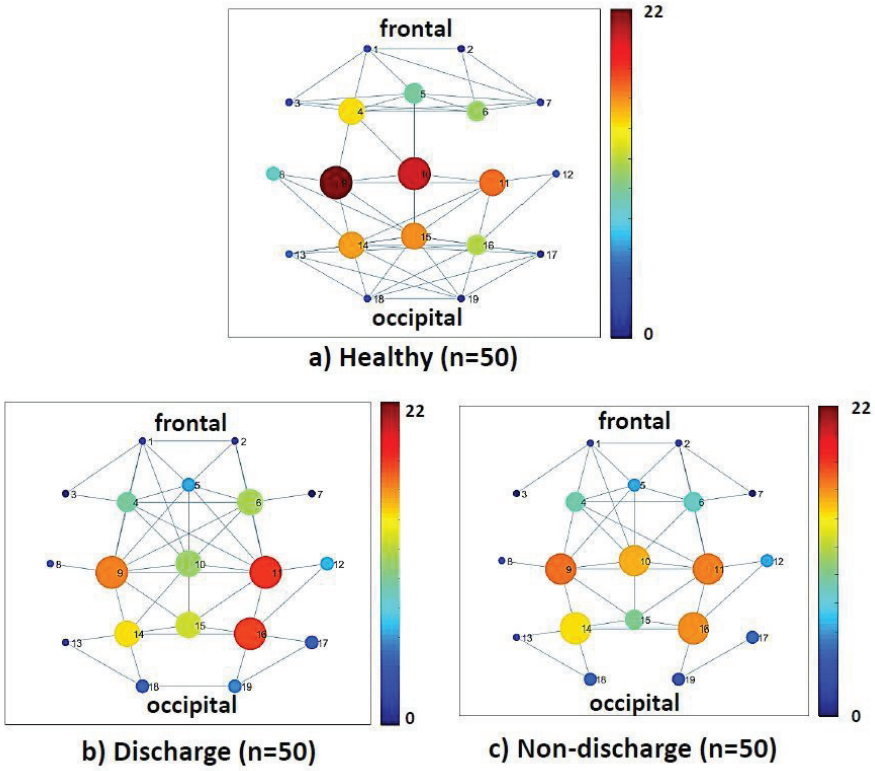

Figure 3.30: Nodal betweenness centrality B_i of all 19 vertices in the alpha 2 bandwidth, represented in a brain graph. The color bar on the right shows the value of B_i.

Figure 3.33 shows the normalized betweenness centrality b_i of the hub vertices (b_i >1.5) for the healthy subjects and the patients during discharge and non-discharge in the alpha 1 band. F3 was a hub region in the brain network of the patients only during non-discharge, and had a significantly higher b_i than during discharge ($p<0.05$). C4 was a hub region for all subjects, but a significantly higher b_i was observed during discharge compared to non-discharge ($p<0.05$) and healthy ($p<0.001$). In the patients' brain network during discharge, Cz was not a hub region, as opposed to during non-discharge and the control group. Pz was only a hub area in the healthy subjects. Figure 3.34 shows the normalized betweenness centrality b_i of the hub vertices for the healthy subjects and the patients during discharge and non-discharge in the alpha 2 band. F3 was only a hub region in the brain network of the healthy individuals. In the patients' brain network during discharge, Cz was not a hub region, as opposed to during non-discharge and the control group. Pz was a hub region in the healthy subjects and in the patients during discharge, but not during non-discharge. As opposed to the healthy subjects, P4 was significantly a hub area in the patients both during discharge ($p<0.05$) and non-discharge ($p<0.05$).

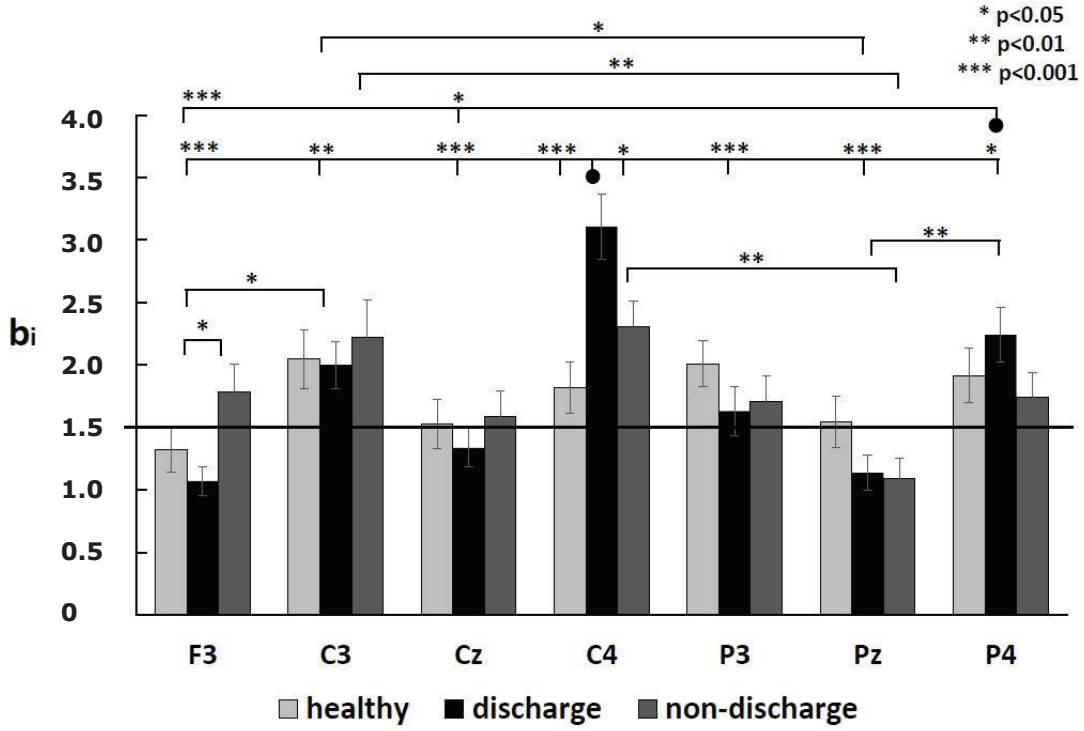

Figure 3.33: Normalized betweenness centrality b_i of the vertices displaying the highest values in the alpha 1 band. Vertices with b_i values >1.5 were considered hubs of the network. [32]

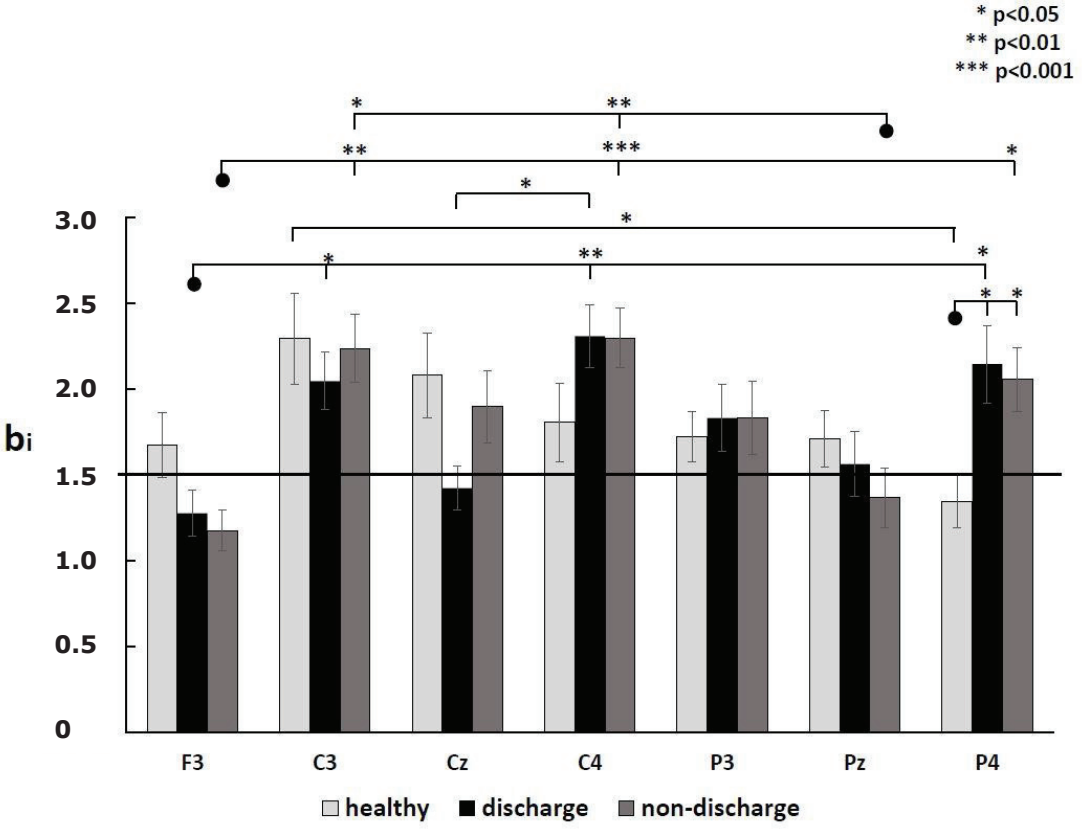

Figure 3.34: Normalized betweenness centrality b_i of the vertices displaying the highest values in the alpha 2 band. Vertices with b_i values >1.5 were considered hubs of the network.

3.4 Discussion

In the current study, scalp recorded EEG data were analyzed by using wavelet–crosscorrelation analysis to derive networks of functional connectivity, and applied graph theory to analyze the spatial distribution of the functional networks. The functional network between the healthy individuals and epilepsy patients, as well as the interictal functional network of the brain of epilepsy patients during epileptiform discharge with during non-discharge were compared. The main findings were that the functional connectivity strength, as well as the functional network configuration in the brain of the epilepsy patients, both at the time of discharge and at the time of non-epileptiform discharge, were altered compared to the healthy subjects. The novel finding of this study is that even though in the patients, the functional connectivity and small-worldness of the brain did not show significant differences between discharge and non-discharge, the centrality and the spatial distribution of the hub regions were different between during epileptiform discharge and during non-discharge.

3.4.1 Wavelet spectra and WCC comparison

After performing wavelet transform on the EEG data, the wavelet spectra showed large differences between the healthy subjects and the patients. The spectral activity at the time of discharge is much higher, and is spread over the theta band in addition to the alpha band compared to during non-discharge and in the healthy brain. Visualizing EEG in a map of wavelet spectra shows at which frequencies the highest spectral activity occurs, and could be helpful for clinical doctors to more easily interpret the neuronal activity between different brain regions [42]. Wavelet–crosscorrelation analysis allowed to construct functional connectivity networks, and reveal the strongest correlation strengths for each group. Visualizing functional connectivity patterns might reveal a lot about brain dynamics and brain function. Functional networks may reveal connections or information beyond the anatomical structure [66]. It has been reported that functional connections undergo spontaneous fluctuations on very short timescales, reflecting responses to sensory input and cognitive tasks [1,85]. On longer timescales however, functional connectivity networks have been found to be robust [86]. In the results of the present study, strong connections seemed to be clustered in the frontal and occipital areas in the healthy subjects, whereas in the patients, strong connections appeared widely over the entire network. This finding is similar to the study described in chapter II, which suggested that the communication in the brain of neuropsychiatric patients may be only possible if all regions of the brain are actively involved [42]. Similar to the study of chapter II, the brain of the epilepsy patients showed significantly higher total functional

connectivity compared to the healthy subjects. Previous research based on EEG has also found increased connectivity in the interictal functional networks in epilepsy patients [17,60,87]. An increased functional connectivity has been reported in the temporal lobes in individuals with temporal lobe epilepsy compared to healthy subjects [55]. Since cognitive dysfunction has been reported in epilepsy patients [72], it could be the case that the higher connectivity in the brain of epilepsy patients might be a compensation mechanism for the loss of optimal brain function. The present study showed a small, non-significant increase in functional connectivity (WCC) in the alpha 1 bandwidth during epileptiform discharge compared to non-discharge in the patients, which is similar to a study of Yamaguchi et. al. based on EEG recordings in epilepsy patients [88]. By using graph theoretical analysis, this study examined whether or not in the alpha bandwidth, the brain network topology of epilepsy patients has significant differences between discharge and non-discharge.

3.4.2 Graph theoretical analysis: Small-worldness

This study examined the small-worldness of the brain network of the healthy subjects, and the patients during epileptiform discharge and during non-discharge. It is believed that the human brain functional network develops for an optimal balance between segregation (specialized processing within dense interconnected brain areas) and functional integration (the ability to rapidly combine specialized information from brain regions) between these specialized brain areas [62,66,77]. This optimal balance has been referred to as complexity [65,89]. The clustering coefficient of a network can be seen as a measure of functional segregation, whereas the characteristic path length can be considered a measure of functional integration [77]. Brain networks with a small-world topology are considered to be optimal for brain functioning and maximizing complexity [1,68,90]. Previous studies have suggested a loss of optimal brain function due to a loss of the optimal small-world topology in the brain network of individuals with neuropsychiatric diseases [61,71].

The results of the present study showed that the network topology of the healthy subjects had a small world configuration ($\gamma >> 1$, $\lambda \geq 1$, and $\sigma > 1$). Networks can gradually transition from a completely small-world topology to a completely random topology ($\gamma \geq 1$, $\lambda \approx 1$, and $\sigma \geq 1$) [67,68]. These findings showed a loss of small-world topology toward a more random, less optimal configuration (decreased clustering and an even shorter path length) in the brain network of the epilepsy patients. These results suggest that the brain network of the epilepsy patients is less optimal and might function less efficient. Decreased γ, λ, and σ in the interictal period of epilepsy patients were also observed in fMRI and electrocorticography studies [55,91]. A study based on MEG concluded that a very low path length may be responsible for a tendency to excessive synchronization and

epileptic seizures in brain tumor patients [63]. The results of the present study are in line with these previous network studies. Synchronization of neurons in healthy brain networks is important for normal functioning and information processing [62]. However, a change in topology due to brain disease might further lower the brain's threshold for synchronization [62], which increases susceptibility to seizures. It has been suggested that brain networks are located dynamically on a critical point between local neuronal synchronization to global synchronization [92]. Several model studies support the notion that a more random topology causes a network to synchronize more easily due to lowering the threshold for synchronization [93–95]. The cause of the randomization of the network could be due to cell loss inflicted by epileptic lesions, resulting in fewer connections [90]. Interestingly, a more random network topology was also found at the time of non-discharge. This suggests a continuous brain dysfunction of epilepsy patients, and continuous susceptibility for seizures during the interictal period.

3.4.3 Graph theoretical analysis: Betweenness Centrality

The current study revealed a decreased nodal centrality of some regions in the patients' brain network during epileptiform discharge. The brain network during non-discharge showed a hub distribution closer to that of the healthy subjects. Hub areas are important to facilitate information transfer in the brain network [1,66], making hubs points of vulnerability to brain dysfunction [82,96]. A change of spatial distribution of hubs may result in a less efficient information flow in the brain network, therefore disrupting the functional connectivity of the brain [79,96]. The brain graphs displaying the nodal centrality in the patients during discharge showed a loss of hubs mainly along the z-line. This may suggest a separate, less efficient flow of information in the left and right hemispheres than in healthy subjects. On the other hand, a very high centrality was found in the right hemisphere (C4) during discharge. This may be interpreted as a compensation mechanism for the inefficient information transfer.

Several measures were computed in present study. The small-worldness σ is a powerful index because it combines the indices γ and λ, and tells more about the topological organization and function of the brain than correlation indices such as WCC. While the optimal network topology of the brain has been reported as being small-world, the optimal functional connectivity in the brain is not clearly defined [1,68]. The present study showed lower small-worldness in the patients' brains even at the time of non-discharge activity, therefore the index σ might aid to distinguish the healthy brain from the epileptic brain.

In order to diagnose epilepsy with higher sensitivity, it might be meaningful to develop a computer-aided diagnosis system to automatically distinguish interictal epileptiform discharge epochs from non-discharge epochs using for example machine learning tech-

niques or automated detection algorithms. The difference in the centrality index between discharge and non-discharge epochs found in our study might be used in future machine learning algorithms.

3.5 Conclusion

In conclusion, the results of this study suggest that graph theoretical analysis of the human brain functional connectivity network derived from the correlation between EEG time series might provide a deeper understanding of the pathophysiological mechanisms underlying brain dysfunction in neuropsychiatric disorders such as epilepsy. The present study provides further evidence for a loss of the optimal small-world configuration of the functional network of epilepsy patients in the direction of a more random network. This more random network seems to push the dynamics of the brain from an optimal intellectual function toward a pathological, seizure-prone state. Furthermore, it was shown that this disturbance in the functional connectivity may be persistently present in the interictal period even when no epileptiform discharges are visible in the EEG. Network indices might therefore aid to distinguish the epileptic brain from the healthy brain, and aid to diagnose epilepsy with a higher sensitivity. The nodal betweenness centrality index might aid to distinguish EEGs at the time of epileptiform discharges from EEGs at the time of non-discharges.

Conflict of interest: The author declares no competing financial interests.

Ethical approval: All procedures performed in studies involving human participants were in accordance with the ethical standards of the Ethics Committee of the Graduate School of Applied Informatics of the University of Hyogo at which the studies were conducted (IRB approval number UHGSAI-2018-9).

Informed consent: Informed consent was obtained from all individual participants included in the study.

Chapter Ⅳ

Conclusions

Overall Summary and Conclusions

In this dissertation, engineering theory and methodology were applied to the medical field of clinical neurophysiology. This research has been conducted in an attempt to explore the functional connectivity and changes in functional activity in the brain derived from EEG data and using wavelet-crosscorrelation analysis and network analysis based on graph theory. The methods and results described in this thesis have made the pathology of the brain of mental disorder and epilepsy patients clear. In the brain of mental disorder patients, strong connectivity patterns were found which seem to compensate for a less efficient information transfer in terms of time. In the epileptic brain, a very short characteristic path length was found which causes the brain in epilepsy patients to synchronize too much, resulting in epileptic seizures to occur easier (seizure-prone state).

The results of chapter II suggest that by using wavelet-crosscorrelation analysis and calculating WCC values, it is possible to abstract the correlation and the connectivity strength between the different parts inside the brain. The connectivity patterns inside the brain were revealed, and compared between healthy individuals and patients who suffer from neuropsychiatric illnesses. The results confirm that the WCC value between the sites in the brain of neuropsychiatric disorder patients who have the diffuse alpha pattern differs from the brain of healthy individuals. The correlation between all sites of the brain in general, as well as the correlation along the coronal and sagittal orientations of the brain, is significantly higher in the patients than in healthy individuals. It can be concluded that the information propagation and connectivity strength between the sites in the entire brain, as well as along the sagittal and coronal orientations could be stronger in the brain of the mental disorder patients than in the healthy individuals.

The results of chapter III suggest that graph theoretical analysis of the human brain functional connectivity network derived from the correlation between EEG time series might provide a deeper understanding of the pathophysiological mechanisms underlying brain dysfunction in neuropsychiatric disorders such as epilepsy. The study in chapter III provides further evidence for a loss of the optimal small-world configuration of the functional network of epilepsy patients in the direction of a more random network. This more random network has a very short path length, and seems to push the dynamics of the brain from an optimal intellectual function toward a pathological, seizure-prone state. Furthermore, it was shown that this disturbance in the functional connectivity may be persistently present in the interictal period even when no epileptiform discharges are visible in the EEG. Network indices might aid to distinguish the epileptic brain from the healthy brain, and aid to diagnose epilepsy with a higher sensitivity. The nodal betweenness centrality index might aid to distinguish EEGs at the time of epileptiform discharges from EEGs at the time of non-discharges.

The results of both studies show that the functional connectivity differs between healthy individuals and neuropsychiatric and epilepsy patients. By revealing the strength of the functional connectivity and the connectivity patterns in the brain of healthy individuals, as well as mental disorder and epilepsy patients, time series analysis techniques such as Wavelet-crosscorrelation analysis could aid in the diagnosis of neuropsychiatric diseases [2]. The brain can be seen as a complex functional network, and performing network analysis based on graph theory provides further characterization and quantification of the functional network of the brain. This provides a deeper understanding of how disturbances in brain function occur by revealing failing network characteristics [1,87]. Combining WCC or other connectivity measures with network measures makes the pathology in the brain clear by revealing the changes in the brain function of individuals suffering from brain disorders. This could lead to a deeper understanding of how the information transfer between brain areas fails, and may reveal the causes of brain dysfunction.

Conducting network analysis in addition to connectivity analysis may lead to a better diagnosis and better treatment of neuropsychiatric diseases and epilepsy in the future. It may become possible to find individuals with a potential brain disorder more easily. Individuals whose wavelet spectra and/or brain graphs have features in between healthy and mental disorder patients could be regarded as potential mental disorder patients. The methods and results described in this thesis may therefore help to predict brain disorders.

.

List of References

[1] Bullmore E and Sporns O; Complex brain networks: graph theoretical analysis of structural and functional systems, *Nature Reviews Neuroscience*, 10, pp.186-198, 2009.

[2] Basset DS and Bullmore E; Human Brain Networks in Health and Disease., *Current Opinion in Neurology*, 22(4), pp.340-347, 2009.

[3] Sand T, Bjork MH, and Vaaler AE; Is EEG a useful test in adult psychiatry?, *Tidsskr Nor Legeforen*, 133(11), pp.1200-1204, 2013.

[4] Teplan M; The fundamentals of EEG measurement, *Measurement science review*, 2(2): pp.1-11, 2002.

[5] "脳波の世界 脳波", http: //brainsc.com/eeg/ [2020/12/22]

[6] Niedermeyer E, and Lopes da Silva S; Electroencephalography. Basic Principles, Clinical Applications, and Related Fields; Fourth edition, Williams and Wilkins, Baltimore, 1999.

[7] "研究のための脳波の基礎知識", http://www.miyukinet.co.jp/jp/seminar/solveBrainfunc/solveBrainfunc.shtml [2020/12/22]

[8] Tatum IV WO; Normal adult EEG; In: Current Practice of Clinical Electroencephalography; 4th edition; ed. J.S. Ebersole, associate eds. A.M. Husain, and D.R. Nordli; Wolters Kluwer Health, Philadelphia, 2014.

[9] Okuma T; Clinical Electroencephalography; Igaku-Shoin Ltd., Tokyo, 1999 (in Japanese).

[10] Kadobayashi I, Inouye T, and Nakamura M; Electroencephalography; Kinpodo, Kyoto, 1983.

[11] Dement WC and Vaughan C; The Promise of Sleep; Dell Publishing, New York, 1999.

[12] Bertrand J, Tremblay J, Lassonde M, Vannasing P, Nguyen DK, Robert M, Bouthillier A, and Lepore F; Recognizing an object from the sum of its parts: an intracranial study on alpha rhythms, *Journal of Cognitive Neuroscience*, 26(8), pp.1797-1805, 2014.

[13] Nunez PL and Srinivasan R; Electric Fields of the Brain. The Neurophysics of EEG; Second edition, Oxford University Press, New York, 2006.

[14] Libenson MH; Practical Approach to Electroencephalography; Saunders Elsevier, Philadelphia, 2010.

[15] Kaplan HI, and BJ Sadock; Synopsis of Psychiatry. Behavioral Sciences. Clinical Psychiatry; 5th edition, Williams and Wilkins, Baltimore, 1988.

[16] Vecchio F, Miraglia F, Curcio G, Della Marcia G, Vollono C, Mazzucchi E, Bramanti P, and Maria Rossini P; Cortical connectivity in Fronto-temporal focal epilepsy from EEG analysis: A study via graph theory, *Clinical Neurophysiology*, 126(6), pp.1108-1116, 2015.

[17] Douw L, de Groot M, van Dellen E, Heimans JJ, Ronner HE, Stam CJ, and Reijneveld JC; Quantitative EEG as a predictive biomarker for Parkinson disease dementia, *Neurology*, 77(2), pp.118-124, 2011.

[18] "International League Against Epilepsy" https://www.ilae.org/guidelines/definition-and-classification [2021/6/13]

[19] Kramer MA, Kolaczyk ED, and Kirsch HE; Emergent network topology at seizure onset in humans; *Epilepsy Research*, 79(2-3), pp.173-186, 2008.

[20] "epilepsy treatment" https://www.nhs.uk/conditions/epilepsy/treatment/ [2021/6/13]

[21] Muldoon SF, Costantini J, Webber WRS, Lesser R, and Bassett DS; Locally stable brain states predict suppression of epileptic activity by enhanced cognitive effort, *NeuroImage: Clinical*, 18, pp. 599-607, 2018.

[22] Binnie CD and Prior PF; Clinical neurophysiology; Volume 2, Elsevier science, Amsterdam, 2003.

[23] Klassen BT, Hentz JG, Shill HA, Driver-Dunckley E, Evidente VGH, Sabbagh MN, Adler CH, and Caviness JN; Quantitative EEG as a predictive biomarker for Parkinson disease dementia, *Neurology*, 77(2), pp.118-124, 2011.

[24] Kirschfeld K; The physical basis of alpha waves in the electroencephalogram and the origin of the "Berger effect", *Biological Cybernetics*, 92(3), pp.177-185, 2005.

[25] Haegens S, Cousijn H, Wallis G, Harrison PJ, and Nobre AC; Inter- and intra-individual variability in alpha peak frequency, *Neuroimage*, 92, pp.46-55, 2014.

[26] Pentilla M, Partanen JV, Soininen H, and Riekkinen PJ; Quantitative analysis of occipital EEG in different stages of Alzheimer's disease, *Clinical Neurophysiology*, 60(1), pp.1-6, 1985.

[27] Dubovik S, Ptak R, Aboulafia T, Magnin C, Gillabert N, Allet L, Pignat J, Schnider A, and Guggisberg AG; EEG alpha band synchrony predicts cognitive and motor performance in patients with ischemic stroke, *Behavioral Neurology*, 26(3), pp.187-189, 2013.

[28] Debener S, Beauducel A, Nessler D, Brocke B, Heilemann H, and Kayser J; Is resting anterior EEG alpha asymmetry a trait marker for depression? Findings for healthy adults and clinically depressed patients, *Neuropsychobiology*, 41(1), pp.31-37, 2000.

[29] Lotz BP; Recurrent attacks of unconsciousness with diffuse alpha activity, *Sleep*, 16(7), pp.671-677, 1993.

[30] Jiang Z, and Zheng L; Inter- and intra-hemispheric EEG coherence in patients with mild cognitive impairment at rest and during working memory task, *Journal of Zhejiang University Science B*, 7(5), pp.357-364, 2006.

[31] Zheng L, Jiang Z, and Yu E; Alpha spectral power and coherence in the patients with mild cognitive impairment during a three-level working memory task, *Journal of Zhejiang University Science B*; 8(8), pp.584-592, 2007.

[32] Carpels SMA, Yamamoto Y, and Mizuno-Matsumoto Y; Graph Theoretical Analysis of Interictal EEG Data in Epilepsy Patients during Epileptiform Discharge and Non-discharge, *International Journal of Affective Engineering*, 20(3), pp.131-142, 2021.

[33] “サンプリング周波数と基本周波数”, http://www.densikairo.com/Development/Public/study_dsp/A5B5A5F3A5D7A5EAA5F3A5B0BCFEC7C8BFF4A4C8B4F0CBDCBCFEC7C8BFF4.html [2020/12/26]

[34] 菊池久和. “エレクトロニクス ウェーブレットのそもそも”, Electronics, Tokyo, 1994.

[35] “Tutorialspoint. Signal sampling theorem”, https://www.tutorialspoint.com/signals_and_systems/signals_sampling_theorem.htm [2020/12/26]

[36] Transnational College of LEX; Who is Fourier? A mathematical adventure; Second edition, Language Research Foundation, Cambridge, 2012.

[37] Mizuno-Matsumoto Y, Motamedi GK, Webber WRS, and Lesser RP; Wavelet-crosscorrelation analysis can help predict whether bursts of pulse stimulation will terminate afterdischarges, *Clinical Neurophysiology*, 113(1), pp.33-42, 2002.

[38] Mizuno-Matsumoto Y, Ukai S, Ishii R, Date S, Kaishima T, Shinosaki K, Shimojo S, Takeda M, Tamura S, and Inouye T; Wavelet-crosscorrelation analysis: Non-stationary analysis of neurophysiological signals, *Brain Topography*, 17(4), pp.237-52, 2005.

[39] 榊原進. “ウェーブレットビギナーズガイド”. Publishing company of Tokyo University of electrical appliances. Tokyo, 1995.

[40] 桜井明, 新井勉. “ウェーブレット入門”. Publishing company of Tokyo University of electrical appliances. Tokyo, 1993.

[41] Kikuchi H, Nakashizuka M, Watanabe H, Watanabe S, and Tomisawa N; Fast wavelet transform and its application to detecting detonation, *IEICE Trans. Fundamentals*, E75-A(8): pp.980-987, 1992.

[42] Carpels SMA, Inoguchi Y, Kobayashi S, Muramatsu A, Yamamoto Y, Ito M, and Mizuno-Matsumoto Y; Comparing the Features of the Diffuse Alpha Pattern with the Normal Alpha Pattern using Wavelet-crosscorrelation Analysis, International Journal of Affective Engineering, 19(1), pp.21-30, 2020.

[43] Nunez PL, Srinivasan R, Westdorp AF, Wijesinghe RS, Tucker DM, Silberstein RB, and Cadusch PJ; EEG coherency: I. Statistics, reference electrode, volume conduction, Laplacians, cortical imaging, and interpretation at multiple scales, *Electroencephalography and Clinical Neurophysiology*, 103(5), pp.499–515, 1999.

[44] Li H, and Nozaki T; Wavelet–crosscorrelation analysis to plane turbulent jet, *International Journal Series B*, 40(1), pp.58–66, 1997.

[45] Lachaux JP, Rodriguez E, Van Quyen M, Lutz A, Martinerie J, and Varela FJ; Studying single-trials of phase synchronous activity in the brain, *International Journal of Bifurcation and Chaos*, 10(10), pp.2429-2439, 2000.

[46] "私のための統計処理", http://www.shiga-med.ac.jp/~koyama/stat/s-index.html [2020/12/21]

[47] 石村貞夫, "SPSSによる分散分析と多重比較の手順," 東京図書, 東京, 2007.

[48] Fisher NI; Statistical analysis of circular data; Cambridge University Press, 1995.

[49] Kim J, Wozniak JR, Mueller BA, Pan W; Testing group differences in brain functional connectivity: using correlations or partial correlations?, *Brain Connectivity*, 5(4), pp.214-231, 2015.

[50] Supekar K, Menon V, Rubin D, Musen M, and Greicius MD; Network analysis of intrinsic functional brain connectivity in Alzheimer disease, *PLoS ONE*, 4(6), 2008.

[51] Gudayol-Ferré E, Pero-Cebollero M, Gonzalez-Garrido AA, and Guardia-Olmos J; Changes in brain connectivity related to the treatment of depression measured through fMRI: a systematic review, *Frontiers in human neuroscience*, 9(582), pp.1-17, 2015.

[52] Fingelkurts AA, Fingelkurts AA, Rytsala H, Suominen K, Isometsa E, and Kahkonen S; Impaired functional connectivity at EEG alpha and theta bands in major depression, *Human Brain Mapping*, 28(3), pp.247-261, 2007.

[53] Carpels SMA, Yamaguchi K, and Mizuno-Matsumoto Y; Using wavelet-crosscorrelation analysis to obtain the features of the diffuse alpha pattern in EEG, *International journal of bioelectromagnetism*, 18(1), pp.8-12, 2016.

[54] Steinmann S, Meier J, Nolte G, Engel AK, Leicht G, and Mulert C; The callosal relay model of interhemispheric communication: new evidence from effective connectivity analysis, *Brain Topography*, 31, pp. 218-226, 2018.

[55] Liao W, Zhang Z, Pan Z, Mantini D, Ding J, Duan X, Luo C, Lu G, and Chen H; Altered functional connectivity and small-world in mesial temporal lobe epilepsy, *PLoS ONE*, 5(1), pp.1-11, 2010.

[56] Bosl WJ, Loddenkemper T, and Nelson CA; Nonlinear EEG biomarker profiles for autism and absence epilepsy, Neuropsychiatric Electrophysiology, 3(1), pp.1-22, 2017.

[57] Smith SMJ; EEG in the diagnosis, classification, and management of patients with epilepsy, *Journal of Neurology, Neurosurgery & Psychiatry*, 76(II), pp.ii2-ii7, 2005.

[58] Pillai J and Sperling MR; Interictal EEG and the Diagnosis of Epilepsy, *Epilepsia*, 47(1), pp.14-22, 2006.

[59] Faust O, Acharya UR, Adeli H, and Adeli A; Wavelet-based EEG processing for computer-aided seizure detection and epilepsy diagnosis, *Seizure*, 26, pp.56-64, 2015.

[60] van Diessen E, Diederen SJH, Braun KPJ, Jansen FE, and Stam CJ; Functional and structural brain networks in epilepsy: What have we learned?, *Epilepsia*, 54(11), pp.1855-1865, 2013.

[61] Stam CJ, Jones BF, Nolte G, Breakspear M, and Scheltens Ph; Small-world Networks and Functional Connectivity in Alzheimer's Disease, *Cerebral Cortex*, 17(1), pp.92-9965, 2007.

[62] Reijneveld JC, Ponten SC, Berendse HW, and Stam CJ; The application of graph theoretical analysis to complex networks in the brain, *Clinical Neurophysiology*, 118(11), pp.2317-2331, 2007.

[63] Bartolomei F, Bosma I, Klein M, Baayen JC, Reijneveld JC, Postma TJ, Heimans JJ, van Dijk BW, de Munck JC, de Jongh A, Cover KS, and Stam CJ; Disturbed functional connectivity in brain tumour patients: Evaluation by graph analysis of synchronization matrices, *Clinical Neurophysiology*, 117(9), pp.2039-2049, 2006.

[64] Fair DA, Dosenbach NUF, Church JA, Cohen AL, Brahmbhatt S, Miezin FM, Barch DM, Raichle ME, Petersen SE, and Schlaggar BL; Development of distinct control networks through segregation and integration, *PNAS*, 104(33), pp.13507-13512, 2007.

[65] He Y, Chen ZJ, and Evans AC; Small-world Anatomical Networks in the Human Brain Revealed by Cortical Thickness from MRI, *Cerebral Cortex*, 17(10), pp.2407-2419, 2007.

[66] Stam CJ and Reijneveld JC; Graph theoretical analysis of complex networks in the brain, *Nonlinear Biomedical Physics*, 1(3), 2007.

[67] Barabasi AL and Posfai M; Network Science; 4th edition, Cambridge University Press, Cambridge, United Kingdom, 2016.

[68] Watts DJ and Strogatz SH; Collective dynamics of 'small-world' networks, *Nature*, 393(4), pp.440-442, 1998.

[69] Strogatz SH; Exploring complex networks, *Nature*, 410(8), pp.268-276, 2001.

[70] Achard S, Salvador R, Whitcher B, Suckling J, and Bullmore E; A Resilient, Low-Frequency, Small-World Human Brain Functional Network with Highly Connected Association Cortical Hubs, *The Journal of Neuroscience*, 26(1), pp.63-72, 2006.

[71] Micheloyannis S, Pachou E, Stam CJ, Breakspear M, Bitsios P, Vourkas M, Erimaki S, and Zervakis M; A Resilient, Small-world networks and disturbed functional connectivity in schizophrenia, *Schizophrenia Research*, 87(1-3), pp.60-66, 2006.

[72] Vlooswijk MCG, Vaessen MJ, Jansen JFA, de Krom MCFTM, Majoie HJM, Hofman PAM, Aldenkamp AP, and Backes WH; Loss of network efficiency associated with cognitive decline in chronic epilepsy, *Neurology*, 77(10), pp.938-944, 2011.

[73] He Y, Chen Z, and Evans A; Structural Insights into Aberrant Topological Patterns of Large-Scale Cortical Networks in Alzheimer's Disease, *The Journal of Neuroscience*, 28(18), pp.4756-4766, 2008.

[74] Boersma M, et al; Network analysis of resting state EEG in the developing young brain: Structure comes with maturation, *Human Brain Mapping*, 32(3), pp. 4756-4766, 2011.

[75] Liu Z, Ke L, Liu H, Huang W, and Hu Z; Changes in Topological Organization of Functional PET Brain Network with Normal Aging, *PLoS ONE*, 9(2), e88690, 2014.

[76] Vecchio F, et al; Human brain networks in physiological aging, 41(4), *Journal of Alzheimer's disease*, 2014.

[77] Rubinov M, and Sporns O; Complex network measures of brain connectivity: Uses and interpretations, *Neuroimage*, 52(3), pp.1059-1069, 2010.

[78] Humphries MD, and Gurney K; Network 'Small-World-Ness': A Quantitative Method for Determining Canonical Network Equivalence, *PLoS ONE*, 3(4), e0002051, 2008.

[79] Sporns O, and Zwi JD; The Small World of the Cerebral Cortex, Neuroinformatics, 2, pp.145-162, 2004.

[80] Bassett DS, and Bullmore E; Small-World Brain Networks, *The Neuroscientist*, 12(6), pp.512-523, 2006.

[81] Barabasi AL and Albert R; Statistical mechanics of complex networks, *Reviews of Modern Physics*, 74(1), pp.47-97 , 2002.

[82] Qiu X, Zhang Y, Feng H, and Jiang D; Positron Emission Tomography Reveals Abnormal Topological Organization in Functional Brain Network in Diabetic Patients, Frontiers in Neuroscience, 10(235), pp.1-11, 2016.

[83] Wang J, Wang X, Xia M, Liao X, Evans A, and He Y; GRETNA: a graph theoretical network analysis toolbox for imaging connectomics, *Frontiers in Human Neuroscience*, 9(386), pp.1-16, 2015.

[84] Achard S, and Bullmore E; Efficiency and Cost of Economical Brain Functional Networks, PLoS ONE, 3(2), e17, 2007.

[85] Honey CJ, Kotter R, Breakspear M, and Sporns O; Network structure of cerebral cortex shapes functional connectivity on multiple time scales, *PNAS*, 104(24), pp.10240-10245, 2007.

[86] Kramer MA, Eden UT, Lepage KQ, Kolaczyk ED, Bianchi MT, and Cash SS; Emergence of Persistent Networks in Long-Term Intracranial EEG Recordings, *The Journal of Neuroscience*, 31(44), pp.15757-15767, 2011.

[87] Stam CJ, and van Straaten ECW; The organization of physiological brain networks, *Clinical Neurophysiology*, 123(6), pp.1067-1087, 2012.

[88] Yamaguchi K, et al; The correlations of the brain for different bandwidths of EEG in interictal paroxysmal rhythmic activity: Using wavelet-crosscorrelation analysis, *Transactions of Japan Society of Kansai Engineering*, 16(2), pp.245-252, 2017 (in Japanese).

[89] Tononi G, Sporns O, and Edelman GM; A measure for brain complexity: Relating functional segregation and integration in the nervous system, *PNAS*, 91(11), pp.5033-5037, 1994.

[90] van Dellen E, Douw L, Baayen JC, Heimans JJ, Ponten SC, Vandertop WP, Velis DN, Stam CJ, and Reijneveld JC; Long-Term Effects of Temporal Lobe Epilepsy on Local Neural Networks: A Graph Theoretical Analysis of Corticography Recordings, *PLoS ONE*, 4(11), e8081, 2009.

[91] Ponten S, Bartolomei F, and Stam CJ; Small-world networks and epilepsy: Graph theoretical analysis of intracerebrally recorded mesial temporal lobe seizures, *Clinical Neurophysiology*, 118(4), pp.918-927, 2007.

[92] Bassett DS, Meyer-Lindenberg A, Achard S, Duke T, and Bullmore E; Adaptive reconfiguration of fractal small-world human brain functional networks, *PNAS*, 103(51), pp.19518-19523, 2006.

[93] Chavez M, Hwang DU, Amann A, and Boccaletti S; Synchronizing weighted complex networks, *Chaos*, 16(1), 015106, 2006.

[94] Percha B, Dzakpasu R, and Zochowski M; Transition from local to global phase synchrony in small world neural network and its possible implications for epilepsy, *Physical Review*, 72(3), 031909, 2005.

[95] Netoff TI, Clewley R, Arno S, Keck T, and White JA; Epilepsy in Small-World Networks, *The Journal of Neuroscience*, 24(37), pp.8075-8083, 2004.

[96] Sporns O, Honey CJ, and Kotter R; Identification and Classification of Hubs in Brain Networks, *PLoS ONE*, 2(10), e1049, 2007.

List of Publications by the Author

Published Journal Papers

1. **Steven M.A. Carpels**, Kozue Yamaguchi, Yuko Mizuno-Matsumoto. Using Wavelet-crosscorrelation Analysis to Obtain the Features of the Diffuse Alpha Pattern in EEG. *International Journal of Bioelectromagnetism (IJBEN)*, Vol. 18, No. 1, pp. 8-12, Dec. 2016.

2. **Steven M.A. Carpels**, Yuji Inoguchi, Shohei Kobayashi, Ayumi Muramatsu, Yusuke Yamamoto, Masato Ito, Yuko Mizuno-Matsumoto. Comparing the features of the diffuse alpha pattern with the normal alpha pattern using wavelet-crosscorrelation analysis. *International Journal of Affective Engineering (IJAE)*, Vol. 19, No. 1, pp. 21-30, Jan. 2020.

3. **Steven M.A. Carpels**, Yusuke Yamamoto, Yuko Mizuno-Matsumoto. Graph Theoretical Analysis of Interictal EEG data in Epilepsy Patients during Epileptiform Discharge and Non-discharge. *International Journal of Affective Engineering (IJAE)*, Vol. 20, No. 3, pp. 131-142, July 2021.

International Conference Paper

1. **Steven M.A. Carpels**, Kozue Yamaguchi, Yuko Mizuno-Matsumoto. Features of diffuse alpha pattern in electroencephalography. 8th International workshop on Biosignal Interpretation (BSI2016), International House Osaka, Osaka, Nov.1-3, 2016 (USB).

Japanese Conference Papers

1. **Steven M.A. Carpels**, Kozue Yamaguchi, Yuko Mizuno-Matsumoto: Comparison of the normal α pattern with the diffuse α pattern along the sagittal orientation in the brain using wavelet-crosscorrelation analysis. 第12回日本感性工学会春季大会, 大阪, 3月29-30日, 2017 (USB).

2. **Steven M.A. Carpels**, Kozue Yamaguchi, Yuko Mizuno-Matsumoto. Resemblance of the connectivity in the brain of patients suffering from epilepsy with small-world networks. 第47回日本臨床神経生理学会学術大会, 横浜市, パシフィコ横浜, 11月29日-12月1日, 2017, 臨床神経生理学, Vol. 45, No.5, p.482, 10月1日, 2017.

3. **Steven M.A. Carpels**, 小林昌平，村松歩，水野（松本）由子．グラフ理論を用いた健常者とてんかん患者の脳内ネットワークの比較．第48回日本臨床神経生理学会学術大会，東京都，東京ファッションタウンビル，11月8-10日，臨床神経生理学，Vol. 46, No. 5, p.424, 2018.

4. **Steven M.A. Carpels**, Yuji Inoguchi, Shohei Kobayashi, Yuko Mizuno-Matsumoto. Comparing the features of the diffuse alpha pattern with the normal alpha pattern using wavelet-crosscorrelation analysis.第14回日本感性工学会春季大会, 長野県上田市, 信州大学繊維学部, p.1-7 (PDF), 3月7-8日, 2019.

Co-author in the following Journal Papers:

1. 山口梢，辻義弘，**Steven M.A. Carpels**, 林伶馬, 猪口祐次，水野（松本）由子. ウェーブレット相互相関解析を用いたてんかん性異常波を含む脳波の帯域別領域別部位間関連性. *日本感性工学会論文誌*, Vol. 16, No. 2, pp. 245-252, doi: 10.5057/jjske.TJSKE-D-17-00013, 4月28日, 2017.

2. 山口梢, 猪口祐次, 佐久間俊, **Steven M.A. Carpels**, 水野（松本）由子．てんかん性異常波の持続時間の違いにおけるウェーブレット相互相関解析を用いた脳波の部位間関連性及び情報伝播の可視化． *電気学会論文誌C*, Vol. 138, No. 8, pp. 1045-1053, 8月1日, 2018.

3. 猪口祐次，小林昌平，**カーペルス M.A. スティーブン**，水野（松本）由子. 情動刺激直後の脳波と心拍変動の時間差解析．*電子情報通信学会和文論文誌*，Vol. J102-D, No. 4, pp. 350-358, Apr. 1, 2019.

4. Yuko Mizuno-Matsumoto, Yuji Inoguchi, Shohei Kobayashi, **Steven M.A. Carpels**, Ayumi Muramatsu. How do the Parasympathetic Nervous System and EEG Respond to Emotional Memory Recall? *IEEJ Transactions on Electrical and Electronic Engineering*, vol. 14, pp. 1082-1090, DOI:10.1002/tee.22903, Jun. 18, 2019.

5. Yuko Mizuno-Matsumoto, Yuji Inoguchi, **Steven M.A. Carpels**, Ayumi Muramatsu, Yusuke Yamamoto. Cerebral Cortex and Autonomic Nervous System Responses during Emotional Memory Processing. *PLoS ONE*, vol. 15, e0229890, DOI: 10.1371/journal.pone.0229890, March 5, 2020.

Co-author in the following Conference Papers:

1. 山口梢, 義弘辻, **S.M.A. Carpels**, 林伶馬, 猪口祐次, 水野（松本）由子. ウエーブレット相互相関解析を用いたてんかん性異常波を含む脳波の帯域別領域別部位間関連性. 第12回日本感性工学会春季大会, 大阪, 3月29-30日, 2017 (USB).

2. 山口梢, **Steven M.A. Carpels**, 猪口祐次, 水野（松本）由子. てんかん性異常波出現時における脳波の経時的部位間関連性変化. ジョイント研究会, 兵庫, 6月6日, 2017 (査読なし).

3. 山口梢, **Steven M.A. Carpels**, 猪口祐次, 水野（松本）由子. てんかん性異常波持続時間の違いにおける脳波の部位間関連性の特徴抽出. 第47回日本臨床神経生理学会学術大会, 横浜市, パシフィコ横浜, 11月29日-12月1日, 2017, 臨床神経生理学, Vol. 45, No. 5, pp. 482, 10月1日， 2017.

4. 関谷まり, 松熊秀明, 尾崎朋文, 小林昌平, **Steven M.A. Carpels**, 水野（松本）由子. 健常女性における経穴の押圧刺激による冷水負荷後の手指表面温度の変化. 第48回日本臨床神経生理学会学術大会, 東京都, 東京ファッションタウンビル, 11月8-10日, 臨床神経生理学, Vol. 46, No. 5, p.439, 2018.

5. 村松歩，小林昌平, **Steven M.A. Carpels**, 水野（松本）由子．スマートフォンを利用した情動刺激における脳波のウェーブレット相互相関解析．第48回日本臨床神経生理学会学術大会, 東京都, 東京ファッションタウンビル, 11月8-10日, 臨床神経生理学, Vol. 46, No. 5, p.424, 2018.

6. 小林昌平, **Steven M.A. Carpels**, 村松歩, 水野（松本）由子. 統合失調症患者の脳内部位間関連性を用いたグラフ理論解析. 第48回日本臨床神経生理学会学術大会, 東京都, 東京ファッションタウンビル, 11月8-10日, 臨床神経生理学, Vol. 46, No. 5, p.491, 2018.

7. 辻義弘, **Steven CARPELS**, 鈴木尚紀, 人見泰正, 西村眞人, 水野（松本）由子: 慢性維持血液透析患者における不定愁訴と悪夢の関係について. 第13回日本感性工学会春季大会, 名古屋市, 名古屋大学工学部, 3月27-28日, 2018.